Determining the Molecular Structure of Animal Silks and Related Peptide Mimics

by

John Bennett Addison

A Dissertation Presented in Partial Fulfillment
of the Requirement for the Degree
Doctor of Philosophy

Approved August 2014 by the
Graduate Supervisory Committee:

Jeffery L. Yarger, Co-Chair
Gregory P. Holland, Co-Chair
Robert Ros
Xu Wang

ARIZONA STATE UNIVERSITY

December 2014

ABSTRACT

An animal's ability to produce protein-based silk materials has evolved independently in many different arthropod lineages, satisfying various ecological necessities. However, regardless of their wide range of uses and their potential industrial and biomedical applications, advanced knowledge on the molecular structure of silk biopolymers is largely limited to those produced by spiders (order Araneae) and silkworms (order Lepidoptera). This thesis provides an in-depth molecular-level characterization of silk fibers produced by two vastly different insects: the caddisfly larvae (order Trichoptera) and the webspinner (order Embioptera).

The molecular structure of caddisfly larval silk from the species *Hesperophylax consimilis* was characterized using solid-state nuclear magnetic resonance (ss-NMR) and Wide Angle X-ray Diffraction (WAXD) techniques. This insect, which typically dwells in freshwater river-beds and streams, uses silk fibers as a strong and sticky nanoadhesive material to construct cocoons and cases out available debris. Conformation-sensitive ^{13}C chemical shifts and ^{31}P chemical shift anisotropy (CSA) information strongly support a unique protein motif in which phosphorylated serine-rich repeats $(pSX)_4$ complex with di- and trivalent cations to form rigid nanocrystalline β-sheets. Additionally, it is illustrated through ^{31}P NMR and WAXD data that these nanocrystalline structures can be reversibly formed, and depend entirely on the presence of the stabilizing cations.

Nanofiber silks produced by webspinners (order Embioptera) were also studied herein. This work addresses discrepancies in the literature regarding fiber diameters and tensile properties, revealing that the nanofibers are about 100 nm in diameter, and are stronger (around 500 MPa mean ultimate stress) than previous works suggested. Fourier-transform Infrared Spectroscopy (FT-IR), NMR and WAXD results find that approximately 70% of the highly repetitive glycine- and serine-rich protein

core is composed of β-sheet nanocrystalline structures. In addition, FT-IR and Gas-chromatography mass spectroscopy (GC-MS) data revealed a hydrophobic surface coating rich in long-chain lipids. The effect of this surface coating was studied with contact angle techniques; it is shown that the silk sheets are extremely hydrophobic, yet due to the microstructural and nanostructural detail of the silk surface, are surprisingly adhesive to water.

DEDICATION

To my family

To my wife

ACKNOWLEDGEMENTS

The first part of this dissertation on caddisfly larval silk is a reprint of two works that were published in Biomacromolecules, the first in April, 2013 (Addison, J. B., (2013). *Biomacromolecules*, 14(4), 1140-1148.) and the second in April, 2014 (Addison, J. B., (2014). *Biomacromolecules*, 15(4), 1269-1275.) I was the lead author for these two works. For these works I would like to thank co-authors Dr. Russell Stewart and Nicholas Ashton (University of Utah) for sample preparation and general research guidance throughout this collaborative effort. The second part, characterizing Embiopteran silks, is a reprint of two manuscripts submitted for publication, the first has been published in *RCS Advances* (Addison, J. B., (2014). *RSC Advances*, 4, 41301-41313.) and the second to the *Journal of Chemical Ecology* (Submitted for publication on September 16th, 2014). I acted as the lead or the co-lead author for the two respective works. For these sections I thank co-author Tom Osborn Popp for his tireless help in pushing this project forward, and additionally Dr. Janice Edgerly (Santa Clara University) for her help with sample preparation and for her excellent research guidance and continued correspondence. Additionally, I would like to thank Warner Weber and Qiushi Mou for their help in collecting and analyzing X-ray diffraction data reported in this dissertation.

Moreover, I would like to thank Dr. Jeff Yarger and Dr. Greg Holland for their constant guidance and support, and all my colleagues and coworkers I had the pleasure of working with in the Yargerlab at ASU.

TABLE OF CONTENTS

CHAPTER Page

LIST OF TABLES

Table Page

LIST OF FIGURES

Figure Page

Figure Page

Figure Page

Chapter 1

INTRODUCTION

The molecular structure and function of silks produced by Lepidoptera (silkworms) and Araneae (spiders) have been extensively studied, but there exist many animal silks, about which relatively little is understood. My dissertation research has focussed primarily on characterizing the molecular structure of silks produced by caddisfly larvae (order Trichoptera) and by webspinners (order Embiidena). So that the reader can better understand my work and its immediate and future contributions to the field, I provide here a brief discussion on the progress and study of other animal silks.

Generally speaking, silk refers to insoluble protein-based biopolymer fibers spun by arthropods, that prior to spinning are soluble silk dopes stored within the animal [1]. Upon extrusion from the body, the silk dope is subjected to chemical and/or physical stimulus inducing aggregation into insoluble fibers [2, 3]. These fibers exhibit remarkable properties highly suited for the lifestyle and habitat of the arthropod. They silks are typically heterogeneous, semicrystalline materials composed of large, highly repetitive proteins. Arguably the most famous silk-producing animal is the domesticated silkworm *Bombyx mori* (order Lepidopetra), which spins a protective silk cocoon around itself prior to passing through the pupal stage. Silk produced by this insect has been coveted for thousands of years as a textile material due to its lustrous finish, strength and dyeability. It has recently gained significant attention outside of the textile industry, especially by the medical industry, because of the versatility and biocompatability of regenerated silk materials [4].

Another extremely famous silk-producing arthropod is the spider (order Araneae). Many spiders can produce up to seven different types of silk, including dragline fibers

(Major Ampullate), prey-wrap (Aciniform) and egg-sac silk (Tubuliform), each with remarkably different physical properties, and each secreted from a separate gland network [5]. Spider silks have gained significant attention from researchers and engineers because of their phenomenal mechanical properties. For example, due to its combination of high strength and elasticity [6], weight for weight the dragline silk fiber from the well-studied orb-weaver *Nephila clavipes* outperforms all synthetic materials including high-grade steel, nylon and Kevlar® [7].

While the most famous uses of silk are as the protective cocoon and prey-capture webs of the silkworm and spider, respectively, the ability to produce silk has evolved in at least 23 different arthropod lineages in 17 different orders, satisfying a variety of ecological necessities [8]. Even within one of the largest insect orders, Hymenoptera, the ability to produce silk has arisen at least 6 times [8]. To name a few other examples: lacewings (order Neuroptera) produce silk cocoons during their final larval instar stage, and in addition some lacewing species produce egg stalk silks with exceptionally high extensibility and toughness [9, 10]. Raspy crickets (order Orthoptera) construct protective shelters by joining together nearby materials (leafs, sticks) with silk fibers and films [11]. This silk-reliant nest construction technique is shared with multiple insect orders with separate lineages; weaver ants for example (order Hymenoptera) build arboreal nests by stitching together leaves using larval silk [12], and some caddisfly larval insects (order Trichoptera), one of which is a primary subject of this thesis, utilize adhesive silk fibers under water to stitch together pebbles, sticks and other available debris into protective cocoons [13, 14]. Webspinner silks (order Embioptera), the other primary focus of this thesis, produce exceptionally fine silk fibers from their forearms that criss-cross and overlap to form silken sheets and tunnels in which they live, forage and reproduce [15, 16]. Silks have also been used for reproductive purposes; the silverfish (order Thysanura) and bristletails (order Archaeognatha) use silk to aid sperm transfer during copulation [17].

Sequence to Structure

In most or all cases, silk biopolymers are relatively large, highly repetitive protein aggregates composed primarily of nonessential amino acids glycine, alanine, and serine [1, 18]. As early as 1907 it has been known that silk fibers are predominantly protein materials [19], but not until much later was the protein content understood to any significant degree. Substantial progress was made towards understanding the molecular structure of silks when the first partial cDNA sequences were published. *Bombyx mori* silkworm fibroin proteins and primary protein sequences were the first to be identified, with other silkworm species soon to follow [20, 21]. It was found that silkworm silk fibers are composed primarily of two proteins named Heavy-chain fibroin (H-fibroin, 350 kDa) and Light-chain fibroin (L-fibroin, 25 kDa) [20], which are covalently linked in a 1:1 stoicheometric ratio with a disulfide bridge [22]. The partial primary protein sequences of various silkworm species revealed several repeat protein motifs including poly(A), poly(GA), GAGAGS, GGX, and GPGXX (X = G, A, Q, Y, L) [20, 21].

Similarly, early cDNA sequencing work for *Nephila clavipes* spider dragline silk (Figure 1.1) revealed that silk protein produced in the major ampullate gland are composed of 2 proteins called major ampullate spidron 1 (MaSp1) and major ampullate spidron 2 (MaSp2), both about 200-350 kDa in length, and these contain the repeat motifs poly(A), poly(GA), GGX (X = Y, L, Q), and/or GPGXX (XX = QQ or GY) [23, 24, 25].

Determining the primary protein sequences of silk fibroin material was considered a major breakthrough because these repetitive motifs were found to adopt particular secondary structures, ultimately giving rise to the fibers outstanding physical properties. In particular, solid-state NMR (ssNMR) and X-ray Diffraction experiments have elucidated the relationship between protein sequence and silk structure

[26, 27, 28, 29, 30, 31, 32, 33, 34, 35]. For example, poly(A) and poly(GA) repeat regions adopt antiparallel β-sheet secondary structures. The protein backbone of these antiparallel β-sheets align parallel to the fiber axis, and additionally hydrophobic or van der Waals interactions between the side chains of adjacent sheets results in the formation of nanocrystalline β-sheet structures with dimensions of a few nanometers.[36, 37] It is largely accepted that these nanocrystalline structures are responsible for the impressive strengths observed for spider and silk fibers [38]. Additionally, GGX and GPGXX motifs have been found to exist in 3_{10} helices and type II β-turns, respectfully. It is believed that the extensibility of silk fibers can be attributed to the stretching and deformation of these motifs [27, 39, 40].

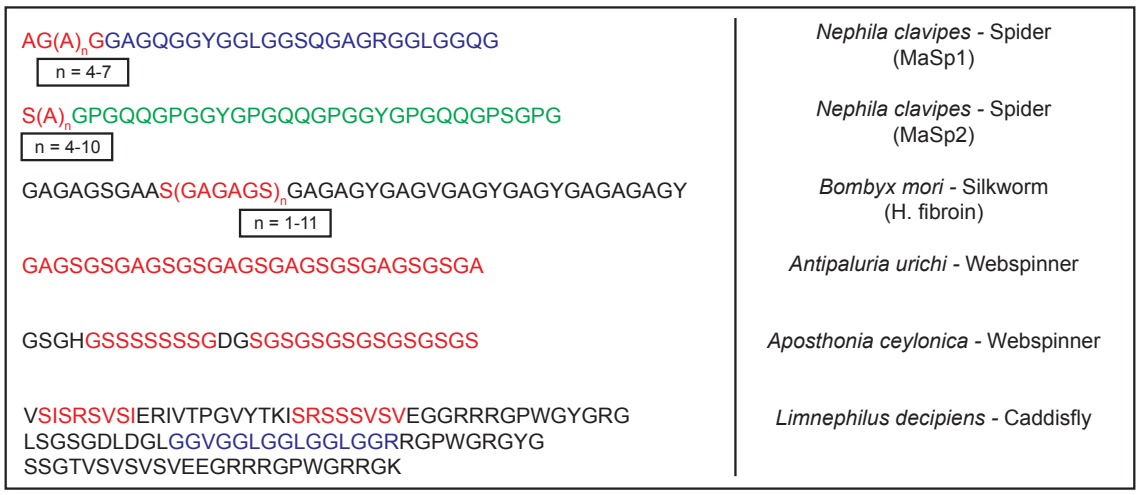

Figure 1.1: Representations of the primary protein sequences from *Nephila clavipes* major ampullate silks [23, 24], *Bombyx mori* Heavy-chain fibroin [20], *Antipaluria urichi* and *Aposthonica ceylonica* webspinner silks [41], and *Limnephilus decipiens* Heavy-chain fibroin [42]. Confirmed or predicted secondary protein structures from repetitive regions are highlighted with red (β-sheet), blue (3_{10}-helix) and green (β-turn). Spider dragline silk from the orb-weaver *Nephila clavipes* contain poly(A), GGX and GPGXX repeat regions that form β-sheets (red), 3_{10} helices (blue) and type II β-turns (green), respectively. *Bombyx mori* silkworm silks contain stretches of $(GAGAGS)_n$ that also are found in β-sheet nanostructures. Webspinner silks are almost entirely composed of poly(S) and poly(GS) sequences, which most likely exist in β-sheet structures. Phosphorylated $(SX)_4$ motifs form caddisfly silks (red) possibly interact with multivalent cations to form rigid β-sheet phosphoserine-cation domains.

Since these early discoveries, cDNA and genomic techniques have determined the partial or complete primary protein sequences for many silk-producing arthropods, including some species of caddisfly larvae [42, 43] and webspinners [41] (Figure 1.1). Like silkworm and spider silks, the two insect silks of interest to this thesis both possess highly repetitive protein sequences that upon careful analysis are good predictive indicators of the silk structure.

Protein Structure Characterization of Silks

Silks are relatively amorphous, heterogeneous structures, making them difficult if not impossible to obtain atomic-level resolution of protein structures with conventional techniques. The vast majority of protein structures in the PDB archive were determined using X-ray crystallography and a small subset with liquid-state NMR, however neither technique apply well for large proteins and for noncrystalline insoluble materials. Thus, determining the overall protein structure and its relation to the repetitive primary protein sequence of silk fibers is challenging and requires the combination of many techniques to gain insight.

The most common characterization techniques used to directly probe the protein secondary structures of these insoluble silk fibers are Fourier-transform Infrared spectroscopy (FT-IR), Raman scattering, Wide-angle X-ray Diffraction (WAXD), small-angle X-ray Diffraction (SAXD), and solid-state nuclear magnetic resonance (ssNMR). FT-IR and Raman techniques cannot directly relate the primary protein sequence to secondary structures, however they are widely used because they are quick, nondestructive, require very little sample, and can probe overall protein structure. It is common to obtain FT-IR profiles for silk materials to quantitatively determine secondary structures. With this technique, infrared radiation is exposed to the silk sample, and the absorbance of that radiation is measured. The protein backbone gives rise to three strong, characteristic amide stretchings denoted the amide I, amide

II, and amide III absorbances, at approximately 1630, 1520 and 1250 wavenumbers, respectively. Based on the absorbance profiles for proteins in known secondary structures, specific peak locations for amide backbone absorbances are assigned to defined structures like parallel and antiparallel β-sheet, α-helix, random coil, and β-turns [44, 45]. These characteristic peak locations are then utilized to quantitatively determine the relative secondary structures within silk fibers from the IR absorbance profiles. For example, quantitative deconvolution of FT-IR profiles have been reported for silkworm [46], spider [47], caddisfly [48], webspinner [49], silverfish [50], and lacewing cocoon silks [51], to name a few. Unfortunately, many researchers ignore frequency-shifting effects from subtle factors like amino acid composition and fiber strain [52], and therefore do not obtain convincing quantitative results. Nevertheless, FT-IR experiments on silk materials are capable of probing general, dominant secondary structures (for example they correctly suggest that silkworm silks and webspinner fibers are dominated by β-sheet secondary structures) and can additionally probe structural changes upon chemical or physical stresses [48, 53].

Undoubtably the most powerful techniques used to elucidate the molecular structure of silk materials have been X-ray diffraction and solid-state NMR. In most silk fibers there exists nanocrystalline β-sheet structures large enough and periodic enough to produce X-ray diffraction patterns [54]. Diffraction patterns have been obtained and analyzed for a variety of arthropod silk fibers, however none have been as extensively studied as silkworm and spider fibers. Previous X-ray studies on spider silks have shown that the silks are both amorphous and semicrystalline, with β-pleated sheets dispersed throughout an amorphous matrix [55, 56, 32]. These experiments are capable of determining important structural information such as the crystal unit cell dimensions, inter-sheet and inter-residue spacings, nanocrystallite dimension and size, orientation of these nanocrystallites with respect to the fiber axis, and total crys-

talline content of the silk material [55, 57]. These parameters show strong correlations to the primary protein sequences. For example, the inter-sheet distances depends on the packing ability of the residue side chains; poly(A) repeat motifs result in slightly larger structures than those composed of poly(GA) because of the smaller side chain of glycine. Also, the total percentage of the fiber that is nanocrystalline varies significantly among arthropod silks. Studies on spider dragline silk fibers show that the crystallinity content ranges from about 30% (*Nephila clavipes*) to 40% (*Latrodectus hesperus*), [32, 58] while fibers from the domesticated silkworm are typically higher, in the range of 40-60% crystallinity [59, 60]. The crystalline fractions come from the repeated protein motifs like poly(A) and poly(GA), thus the primary protein sequence for silks should yield predictive power. Indeed, protein secondary structure within spider dragline silk fibers has been shown to correlate quantitatively with silk primary protein sequences [35, 58].

The information available through X-ray diffraction is limited, however, because silks are largely amorphous, heterogeneous materials. Solid-state NMR has been exceptionally useful towards the study of silk fibers because it is capable of determining angstrom-scale information on large or insoluble biomolecules. Thorough discussions of both the theoretical and practical aspects of solid-state NMR experiments can be found easily in print [61, 62], however considering its heavy use in this dissertation, a brief introduction is provided. The most common and most fundamental ssNMR experiment is the Cross-Polarization under Magic Angle Spinning (CP-MAS) experiment. In combination, Cross Polarization (CP) and Magic Angle Spinning (MAS) address two major experimental issues in obtaining useful NMR data on biomolecules in the solid state: 1) that molecular motion is restricted in the solid state, and 2) adequate signal-to-noise is difficult to obtain for dilute nuclei like ^{13}C and ^{15}N because of low isotopic abundance and long T_1 relaxation times. Unlike in the liquid state

where molecules tumble sufficiently fast, samples in the solid state do not undergo sufficient molecular motion to average away anisotropic parameters such as dipolar coupling between nearby nuclei and the chemical shift anisotropy (CSA). When in an external magnetic field B_0, the hamiltonian expressions for these interactions contain orientation-dependent terms, $(1 - 3\cos^2\theta)$, where θ is the angle between the interaction vector and B_0. These orientation-dependent interactions result in significant line broadening effects that can render data effectively useless. However, the interactions can be partially or completely averaged away by artificially spinning a solid sample about the magic angle ($\theta_M = 54.74\ ^\circ$, equivalent to the apex of a cube, the angle at which the orientation-dependent term goes to zero). This trick is called Magic Angle Spinning (MAS), and is a staple of most solid-state NMR experiments. Cross-Polarization NMR experiments utilize the heteronuclear dipolar coupling interaction between two nuclei to transfer magnetization from the abundant spin (typically ^{1}H) to the dilute nuclei (often ^{13}C and ^{15}N in the case of biomolecules). This magnetization transfer is achieved by first polarizing the abundant spin, then applying radio frequency (RF) spin-lock fields on both nuclei such that two spins are at matching energy levels and satisfy the Hartmann Hahn condition [63]. This is extremely useful for two primary reasons. First, the signal for dilute spins with lower gyromagnetic ratios (^{13}C and ^{15}N) are enhanced theoretically by a factor of γ_I / γ_S, where γ_I and γ_S are the gyromagnetic ratios of the donor spin and acceptor spin, respectively. Thus in the case for ^{1}H - ^{13}C Cross-Polarization experiments, the signal is enhanced by a factor of 4 relative to direct ^{13}C observation. Secondly, the wait time necessary to collect multiple scans during a CP experiment depends on the T_1 relaxation behavior of the donor nucleus ^{1}H, which is significantly shorter than for the dilute nucleus. Data can therefore be collected much faster by simply acquiring more scans in a given timeframe. Hence, the CP-MAS NMR experiment is widely used in solid-state

NMR, and it is one of the most fundamental building blocks for more complicated experiments.

For the last 30 years, ssNMR has been extensively utilized to probe in depth the molecular structure of both spider and silkworm silks. Provided here is a brief discussion of the information gained, but for an excellent and in-depth summary of these works the reader is encouraged to read two recent reviews by Asakura and Yarger [26, 64]. NMR techniques are widely used to study the conformation and local structure of proteins partly because of the sensitivity of specific resonances to local protein secondary structure. Namely, the ^{13}C chemical shift values for the Cα, Cβ and C=O can determine if a particular residue exists in a β-sheet, helical, β-turn or random-coil environment [65, 66, 67]. Solid-state NMR provides a huge advantage over X-ray techniques in this sense because it can gain information on both the crystalline β-sheets and on the amorphous regions. Additionally, ssNMR is capable of directly correlating the primary protein sequence with specific structures. CP-MAS NMR experiments were first applied to silk fibroin as early as 1983 by Saito et al. [68] in the study of silkworm silks. The authors showed that both glycine and alanine residues within silkworm silk existed in predominantly a β-sheet environment, directly correlating poly(A) and poly(GA) repeat motifs to specific β-sheet structures. In 1994, Simmons et al. [34] used ^{13}C CP-MAS NMR to show for the first time that poly(A) motifs within *Nephila clavipes* dragline silk (major ampullate) exist in a β-sheet secondary structure. With the prior knowledge from X-ray diffraction and FT-IR data that *N. clavipes* silks contained antiparallel β-sheet nanocrystallites [54, 69], it became clear that these crystalline regions are indeed composed of poly(A).

Since these early results, more advanced ssNMR experiments have greatly progressed the molecular-level understanding of silkworm and spider silks. For example, two-dimensional ^{13}C double-quantum single-quantum correlation experiments (DO-

QSY) on isotopically-enriched *Nephila edulis* dragline fibers confirmed that alanine residues are predominantly found in β-sheet structures while glycine residues are partially incorporated in β-sheets and otherwise found in 3_1-helical structures [27]. 2D spin-diffusion and double-quantum single-quantum ^{13}C - ^{13}C correlation experiments have similarly shown that both alanine and glycine residues within *N. clavipes* major ampullate silks exist in β-sheet and 3_1-helical conformational environments [70, 71]. It was suggested that the poly(A) and flanking poly(GA) repeats from the MaSp1 and MaSp2 proteins form the β-sheet structures, while the 3_{10}-helical structures arise from the GGX motifs. 2D $^{15}N/^{13}C$ heteronuclear correlation (HETCOR) experiments on *Argiope aurantia* dragline silks suggested by investigating the ^{15}N chemical shift of the proline resonance that GPGXX motifs within MaSp2 proteins exist in type II β-turns [30].

It should be noted that prior to the works summarized in this thesis, there existed virtually no solid-state NMR data in the literature on silks produced by arthropods other than silkworms or spiders. For example, most comprehensive molecular-level works characterizing webspinner silks to date used FT-IR to probe the overall silk secondary structure [49, 72]. Thus, the works presented herein represent the most in-depth molecular-level characterization of fibroin produced by caddisfly larvae and by webspinners.

Study Subjects: Caddisfly (Trichoptera) and Webspinner (Embioptera)

The study of silk materials produced by two vastly different arthropods is presented in this thesis. Sufficient information on these animals and their silks is included in later appropriate chapters, and is briefly introduced here.

Caddisfly larvae, from the order Trichoptera, utilize adhesive silk fibers spun from adapted salivary glands to stitch together available debris into elaborate structures used for protection and camouflage (Figure 1.2 A, B) [73, 74, 13, 14]. Although

Figure 1.2: Optical images depicting the caddisfly larvae and the webspinner, and the respective roles of their silks. An *Hesperophylax consimilis* larvae seen in (A) utilize adhesive silk fibers in freshwater rivers and streams to stitch together available debris into protective cases and cocoons (A, B). Webspinners are typically small (approximately 1.5 cm in length) tropical or subtropical insects that spin silk out of their forearms (C) into protective silken galleries composed of sheets and tunnels (D). The webspinner and its silk seen in (C) and (D) are of the species *Antipaluria urichi*. The images from (A) and (B) are borrowed from Figure 2.1, while the images from (C) and (D) are borrowed from figures 4.1 and 5.1, respectively.

the caddisfly dwells underwater, typically in freshwater streams and riverbeds, the insect is remarkably homologous to the terrestrial silkworm (order Lepidoptera). Trichopteran silks are composed primarily of two proteins H-fibroin (250-500 kDa) and L-fibroin (25 kDa) covalently linked in a 1:1 molar ratio with a disulfide linkage [75, 42, 43]. The partial H-fibroin primary protein sequences have been determined for a few Trichopteran species, revealing repetitive protein motifs shared with Lepidopteran silks including GPXGX, GGX and $(SX)_n$ [21, 42, 43] (see Figure 1.1 or

Figure 2.2).

Interestingly, it has been shown that caddisfly silks contain a substantial amount of phosphorus [76, 77]. The phosphorus appears to come from seryl residues that are heavily phosphorylated within the silks; Stewart et al. (2010) [77] showed that approximately 60% of all serine residues within some caddisfly silk species are phosphorylated, and the phosphorylation is mostly localized to the highly conserved $(SX)_4$ repeat motif (highlighted in red for the partial caddisfly protein sequence in Figures 1.1 and 2.2). The high concentration of negatively charged phosphates from $(SX)_4$ repeat motifs implies an electrostatic-driven structural arrangement. The observation that caddisfly silks contain high levels of divalent cations Ca^{2+} and Mg^{2+} led to a proposed model in which alternating phosphorylated serine residues interact with divalent cations to form rigid β-sheet structures in caddisfly silk [77]. It is this proposed molecular structure that is thoroughly investigated within this work.

Embiopterans (often called webspinners or embiids) are community-based insects, typically of tropical or sub-tropical habitat, that produce silken galleries and sheets using exceptionally fine silk fibers in which they live and breed (Figure 1.2 C, D) [78, 79]. They secrete many silk fibers at once from the surface of the basal segment of their front feet [78]. These fibers overlap and criss-cross to form sheets and tunnels that protect the insects foraging beneath. Partial protein sequences have been identified for a few webspinner species [80, 41]. Results revealed that webspinner silk proteins are approximately 70 kDa in molecular weight, are dominated by glycine, serine and alanine, and are composed primarily of highly repetitive motifs such as poly(GS), poly(S) and GAGSGS [72, 80, 41] (see Figures 1.1 and 4.1 for representations of webspinner repetitive protein sequences). The molecular structure of webspinner silk remains largely uncharacterized, however previous Fourier-transform infrared spectroscopy studies on embiopteran silks have suggested that the fibers are

dominated by β-sheet secondary structures within the protein core, presumably from said repetitive protein motifs [80, 41, 49, 72]. In addition to deterring predators, these protective sheets are quite water-repellant, a trait that could be an adaptation to prevent the drowning of the insects during tropical, often torrential rainfall. This work investigates the molecular-level protein structure of the fiber core and probes the composition and functional use of a hydrophobic, alkane-rich surface coating surrounding the silk fibers.

Bioinspired Materials

The fantastic physical properties as well as biocompatibility of silk materials have given researchers and engineers plenty of reason to flatter nature through mimicry. Spiders produce fibers that dramatically outperform those produced by silkworms, however unlike the silkworm, which has been domesticated and can cheaply produce large quantities of silk, spiders are canibalistic creatures and cannot be domesticated for mass-production [81]. For perspective, it took 1 million spiders, over 100 people and 4 years to produce a single 11 foot by 4 foot silk cloth [82]. Thus, there exists a serious effort to spin synthetic spider silks with matching physical properties [83, 84, 85, 86, 87]. Synthetic spider silk fibers will undoubtably prove to be useful for industrial and biomedical applications, but silk-based synthetic biomaterals are not limited to fibers. In addition to synthetic fibers, spider silk-based films, hydrogels, nanoparticles, foams and non-woven mesh materials have been created for a wide variety of biomedical applications including drug delivery, implant coating and tissue scaffolding, to name a few [88, 89, 90].

Spider silk-based synthetic materials must be produced through artificial protein expression, like through ecoli or yeast, but silkworm silk is plentiful, cheap, biocompatible [91], shows slow degredation rates [92], and can likewise be reconstituted into a variety of materials including fibers, films, hydrogels, sponges, and nanospheres [4].

An additional desirable property of silk materials is their ease of chemical modification or as substrate for composite materials. For example, hydroxyapatite-silk fibroin materials have been synthesized with the goal of preparing artificial tooth or bone roots and scaffolding [93]. Chemical modification of tyrosine residues within silkworm fibroin using diazonium coupling chemistry was developed by Murphy et al. [94], allowing for incorporation of a wide variety of chemistry functional groups, and thus better control of the physical properties of the regenerated silk materials. Silkworm silks have also been chemically modified using isocyanates [95], epoxides [96, 97], aromatic acid anhydrides [98], small peptides [99, 100], and gold nanoparticles [101], all further broadening the applicability of such materials.

Without doubt, the primary inspiration for these synthetic silk-based materials has been silkworm and spider silks. However, there also exist several examples of synthetic materials inspired by other arthropod biopolymers. One example of this is the green lacewing egg-stalk silk [10]. Lacewings lay their eggs on top of silken egg-stalks to protect them from predators and caniballism. The silks are fairly short and simple in that they are only around 1/4 the length of spider and silkworm proteins, and over 70% of the protein content consists of highly-repetitive regions with 16 AA periodicity [10]. Bauer and Scheibel (2012) [102] created synthetic egg-stalks from recombinant lacewing silk protein purified from ecoli that, at least at standard temperatures and low humidity, performed equally well to the native silks. In addition to broadening the scope of model silks for artificial materials, synthetic lacewing egg-stalk silks are intriguing because of the shorter length and the simplicity of the protein sequence, and thus fewer engineering problems for biomicry in comparison to spider and silkworm silks.

Bioadhesives produced by arthropods, especially those that function underwater, are an additional class of polymers that are gaining attention. Marine organisms

such as the muscles, sandcastle worms and the caddisfly have evolved proteinaceous adhesive materials that can adhere even to polar substrate under water [103]. Progress in understanding the materials by these subjects have served as inspiration for the synthetic production of underwater-based adhesives [104, 76, 105].

Final Remarks

Studying new and relatively uncharacterized silk materials not only improves the general understanding of silk-based biopolymers found in nature, but also provides engineers with more directed information for the creation of useful bioinspired materials. The results presented in this thesis therefore should be of interest to biologists, chemists and engineers studying proteinaceous biopolymers and related bio-inspired materials.

REFERENCES

[1] C Craig. Evolution of arthropod silks. *Annual review of entomology*, 1997.

[2] Fritz Vollrath. Liquid crystalline spinning of spider silk. *Nature*, 2001.

[3] C Wong Po Foo, E Bini, J Hensman, D P Knight, R V Lewis, and D L Kaplan. Role of pH and charge on silk protein assembly in insects and spiders. *Applied Physics A*, 82(2):223–233, 2006.

[4] Danielle N Rockwood, Rucsanda C Preda, Tuna Yücel, Xiaoqin Wang, Michael L Lovett, and David L Kaplan. Materials fabrication from Bombyx mori silk fibroin. *Nature Protocols*, 6(10):1612–1631, September 2011.

[5] Fritz Vollrath. Strength and structure of spiders' silks. *Reviews in Molecular Biotechnology*, 74(2):67–83, August 2000.

[6] John M Gosline, Mark W Denny, and M Edwin DeMont. Spider silk as rubber. *Nature*, 309(5968):551–552, June 1984.

[7] J M Gosline, P A Guerette, C S Ortlepp, and K N Savage. The mechanical design of spider silks: from fibroin sequence to mechanical function. *The Journal of Experimental Biology*, 202(Pt 23):3295–3303, December 1999.

[8] Tara D Sutherland, James H Young, Sarah Weisman, Cheryl Y Hayashi, and David J Merritt. Insect silk: one name, many materials. *Annual review of entomology*, 55:171–188, 2010.

[9] P Duelli. A 'missing link' in the evolution of the egg pedicel in lacewings? *Experientia*, 42(6):624–624, June 1986.

[10] Sarah Weisman, Shoko Okada, Stephen T Mudie, Mickey G Huson, Holly E Trueman, Alagacone Sriskantha, Victoria S Haritos, and Tara D Sutherland. Fifty years later: the sequence, structure and function of lacewing cross-beta silk. *Journal of structural biology*, 168(3):467–475, December 2009.

[11] Andrew A Walker, Sarah Weisman, Jeffrey S Church, David J Merritt, Stephen T Mudie, and Tara D Sutherland. Silk from Crickets: A New Twist on Spinning. *PLoS ONE*, 7(2):e30408, February 2012.

[12] R H Crozier, P S Newey, and E A Schluens. A masterpiece of evolution—Oecophylla weaver ants (Hymenoptera: Formicidae). *Myrmecological News*, 13:57–71, December 2009.

[13] Gary LaFontaine. *Caddisflies*. The Lyons Press, April 1989.

[14] Glenn B Wiggins. *The caddisfly family Phryganeidae (Trichoptera)*. University of Toronto Press Incorporated, 1998.

[15] E S Ross. A synopsis of the embiidina of the United States. *Proceedings of the Entomological Society of Washington*, 86(1):82–93, 1984.

[16] Edward S Ross. Webspinners (Embiidina). In John L Capirena, editor, *Encyclopedia of Entomology*, pages 4169–4172. Springer Netherlands, 2008.

[17] Jacques Bitsch. Ultrastructure of the phallic glands of the firebrat, Thermobia domestica (packard) (Thysanura : Lepismatidae). *International Journal of Insect Morphology and Embryology*, 19(2):65–78, January 1990.

[18] C Craig, M Hsu, and D Kaplan. A comparison of the composition of silk proteins produced by spiders and insects. *International journal of biological ...*, 1999.

[19] E Fischer. About spider silk. *Hoppe-Seyler's Z Physiol Chem*, pages 440–450, 1907.

[20] Yoshihide Tsujimoto and Yoshiaki Suzuki. The dna sequence of bombyx mori fibroin gene including the 5 flanking, mRNA coding, entire intervening and fibroin protein coding regions. *Cell*, 18(2):591–600, October 1979.

[21] F Sehnal and M Zurovec. Construction of silk fiber core in Lepidoptera. *Biomacromolecules*, 5(3):666–674, 2004.

[22] Tetsuo Ohmachi, Hideo Nagayama, and Kensuke Shimura. The isolation of a messenger RNA coding for the small subunit of fibroin from the posterior silkgland of the silkworm, Bombyx mori. *FEBS letters*, 146(2):385–388, September 1982.

[23] M Xu and R V Lewis. Structure of a protein superfiber: spider dragline silk. *Proceedings of the National Academy of Sciences of the United States of America*, 87(18):7120–7124, September 1990.

[24] Michael B Hinman and Randolph V Lewis. Isolation of a clone encoding a second dragline silk fibroin. Nephila clavipes dragline silk is a two-protein fiber. *The Journal of biological chemistry*, 267(27):19320–19324, 1992.

[25] C Y Hayashi, N H Shipley, and R V Lewis. Hypotheses that correlate the sequence, structure, and mechanical properties of spider silk proteins. *International Journal of Biological Macromolecules*, 24(2-3):271–275, March 1999.

[26] Tetsuo Asakura, Yu Suzuki, Yasumoto Nakazawa, Gregory P Holland, and Jeffery L Yarger. Elucidating silk structure using solid-state NMR. *Soft Matter*, 9(48):11440–11450, 2013.

[27] J D van Beek. The molecular structure of spider dragline silk: Folding and orientation of the protein backbone. *Proceedings of the National Academy of Sciences*, 99(16):10266–10271, July 2002.

[28] L Beaulieu, H Schäfer, M Demura, and T Asakura. Solid-state NMR determination of the secondary structure of Samia cynthia ricini silk. *Nature*, 2000.

[29] Gregory P Holland, Melinda S Creager, and Janelle E Jenkins. Determining Secondary Structure in Spider Dragline Silk by Carbon Carbon Correlation Solid-State NMR Spectroscopy. *Journal of the ...*, 2008.

[30] M S Creager, E B Butler, R V Lewis, J L Yarger, and G P Holland. Solid-state NMR evidence for elastin-like β-turn structure in spider dragline silk. *Chemical Communications*, 46(36):6714–6716, 2010.

[31] Xiangyan Shi, Jeffery L Yarger, and Gregory P Holland. Elucidating proline dynamics in spider dragline silk fibre using 2H-13C HETCOR MAS NMR. *Chemical Communications*, 50(37):4856–4859, May 2014.

[32] Sujatha Sampath, Thomas Isdebski, Janelle E Jenkins, Joel V Ayon, Robert W Henning, Joseph P R O Orgel, Olga Antipoa, and Jeffery L Yarger. X-ray diffraction study of nanocrystalline and amorphous structure within major and minor ampullate dragline spider silks. *Soft Matter*, 8(25):6713–6722, 2012.

[33] Tetsuo Asakura, Kosuke Ohgo, Kohei Komatsu, Masakazu Kanenari, and Kenji Okuyama. Refinement of Repeated β-turn Structure for Silk I Conformation of Bombyx moriSilk Fibroin Using 13C Solid-State NMR and X-ray Diffraction Methods. *Macromolecules*, 38(17):7397–7403, August 2005.

[34] A Simmons, E Ray, and LW Jelinski. Solid-state 13C NMR of Nephila clavipes dragline silk establishes structure and identity of crystalline regions. *Macromolecules*, 27(18):5235–5237, 1994.

[35] Janelle E Jenkins, Melinda S Creager, Randolph V Lewis, Gregory P Holland, and Jeffery L Yarger. Quantitative Correlation between the protein primary sequences and secondary structures in spider dragline silks. *Biomacromolecules*, 11(1):192–200, 2009.

[36] Z Yang, DT Grubb, and LW Jelinski. Small-angle X-ray scattering of spider dragline silk. *Macromolecules*, 30(26):8254–8261, 1997.

[37] Gregory P Holland, Randolph V Lewis, and Jeffery L Yarger. WISE NMR characterization of nanoscale heterogeneity and mobility in supercontracted Nephila clavipes spider dragline silk. *J. Am. Chem. Soc*, 126(18):5867–5872, 2004.

[38] Sinan Keten and Markus J Buehler. Atomistic model of the spider silk nanostructure. *Applied physics letters*, 96(15):153701, 2010.

[39] Nathan Becker, Emin Oroudjev, Stephanie Mutz, Jason P Cleveland, Paul K Hansma, Cheryl Y Hayashi, Dmitrii E Makarov, and Helen G Hansma. Molecular nanosprings in spider capture-silk threads. *Nature Materials*, 2(4):278–283, March 2003.

[40] Yi Liu and Zhengzhong Shao. Elasticity of spider silks. *Biomacromolecules*, 9:1782–1786, 2008.

[41] Matthew A Collin, Janice S Edgerly, and Cheryl Y Hayashi. Comparison of fibroin cDNAs from webspinning insects: insight into silk formation and function. *Zoology (Jena, Germany)*, 114(4):239–246, September 2011.

[42] N Yonemura, F Sehnal, and K Mita. Protein composition of silk filaments spun under water by caddisfly larvae. *Biomacromolecules*, 7(12):3370–3378, 2006.

[43] Naoyuki Yonemura, Kazuei Mita, Toshiki Tamura, and František Sehnal. Conservation of Silk Genes in Trichoptera and Lepidoptera. *Journal of molecular evolution*, 68(6):641–653, May 2009.

[44] D M Byler and H Susi. Examination of the secondary structure of proteins by deconvolved FTIR spectra. *Biopolymers*, 25(3):469–487, March 1986.

[45] S Cai and B R Singh. Identification of β-turn and random coil amide III infrared bands for secondary structure estimation of proteins. *Biophysical Chemistry*, 1999.

[46] Md Majibur Rahman Khan, Hideaki Morikawa, Yasuo Gotoh, Mikihiko Miura, Zha Ming, Yuji Sato, and Masayuki Iwasa. Structural characteristics and properties of Bombyx mori silk fiber obtained by different artificial forcibly silking speeds. *International Journal of Biological Macromolecules*, 42(3):264–270, April 2008.

[47] Shengjie Ling, Zeming Qi, David P Knight, Zhengzhong Shao, and Xin Chen. Synchrotron FTIR Microspectroscopy of Single Natural Silk Fibers. *Biomacromolecules*, 12(9):3344–3349, September 2011.

[48] Nicholas N Ashton, Daniel R Roe, Robert B Weiss, Thomas E Cheatham, III, and Russell J Stewart. Self-Tensioning Aquatic Caddisfly Silk: Ca 2+-Dependent Structure, Strength, and Load Cycle Hysteresis. *Biomacromolecules*, 14(10):3668–3681, October 2013.

[49] Matthew A Collin, Edina Camama, Brook O Swanson, Janice S Edgerly, and Cheryl Y Hayashi. Comparison of embiopteran silks reveals tensile and structural similarities across Taxa. *Biomacromolecules*, 10(8):2268–2274, August 2009.

[50] Andrew A Walker, Jeffrey S Church, Andrea L Woodhead, and Tara D Sutherland. Silverfish silk is formed by entanglement of randomly coiled protein chains. *Insect biochemistry and molecular biology*, 43(7):572–579, July 2013.

[51] Sarah Weisman, Holly E Trueman, Stephen T Mudie, Jeffrey S Church, Tara D Sutherland, and Victoria S Haritos. An Unlikely Silk: The Composite Material of Green Lacewing Cocoons. *Biomacromolecules*, 9(11):3065–3069, November 2008.

[52] P Papadopoulos, J Sölter, and F Kremer. Structure-property relationships in major ampullate spider silk as deduced from polarized FTIR spectroscopy. *The European physical journal. E, Soft matter*, 24(2):193–199, October 2007.

[53] Shengjie Ling, Zeming Qi, David P Knight, Yufang Huang, Lei Huang, Huan Zhou, Zhengzhong Shao, and Xin Chen. Insight into the Structure of Single Antheraea pernyi Silkworm Fibers Using Synchrotron FTIR Microspectroscopy. *Biomacromolecules*, 14(6):1885–1892, June 2013.

[54] J O Warwicker. Comparative studies of fibroins. II. The crystal structures of various fibroins. *Journal of Molecular Biology*, 2(6):350–362, December 1960.

[55] DT Grubb and LW Jelinski. Fiber morphology of spider silk: the effects of tensile deformation. *Macromolecules*, 30(10):2860–2867, 1997.

[56] C Riekel, C Bränden, C Craig, C Ferrero, F Heidelbach, and M Müller. Aspects of X-ray diffraction on single spider fibers. *International Journal of Biological Macromolecules*, 24(2-3):179–186, March 1999.

[57] Lawrence F Drummy, B L Farmer, and Rajesh R Naik. Correlation of the ?-sheet crystal size in silk fibers with the protein amino acid sequence. *Soft Matter*, 3(7):877–882, 2007.

[58] Janelle E Jenkins, Sujatha Sampath, Emily Butler, Jihyun Kim, Robert W Henning, Gregory P Holland, and Jeffery L Yarger. Characterizing the secondary protein structure of black widow dragline silk using solid-state NMR and X-ray diffraction. *Biomacromolecules*, 14(10):3472–3483, October 2013.

[59] Ku Liang, Yu Gong, Jianlong Fu, Shi Yan, Yuanyuan Tan, Rong Du, Xueqing Xing, Guang Mo, Zhongjun Chen, Quan Cai, Dongbai Sun, and Zhonghua Wu. Microstructural change of degummed Bombyx mori silk: an in situ stretching wide-angle X-ray-scattering study. *International Journal of Biological Macromolecules*, 57:99–104, June 2013.

[60] Tetsuo Asakura, Juming Yao, Tsutomu Yamane, Kosuke Umemura, and Anne S Ulrich. Heterogeneous Structure of Silk Fibers from BombyxmoriResolved by 13C Solid-State NMR Spectroscopy. *J. Am. Chem. Soc*, 124(30):8794–8795, July 2002.

[61] K Schmidt-Rohr and H W Spiess. *Multidimensional Solid-State NMR and Polymers*. Academic Press, 1 edition, November 1994.

[62] H Saito, I Ando, and A Naito. *Solid State NMR Spectroscopy for Biopolymers*. Springer, July 2006.

[63] S Hartmann. Nuclear double resonance in the rotating frame. *Physical Review*, 1962.

[64] Tetsuo Asakura, Yu Suzuki, Yasumoto Nakazawa, Koji Yazawa, Gregory P Holland, and Jeffery L Yarger. Silk structure studied with nuclear magnetic resonance. *Progress in Nuclear Magnetic Resonance Spectroscopy*, 69(Complete):23–68, 2013.

[65] DS Wishart, CG Bigam, A Holm, RS Hodges, and BD Sykes. 1 H, 13 C and 15 N random coil NMR chemical shifts of the common amino acids. I. Investigations of nearest-neighbor effects. *Journal of biomolecular NMR*, 5(1):67–81, 1995.

[66] Akira Shoji, Takuo Ozaki, Hazime Saito, Ryoko Tabeta, and Isao Ando. Conformational characterization of solid polypeptides by carbon-13 NMR recorded by the cross polarization-magic angle spinning method: conformation-dependent carbon-13 chemical shifts of oligo- and poly(γ-benzyl L-glutamates) and sequential copolymers of γ-benzyl and γ-methyl L-glutamates and qualitative evaluation of side-chain orientation. *Macromolecules*, 17(8):1472–1479, August 1984.

[67] Hans R Kricheldorf and Detlef Mueller. Secondary structure of peptides. 3. Carbon-13 NMR cross polarization/magic angle spinning spectroscopic characterization of solid polypeptides. *Macromolecules*, 16(4):615–623, July 1983.

[68] Hazime Saito, Yoshihiro Iwanaga, Ryoko Tabeta, Mitsuaki Narita, and Tetsuo Asakura. A high resolution 13C NMR study of silk fibroin in solid state by the cross polarization-magic angle spinning method: Conformational characterization utilizing conformation-dependent 13C chemical shifts. *Chemistry Letters*, (4):427–430, 1983.

[69] Zhengyu Dong, Randolph V Lewis, and C Russell Middaugh. Molecular mechanism of spider silk elasticity. *Archives of biochemistry and biophysics*, 284(1):53–57, January 1991.

[70] Gregory P Holland, Melinda S Creager, Janelle E Jenkins, Randolph V Lewis, and Jeffery L Yarger. Determining Secondary Structure in Spider Dragline Silk by Carbon Carbon Correlation Solid-State NMR Spectroscopy. *J. Am. Chem. Soc*, 130(30):9871–9877, 2008.

[71] G P Holland, J E Jenkins, M S Creager, R V Lewis, and J L Yarger. Quantifying the fraction of glycine and alanine in β-sheet and helical conformations in spider dragline silk using solid-state NMR. *Chemical Communications*, (43):5568–5570, 2008.

[72] Shoko Okada, Sarah Weisman, Holly E Trueman, Stephen T Mudie, Victoria S Haritos, and Tara D Sutherland. An Australian webspinner species makes the finest known insect silk fibers. *International Journal of Biological Macromolecules*, 43(3):271–275, October 2008.

[73] K M Kjer, R J Blahnik, and R W Holzenthal. Phylogeny of caddisflies (Insecta, Trichoptera). *Zoologica Scripta*, 31(1):83–91, 2002.

[74] J C Morse. Phylogeny of trichoptera. *Annual review of entomology*, 42(1):427–450, 1997.

[75] Kensuke Shimura, Aiko Kikuchi, Kohei Ohtomo, Yōtarō Katagata, and Akio Hyodo. Studies on Silk Fibroin of Bombyx mori. I. Fractionation of Fibroin Prepared from the Posterior Silk Gland. *The Journal of Biochemistry*, 80(4):693–702, 1976.

[76] Russell J Stewart, Ching Shuen Wang, and Hui Shao. Complex coacervates as a foundation for synthetic underwater adhesives. *Advances in Colloid and Interface Science*, 167:85–93, 2011.

[77] R J Stewart and C S Wang. Adaptation of Caddisfly Larval Silks to Aquatic Habitats by Phosphorylation of H-Fibroin Serines. *Biomacromolecules*, 11(4):969–974, 2010.

[78] J S Edgerly, J A Davilla, and N Schoenfeld. Silk Spinning Behavior and Domicile Construction in Webspinners - Springer. *Journal of Insect Behavior*, 15(2):219–242, 2002.

[79] Janice S Edgerly. Life Beneath Silk Walls: A Review of the Primitively Social Embiidina. In J C Choe and B Crespi, editors, *The Evolution of Social Behavior in Insects and Arachnids*, pages 14–25. Cambridge University Press, 1997.

[80] Matthew A Collin, Jessica E Garb, Janice S Edgerly, and Cheryl Y Hayashi. Characterization of silk spun by the embiopteran, Antipaluria urichi. *Insect biochemistry and ...*, 39:79–82, 2009.

[81] Laurel R Fox. Cannibalism in natural populations. *Annual review of ecology and systematics*, pages 87–106, 1975.

[82] Hadley Leggett. 1 Million Spiders Make Golden Silk for Rare Cloth, September 2009.

[83] Amy E Albertson, Florence Teulé, Warner Weber, Jeffery L Yarger, and Randolph V Lewis. Effects of different post-spin stretching conditions on the mechanical properties of synthetic spider silk fibers. *Journal of the Mechanical Behavior of Biomedical Materials*, 29:225–234, January 2014.

[84] Florence Teulé, Bennett Addison, Alyssa R Cooper, Joel Ayon, Robert W Henning, Chris J Benmore, Gregory P Holland, Jeffery L Yarger, and Randolph V Lewis. Combining flagelliform and dragline spider silk motifs to produce tunable synthetic biopolymer fibers. *Biopolymers*, 97(6):418–431, October 2011.

[85] Lingling Xu, Jan K Rainey, Qing Meng, and Xiang-Qin Liu. Recombinant Minimalist Spider Wrapping Silk Proteins Capable of Native-Like Fiber Formation. *PLoS ONE*, 7(11):e50227, November 2012.

[86] Paul Geurts, Liang Zhao, Yang Hsia, Eric Gnesa, Simon Tang, Felicia Jeffery, Coby La Mattina, Andreas Franz, Leah Larkin, and Craig Vierra. Synthetic Spider Silk Fibers Spun from Pyriform Spidroin 2, A Glue Silk Protein Discovered in Orb-Weaving Spider Attachment Discs. *Biomacromolecules*, 11(12):3495–3503, 2010.

[87] Gustavo R Plaza, Paola Corsini, Enrico Marsano, José Pérez-Rigueiro, Lautaro Biancotto, Manuel Elices, Christian Riekel, Fernando Agulló-Rueda, Eva Gallardo, José M Calleja, and Gustavo V Guinea. Old Silks Endowed with New Properties. *Macromolecules*, 42(22):8977–8982, November 2009.

[88] John G Hardy, Lin M Römer, and Thomas R Scheibel. Polymeric materials based on silk proteins. *Polymer*, 49(20):4309–4327, September 2008.

[89] Kristin Schacht and Thomas Scheibel. Processing of recombinant spider silk proteins into tailor-made materials for biomaterials applications. *Current opinion in biotechnology*, 29:62–69, 2014.

[90] Jonathan A Kluge, Olena Rabotyagova, Gary G Leisk, and David L Kaplan. Spider silks and their applications. *Trends in biotechnology*, 26(5):244–251, May 2008.

[91] L Meinel, S Hofmann, V Karageorgiou, and C Kirker-Head. The inflammatory responses to silk films in vitro and in vivo. *Biomaterials*, 2005.

[92] Rebecca L Horan, Kathryn Antle, Adam L Collette, Yongzhong Wang, Jia Huang, Jodie E Moreau, Vladimir Volloch, David L Kaplan, and Gregory H Altman. In vitro degradation of silk fibroin. *Biomaterials*, 26(17):3385–3393, June 2005.

[93] Rei Nemoto, Satoshi Nakamura, Tetsuhiko Isobe, and Mamoru Senna. Direct Synthesis of Hydroxyapatite-Silk Fibroin Nano-Composite Sol via a Mechanochemical Route. *Journal of Sol-Gel Science and Technology*, 21(1/2):7–12, 2001.

[94] A Murphy and P John. Modification of silk fibroin using diazonium coupling chemistry and the effects on hMSC proliferation and differentiation. *Biomaterials*, 2008.

[95] T Arai, H Ishikawa, and G Freddi. Chemical modification of Bombyx mori silk using isocyanates. *Journal of applied ...*, 2001.

[96] Z Cai and G Jiang. Chemical modification of Bombyx mori silk with epoxide EPSIB. *Journal of applied polymer science*, 2004.

[97] Z Cai. Using an aqueous epoxide in Bombyx mori silk fabric finishing. *Textile Research Journal*, 2003.

[98] M Tsukada, Y Goto, G Freddi, and H Shiozaki. Chemical modification of silk with aromatic acid anhydrides. *Journal of applied polymer science*, 45(7):1189–1194, 1992.

[99] Susan Sofia, Mary Beth McCarthy, Gloria Gronowicz, and David L Kaplan. Functionalized silk-based biomaterials for bone formation. *Journal of Biomedical Materials Research Part A*, 54(1):139–148, 2000.

[100] T Kardestuncer, M B McCarthy, V Karageorgiou, D Kaplan, and G Gronowicz. RGD-tethered Silk Substrate Stimulates the Differentiation of Human Tendon Cells. *Clinical Orthopaedics and Related Research*, 448:234–239, July 2006.

[101] Tzahi Cohen-Karni, Kyung Jae Jeong, Jonathan H Tsui, Gally Reznor, Mirela Mustata, Meni Wanunu, Adam Graham, Carolyn Marks, David C Bell, Robert Langer, and Daniel S Kohane. Nanocomposite gold-silk nanofibers. *Nano letters*, 12(10):5403–5406, October 2012.

[102] Felix Bauer and Thomas Scheibel. Artificial Egg Stalks Made of a Recombinantly Produced Lacewing Silk Protein. *Angewandte Chemie International Edition*, 51(26):6521–6524, May 2012.

[103] Russell J Stewart. Protein-based underwater adhesives and the prospects for their biotechnological production. *Applied microbiology and biotechnology*, 89(1):27–33, 2011.

[104] H Shao. Biomimetic underwater adhesives with environmentally triggered setting mechanisms. *Advanced Materials*, 2010.

[105] Bruce P Lee, P B Messersmith, J N Israelachvili, and J H Waite. Mussel-Inspired Adhesives and Coatings. *Annual Review of Materials Research*, 41(1):99–132, August 2011.

Chapter 2

β-SHEET NANOCRYSTALLINE DOMAINS FORMED FROM PHOSPHORYLATED SERINE-RICH MOTIFS IN CADDISFLY LARVAL SILK: A SOLID-STATE NMR AND XRD STUDY

2.1 Abstract

Adhesive silks spun by aquatic caddisfly (order Trichoptera) larvae are used to build both intricate protective shelters and food harvesting nets underwater. In this study, we use ^{13}C and ^{31}P solid-state Nuclear Magnetic Resonance (NMR) and Wide Angle X-ray Diffraction (WAXD) as tools to elucidate molecular protein structure of caddisfly larval silk from the species *Hesperophylax consimilis*. Caddisfly larval silk is a fibroin protein based biopolymer containing mostly repetitive amino acid motifs. NMR and X-ray results provide strong supporting evidence for a structural model in which phosphorylated serine repeats $(pSX)_4$ complex with divalent cations Ca^{2+} and Mg^{2+} to form rigid nanocrystalline β-sheet structures in caddisfly silk. ^{13}C NMR data suggests that both phosphorylated serine and neighboring valine residues exist in a β-sheet secondary structure conformation while glycine and leucine residues common in GGX repeats likely reside in random coil conformations. Additionally, ^{31}P chemical shift anisotropy (CSA) analysis indicates that the phosphates on phosphoserine residues are doubly ionized, and are charge-stabilized by divalent cations. Positively charged arginine side chains also likely play a role in charge stabilization. Finally, WAXD results finds that the silk is at least 7-8% crystalline, with β-sheet inter-plane spacings of 3.7 and 4.5 Å.

2.2 Introduction

Caddisfly larvae (order Trichoptera) spin silk under water. In addition to building nets for food capture, the larvae use the silk to stitch together debris into elaborate structures for protection and camouflage (Figure 2.1A, 2.1B) [1, 2, 3, 4]. The ability of the silk to adhere to virtually any surface underwater has attracted researchers, as it could serve as a model for new biocompatible water-borne adhesives [5, 6]. Caddisfly silk is not well characterized at the molecular level, however its close relation to the well-studied domesticated silkworm moth (order Lepidoptera) provides a starting point for understanding secondary and tertiary hierarchical structures. The silks produced by the two orders are homologous. On the protein level, both silkworm and caddisfly fibers are composed of heavy chain fibroin (H-fibroin, 250-500 kDa) and light-chain fibroin (L-fibroin, 25 kDa), which are covalently linked in a 1:1 molar ratio through a disulfide bridge [7, 8, 9]. While very different from the sticky sericin layer that coats silkworm silk, caddisfly silk also contains a carbohydrate-rich peripheral layer engulfing the fiber [10]. Additional similarities are observed at the amino acid level. Partial H-fibroin primary protein sequences have been determined for both orders, revealing common repetitive stretches including GPXGX, GGX and $(SX)_n$ motifs [11, 8, 9]. Repeat regions identified in the partial H-fibroin sequence for the caddisfly species *L. decipiens* have been color-coded and aligned in Figure 2.2 to illustrate important protein motifs. The prevalent $(SX)_4$ repeats shown in red and the GGX regions in blue are found in species of each of the three suborders of trichoptera [12]. Comparison of the primary protein sequences reveals that glycine is the most commonly found residue in both fibers, and serine is the second and third most common residue in caddisfly and silkworm silks, respectively [10, 12]. Alanine however, a dominant residue in silkworm silks, is poorly represented in caddisfly

silk. This contrast is intriguing because alanine plays an important structural role in silkworm and spider silks [13, 14, 15].

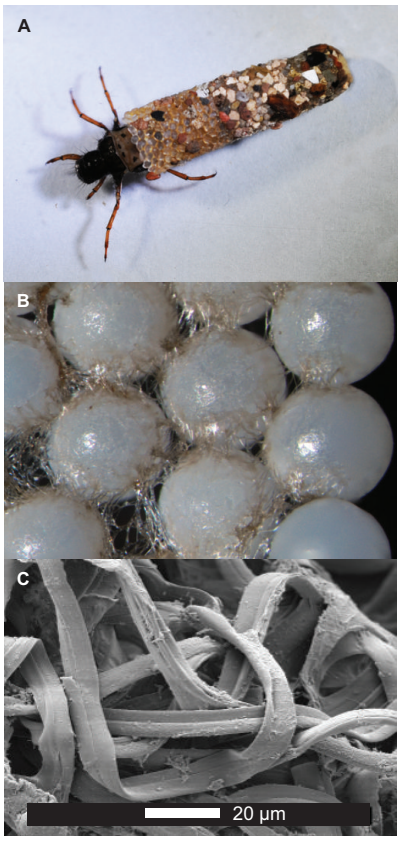

Figure 2.1: (A) A caddisfly larva from the species *H. consimilis* has stitched together debris under water using adhesive silk fibers. (B) Detailed image of silk attached to 0.5 mm zirconia spheres. (C) SEM micrograph of caddisfly silk.

Another interesting difference is that caddisfly silks contain a substantial amount of phosphorus, an element that is effectively absent from silkworm silks [5, 12, 16]. In addition to estimating that nearly 60% of serine residues in caddisfly silk are phosphorylated, a study by Stewart et al. [12] showed that the phosphorylation appears to be localized to the highly conserved $(SX)_4$ repeat motifs where X residues are typically hydrophobic or basic. In particular, each alternating serine residue in the D-repeat seen in Figure 2.2 is phosphorylated [12]. The introduction of multiple negatively charged phosphates to $(SX)_4$ repeat motifs implies an electrostatic-driven

structural arrangement. The additional observation that caddisfly silk is relatively high in divalent cations Ca^{2+} and Mg^{2+} led to a proposed model in which alternating phosphorylated serine residues interact with divalent cations to form rigid β-sheet structures in caddisfly silk [12].

Figure 2.2: Partial amino acid sequences of Heavy-chain Fibroin protein from the caddisfly species *Limnephilus decipiens*. The H-fibroin sequence is continuous, however repeat regions are aligned for convenience. Phosphorylated $(SX)_4$ motifs found in the D-repeat shown in red are proposed to exist in calcium-phosphoserine sheets. In support of the sheet model, proline residues often found in β-turn secondary structures appear shortly after every $(SX)_4$ region. The sequence for the H-fibroin protein is taken from GenBank [AB214509].

There are many arguments in favor of phosphorylated $(SX)_4$ motifs forming nanocrystalline β-sheets in caddisfly silks [12, 17]. First, poly(A) and poly(GA) repeat regions are absent from the caddisfly H-fibroin sequence. These motifs are primarily responsible for the impressive mechanical properties of terrestrial silks because they form three-dimensional crystalline β-sheet nanostructures within the fibers [18, 13, 19]. Previous X-ray diffraction studies on caddisfly silk fibers suggest a significant crystalline component [10, 20, 21], therefore some repeat regions other than poly(A) or poly(GA) must be responsible for this hierarchical structure. Second, serine residues in the highly prevalent $(SX)_4$ repeat motifs are heavily phosphorylated. The incorporation of multiple localized negative charges may explain why the silk contains high levels of calcium and magnesium cations [12]. Third, the H-fibroin sequence shows

a conserved proline-glycine motif (underlined and bolded in Figure 2.2) shortly after every $(SX)_4$ motif [8, 9]. Prolines are often found at the beginning and end of β-strands, and are prevalent in β-turn secondary structures in other well-characterized silks [22]. The prevalence and conserved location of proline residues in the caddisfly silk H-fibroin sequence could be explained if $(SX)_4$ repeat regions formed β-sheet nanostructures. Additionally, valine and isoleucine are often found as the X residue in $(SX)_4$ motifs. As hydrophobic beta-branched amino acids, the bulkiness of valine and isoleucine near the peptide backbone significantly favors a β-sheet environment as opposed to α-helical secondary structures [23, 24]. Computer modeling of the motif of interest also identified a significant boost in strength when the serines are phosphorylated and when calcium cations are present [25]. The introduction of calcium to multi-phosphorylated peptides has been previously shown to induce β-sheet conformations; this mechanism may be relevant to the formation of neurofilament tangles in Alzheimer's disease patients [26, 27, 28]. In caddisfly silk, this molecular arrangement possibly serves as a structural replacement for sheet-forming poly(A) and poly(GA) repeats in spider and silkworm silks. In this study, we put this hypothesis to test by using solid-state NMR and wide angle X-ray diffraction (WAXD) to probe the molecular structure of caddisfly larval silk.

2.3 Materials and Methods

Materials In the late spring, fifth instar larvae of the species *Hesperophylax consimilis* were collected from the upper Red Butte creek in Salt Lake county Utah. The larvae were transported in ice water back to the lab. The animals were kept in 11°C dechlorinated tap water which was filtered and bubbled.

For use as a larval food source, yeast were grown in yeast minimal media (10 g/L ^{13}C-glucose, 0.9 g/L yeast nitrogen base without amino acids, and 2.5 g/L ^{15}N

ammonium sulfate). Yeast cells were collected by centrifugation, dried, and used to make food pellets. Food pellets were prepared using 40mg/ml of 300 bloom gelatin and 300mg/ml of dry yeast (^{13}C, ^{15}N) in DI water. This mixture was heated to 100°C and cooled on ice. The resultant food pellet was insoluble in the chilled aquarium water, an important requirement. Fifty caddisfly larvae were removed from their cases and provided $1mm^3$ blocks of polytetrafluoroethylene (PTFE) as construction material. After 3 days the larvae rebuilt their cases with the PTFE. They were removed from their PTFE cases and placed back into their original stone cases and allowed to feed on the previously prepared food pellet. After three days, the larvae were once again removed from their cases, washed in dechlorinated tap water, introduced into a second aquarium with clean dechlorinated tap water, provided PTFE, and allowed to build for 3 days. The PTFE cases were removed and set aside for future use. The same larvae were placed back in their cases and allowed to feed, starting the cycle over again. This was repeated an additional 9 times resulting in 10 harvesting of PTFE cases. With a pair of fine forceps, the ^{13}C, ^{15}N enriched silk was carefully separated from the PTFE, rinsed in dechlorinated tap water, and stored in tap water at 11°C until further use. For all experiments conducted on naturally-abundant silk, identical harvesting techniques were used except fish food pellets were used for feeding.

Phosphoserine salts were prepared by dissolving L-O-Phosphoserine (Sigma Aldrich) in ultrapure water (EMD), adding equimolar amounts of cation-chloride salts, and adjusting the solution to pH = 7 with NaOH. The solvent was slowly evaporated at room temperature overnight.

Scanning Electron Microscopy. The silk sample was removed from the buffer solution and mounted onto the sample holder with the aid of double-sided carbon tape. It was then Au/Pd coated in a Denton vacuum sputter coater desk II for 180 seconds at a deposition rate of 5 nm/min using a current of 20 milliamps under a

pressure of 200 millitorr. This results in a deposition of approximately 15 nm to prevent charging the sample. The SEM was performed using a XL30 Environmental SEM-FEG built by FEI. The secondary electron (SE) detector was used for imaging. Measurements were collected under a vacuum pressure of less than 9 x 10^{-5} mbar and with a beam current of 5.00 kV. The beam diameter at the sample was 21 Angstroms with a current of 98 pA.

Solid-State NMR. All ^{13}C solid-state NMR experiments were conducted on a 400 MHz Varian Wide-Bore spectrometer equipped with a 3.2 mm triple-resonance MAS probe. The enriched silk was originally packed in its natural (hydrated) environment in a 3.2 mm zirconium rotor fitted with a Torlon cap and drive tip. The sample was spun at the magic angle at 8.5 kHz, a spinning speed chosen such that the carbonyl spinning side band would not overlap with any glycosidic resonances near 75 ppm. ^{13}C chemical shifts were referenced externally to TMS at 0 ppm by setting the downfield adamantane resonance to 38.56 ppm. ^{1}H $\rightarrow$ ^{13}C Cross-Polarization (CP) conditions were matched by using a square 70 kHz contact pulse on the ^{13}C channel, which was matched to the -1 Hartmann-Hahn side band of a 1 ms ramped ($\sim$15%) CP spin-lock pulse on the proton channel. Two-pulse phase-modulated[29] (TPPM) proton decoupling at 100 kHz was applied during acquisition using a 7° phase angle, and a 5 second relaxation delay separated each of 4096 transients. Direct Detection under Magic Angle Spinning (DD-MAS) experiments were performed using a 3.5 μs $\pi/2$ pulse on the ^{13}C channel, and 20,480 transients were averaged. A fast (1 second) relaxation delay was chosen to highlight resonances with fast relaxation properties. 100 kHz TPPM proton decoupling was applied during acquisition.

Two dimensional ^{13}C - ^{13}C correlation experiments were performed using the Dipolar Assisted Rotational Resonance (DARR) experiment [30, 31]. Assisted transfer of magnetization was established using a continuous wave (CW) radio-frequency pulse

on the ^{1}H channel for 50 ms at the second rotational resonance condition. The acquisition parameters used were 64 scan averages, 2 second recycle delay, 50 kHz spectral width and 1024 complex points collected in the direct dimension, and 25 kHz spectral width and 64 complex points collected in the indirect dimension. 100 kHz TPPM decoupling was applied to the ^{1}H channel during acquisition.

The ^{1}H $\rightarrow$ ^{31}P - ^{13}C double cross-polarization (DCP) experiment was conducted on dry caddisfly silk with a 3.2 mm Varian triple resonance MAS probe [32, 33]. The sample was spun at a slow speed (5 kHz MAS) to favor the zero-quantum transition during the second polarization transfer step [34]. The highly sensitive DCP conditions were carefully calibrated using crystalline L-O-Phosphoserine (Sigma Aldrich). The experimental parameters for the initial ^{1}H $\rightarrow$ ^{31}P CP step were a 3 μs ^{1}H $\pi/2$ pulse, a 1 ms ramped ^{1}H spin-lock pulse centered at 80 kHz radio frequency (rf) field strength, and a ^{31}P square contact pulse matched to the -1 spinning side band of the Hartmann-Hahn profile. Then ^{31}P transverse magnetization was transferred to ^{13}C using a 5 ms ramped spin-lock pulse centered at 80 kHz RF field strength on the ^{31}P channel, and a square contact pulse on the ^{13}C channel matched to the -2 side band of the Hartmann-Hahn profile, during which a 133 kHz continuous wave RF field was applied to the proton channel to ensure that all ^{13}C transverse magnetization was obtained only through nearby ^{31}P nuclei. Two-pulse phase modulated (TPPM) decoupling at 100 kHz RF field strength and 7° phase angle was applied to the ^{1}H channel during acquisition. Acquisition parameters were 100 kHz spectral width, 2048 complex points, 65,536 scan averages and a 1 second recycle delay.

^{31}P solid-state NMR experiments were conducted on a 400 MHz Bruker Avance III instrument equipped with a 4 mm double resonance MAS probe. ^{31}P chemical shifts were referenced externally to crystalline ammonium phosphate at 0.8 ppm. All

samples were spun at the magic angle at 4 kHz. Typical $^{1}H \rightarrow {}^{31}P$ CP experiments were performed with a 2 ms CP contact time, 20 ms acquisition time and a 5 second relaxation delay. Static CP spectra were observed using a Hahn spin-echo refocusing period of 20 μs. All experiments were collected using 80 kHz TPPM proton decoupling during acquisition. Data Fitting: All ^{31}P chemical shift anisotropy (CSA) parameters were extracted from the spectra according to the Herzfeld-Berger [35] convention using DMFIT software [36].

Wide Angle X-ray Diffraction. Caddisfly larval silk was mounted onto a cardboard washer for WAXD measurements using a small amount of super glue at either end. WAXD measurements were collected using the synchrotron x-ray research facility at the Advanced Photon Source (APS) at Argonne National Laboratory. The BioCARS beamline 14 BM-C (bending magnet) was used with an approximate x-ray wavelength of 0.9787 angstroms and fixed energy of 12.668 keV. The detector used was the ADSC Quantum-315 with a beam size of approximately 130 x 340 μm (FWHM) . The fiber samples were aligned parallel to the axis of the beamstop with a sample to detector distance of 300 mm and a beamstop to detector distance of 50 mm. Five trials with an exposure time of 60 seconds each were collected per sample with 5 similar backgrounds and then background subtracted to remove air scattering. Cerium dioxide (CeO_2) was used as a calibrant in the FIT2D x-ray processing software to analyze the 2D diffraction patterns.

2.4 Results and Discussion

Caddisfly larval silk from the species *Hesperophylax consimilis* was studied using solid-state NMR and wide angle X-ray diffraction, and all experimental results refer to data collected on this species. *H. consimilis* larvae utilize silk to construct protective casings from available debris, as seen in Figure 2.1A and 2.1B. Unlike the cylindrical

silk fibers produced by spiders, caddisfly fibers appear in the SEM micrograph as a fusion of two fibers into a flat ribbon (Figure 2.1C). The protein-based biopolymer is composed of both H and L-fibroin protein. The H-fibroin sequence is not described in the literature for the species *H. consimilis*, thus the partial H-fibroin sequence for the closely related species *L. decipiens* is shown in Figure 2.2. Repetitive $(SX)_4$ motifs illustrated in Figure 2.2 have been identified in multiple caddisfly species through gene sequencing,[8, 9] and tandem Mass-Spectrometry data on silk from *H. consimilis* larvae confirm that identical repeat sequences seen in Figure 2.2 are present in the *H. consimilis* H-fibroin protein [12]. As previously mentioned, one striking observation is the apparent lack of poly(A) and poly(GA) repeat motifs found in silkworm H-fibroin sequences. Instead, heavily phosphorylated runs of $(SX)_4$ highlighted in red are a dominant repetitive motif found in caddisfly silk.

Solid-State NMR on Caddisfly Silk. In order to investigate the molecular structure of caddisfly silk and any links to the primary protein sequence, both ^{13}C and ^{31}P solid-state NMR techniques were utilized. $^{1}H \rightarrow {}^{13}C$ CP-MAS spectra for naturally-abundant caddisfly silk exhibits relatively poor signal to noise, as seen in Figure 2.3, thus advanced analysis of the silk is difficult to impossible without isotopic enrichment. Caddisfly larvae were fed with (^{13}C, ^{15}N) yeast, and the resulting silk was collected and analyzed. The signal to noise ratios observed for the naturally-abundant and enriched silks were used to estimate the amount of isotopic enrichment at 6 to 8% (Supplemental Figure 2). ^{13}C NMR data from isotopically enriched caddisfly silk are shown in Figure 2.4. The data was collected with the silk hydrated in the same water from which it was obtained, therefore preserving its native environment. Many overlapping resonances make interpretation and chemical shift assignments challenging, but some information can nevertheless be extracted from the $^{1}H \rightarrow {}^{13}C$ CP-MAS and DD-MAS spectra in Figure 2.4. The assortment of resonances near 75 ppm and

105 ppm are characteristic of carbohydrates, and are assigned to a carbohydrate-rich surface coating of the silk. Consistent with this assignment, TEM micrograph images obtained from histological sections of the fibers show a clear peripheral carbohydrate layer [10]. Spider silks are also thought to have peripheral surface coatings, but the proposed lipid and/or carbohydrate layer of spider silk is only 10-100 nm thick [37]. This makes the overall mole percentage small and therefore hard to detect using solid-state NMR. While the surface of spider silk fibers is smooth, atomic force micrographs of caddisfly silks show small (∼150 nm) spherical subunits [25, 17]. The lumpy topography of the caddisfly silk surface provides additional contact area for adhering to surfaces due to an increased area-to-volume ratio. The contrast between the CP and DD-MAS experiments in Figure 2.4 is useful because resonances that exist in a mobile, water-solvated environment will typically show short T_1 relaxation times relative to rigid regions. Hydrated residues therefore exhibit enhanced signal intensity in the DD-MAS spectrum when using short (1 second) recycle times. Additionally, sharpened signals are observed for hydrated residues due to the longer T_2 relaxation times. The contrast between unmodified and phosphorylated serine Cβ resonances at 62 and 64 ppm, respectively, is a very signifiant result. When comparing the $^{1}H \rightarrow {}^{13}C$ CP-MAS spectrum to the DD-MAS spectrum, one notices that the degree of sharpening is significantly more pronounced for unmodified serine Cβ, suggesting higher mobility. This supports the idea that phosphorylated serine residues reside in nanocrystalline β-sheet structures while unmodified serine residues are found in less rigid secondary structures. This is a commonly observed phenomenon when studying wet spider silks to show differences between rigid and mobile motifs. In spider silks, the alanine Cβ resonance at 21 ppm associated with rigid poly(A) β-sheet regions is strongly observed during CP but has significantly reduced signal when using DD-MAS techniques with a fast relaxation delay because of its long T_1 relaxation time

[38, 39]. Conversely, alanine in a disordered helical conformation exhibits short T_1 and long T_2 relaxation times. As a result, narrowed line widths are observed for the mobile alanine environments in the DD-MAS experiment on wet spider silks.

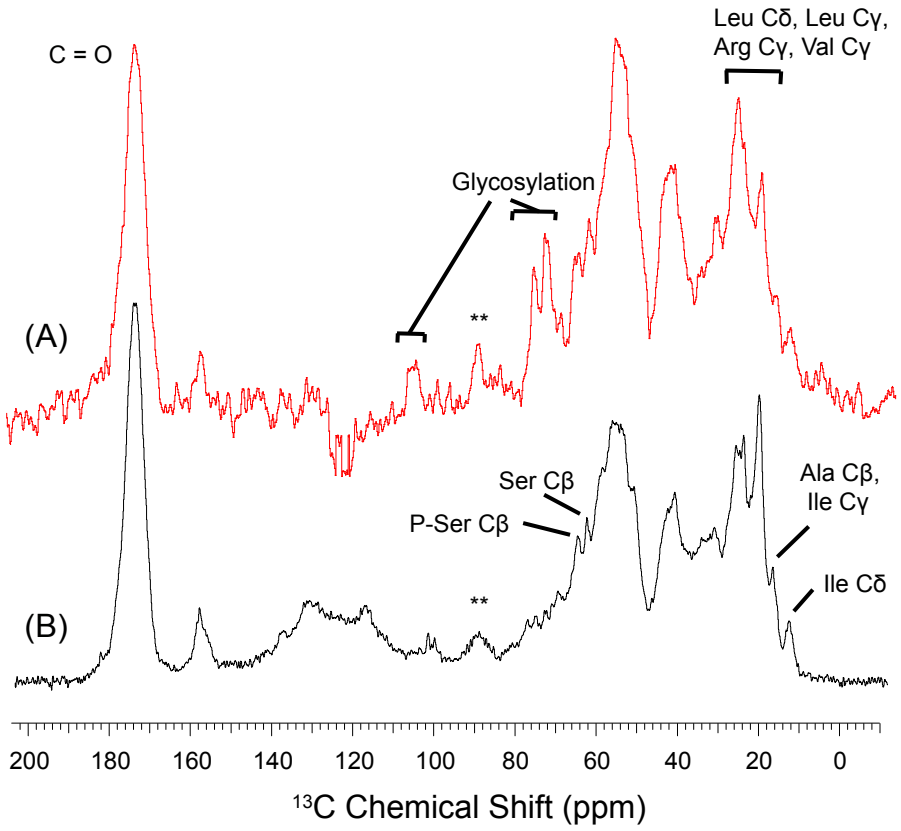

Figure 2.3: $^{1}H \rightarrow {}^{13}C$ CPMAS spectra of hydrated natural caddisfly silk (A) is compared to isotopically enriched silk (B). A substantial background was observed for the natural sample, and the apparent dip near 130 ppm seen in (A) is an artifact of background subtraction. Carbonyl spinning side bands are marked with a double asterisk.

Interpretation of the one-dimensional (1D) solid-state NMR data is limited because of the many overlapping resonances. In order to extract accurate chemical shifts for specific amino acid resonances in caddisfly silk, two dimensional (2D) ^{13}C - ^{13}C correlation NMR was necessary. The chemical shifts of amino acid backbone and side-chain resonances are very sensitive to secondary structure, and can be used to identify helical, turn and β-sheet components of a protein [40, 41, 42, 43, 44]. Figure

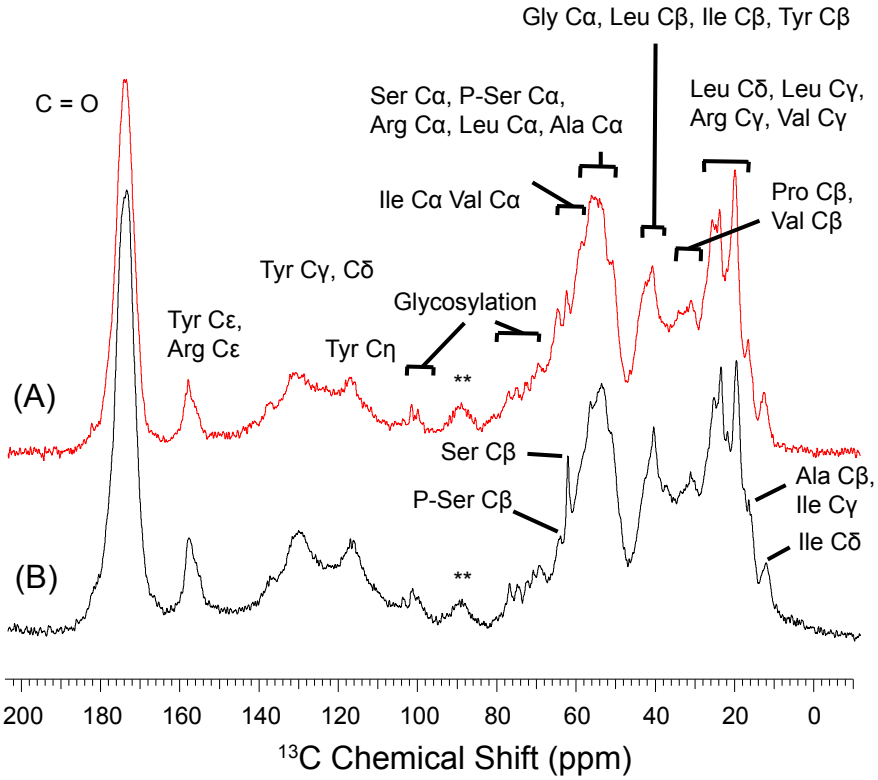

Figure 2.4: ^{13}C NMR of isotopically enriched caddisfly silk from the species *H. consimilis* in its natural (water-hydrated) environment. The two spectra shown are (A): ^{1}H $\rightarrow$ ^{13}C CP-MAS NMR using a 1 ms CP contact time and 4096 scan averages, and (B): ^{13}C DD-MAS NMR using fast (1 second) repetition and 20,480 scan averages. Samples were spun at 8500 Hz MAS. Approximate assignments for common amino acids are indicated, and the carbonyl spinning side bands are marked with a double asterisks.

2.5 shows expanded regions of a ^{13}C - ^{13}C Dipolar Assisted Rotational Resonance (DARR) experiment using 50 ms mixing time. Off-diagonal cross peaks resulting from magnetization exchange between ^{13}C nuclei can be observed. The strong signals observed from glycine, valine, leucine and isoleucine residues are assigned and are compared to known chemical shifts from the literature (Table 2.1). The glycine Cα-CO correlation seen in Figure 2.5A is fairly strong, allowing for accurate chemical shift measurements. Both chemical shift values for glycine Cα and CO agree nearly perfectly with an average random coil conformation, suggesting that a large range of

backbone dihedral angles are available such that glycine does not adopt any identifiable secondary structure in caddisfly silk. Leucine residues are also often seen in GGX repeats, and assigned chemical shifts again agree with a random coil conformation. The data does not necessarily mean that there is no secondary structure in this region. Fast dynamic averaging may play a role, and the chemical shifts of many helical conformations overlap with random coil shifts. Interestingly, glycine-heavy GGX motifs are well known for forming 3_1-helical structures in spider and silkworm silks[45, 46, 47]. 3_1-helical structures may indeed be prevalent in caddisfly fibers, but the current NMR data better supports a random coil configuration or very loose helical structure. Conversely, the ^{13}C chemical shifts extracted for valine resonances prevalent in $(SX)_4$ motifs seem to agree with β-sheet secondary structure. Fortunately, the off-diagonal cross peaks observed for valine are sufficiently strong even though it only accounts for approximately 4% of the total amino acid content [12].

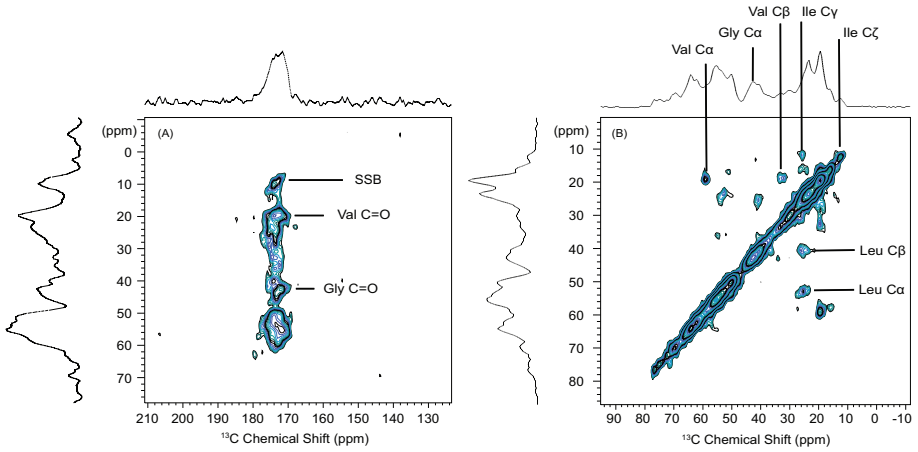

Figure 2.5: 2D ^{13}C - ^{13}C DARR experiment at 50 ms mixing time on isotopically enriched caddisfly silk. (A) shows the expanded carbonyl cross peaks, while (B) shows the expanded aliphatic region. At this mixing time, cross peaks from large hydrophobic residues are dominant. The ^{13}C chemical shifts extracted from this DARR experiment are tabulated in Table 2.1.

Although expected to make up a large percentage (∼15%) of the total amino acid content in caddisfly silk, the chemical shifts for serine and phosphoserine cannot

confidently be extracted from the 2D ^{13}C-^{13}C correlation NMR experiment. This is possibly a result of inconsistent isotope uptake and/or metabolism between various amino acids; it is clear from Figure 2.3 that isotopic enrichment is not the same for all amino acids. Selective enrichment of amino acids in spider silks has been challenging even when only a single enriched amino acid is provided, thus we cannot expect consistent isotopic uptake when feeding labeled yeast extract to the caddisfly larvae [48]. Confidently identifying phosphoserine chemical shifts would be exceptionally useful towards supporting or opposing the proposed model. We therefore used a ^{1}H $\rightarrow$ ^{31}P - ^{13}C double cross polarization (DCP) experiment to selectively observe ^{13}C nuclei that are in dipolar contact with ^{31}P nuclei. Figure 2.6 compares ^{13}C NMR spectra of dried caddisfly silk under standard CP conditions (red) and under DCP conditions (black) at 5 kHz MAS. The silk in this experiment had been dried and therefore no longer in its natural environment. Nonetheless, ^{13}C NMR data (Supplemental Figure 3) suggests that the silk is structurally identical before dehydration and after re-hydration, thus no structural changes occur upon dehydration. The DCP experiment confirms that serine is in fact phosphorylated, and selects the phosphoserine Cα and Cβ chemical shifts. The values for phosphoserine Cα and Cβ are listed in Table 2.1. Comparison to chemical shifts listed in the literature reveals that the caddisfly silk phosphoserine Cα resonance is shifted upfield and Cβ downfield with respect to random coil. This observed trend is indicative of a β-sheet secondary structure, therefore the data is in agreement with a sheet-based model for $(pSX)_4$ motifs in caddisfly silk.

The DCP experiment revealed additional useful information towards understanding the molecular structure of caddisfly silk. Arginine side chain resonances, especially those closer to the positively charged guanidinium group, are also observed in the DCP experiment. This suggests that arginine residues play a significant role in

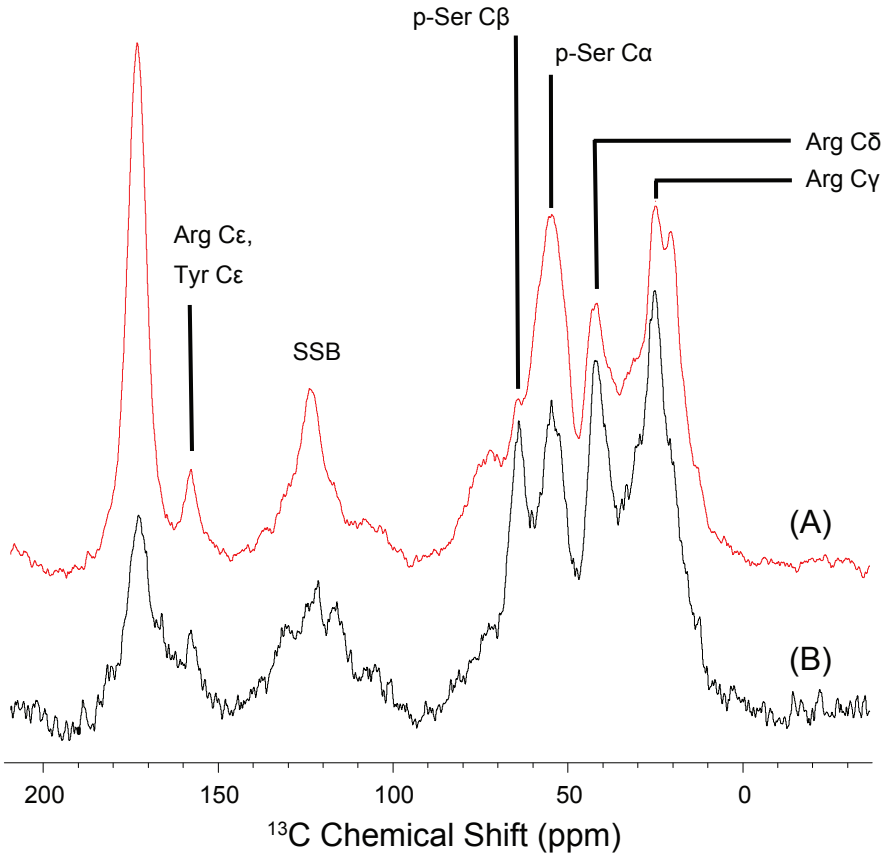

Figure 2.6: $^{1}H \rightarrow {}^{13}C$ CP-MAS NMR at 5 kHz of dry caddisfly silk (A) is compared to a $^{1}H \rightarrow {}^{31}P \rightarrow {}^{13}C$ Double Cross-Polarization (DCP) experiment (B). Only ^{13}C nuclei that are in dipolar contact with ^{31}P nuclei should have observed signal. The ^{13}C chemical shifts extracted for pSer Cα and Cβ indicate that phosphoserine exists in a β-sheet conformation within caddisfly silk.

stabilizing negatively charged phosphate groups in caddisfly silk. While the arginine assignments listed in Table 2.1 align with random coil conformations, it should be noted that distant side chain resonances are not very sensitive to secondary structure and therefore should not be used here to suggest local environments [42]. The DCP experiment also suggests that tyrosine may be phosphorylated in caddisfly silks. Secondary structure motifs involving phosphotyrosine may be prevalent in caddisfly silks, but selective isotopic labeling of tyrosine may be necessary before a full investigation would be possible.

Table 2.1: ^{13}C chemical shifts observed from caddisfly silk are compared to shifts from model polypeptides with known secondary structures [40, 41, 42, 43, 44]. Caddisfly silk chemical shifts were extracted from either the ^{13}C - ^{13}C DARR experiment (Figure 2.6) or the DCP experiment (Figure 2.7). Only assignments that could be made with any confidence are listed. All values are relative to TMS at 0 ppm.

Residue	Caddisfly silk	β-sheet	α-helix	random coil
Gly C=O	173.5	171.8	174.9	173.2
Gly Cα	43.3	42.0	46.0	43.4
Ile C=O		172.7	174.9	174.7
Ile Cα	58	57.8	63.9	59.4
Ile Cβ		39.4	34.8	37.1
Ile Cγ1	16			15.7
Ile Cγ2				25.5
Ile Cδ	12.1			11.2
Leu C=O		170.3	175.7	175.9
Leu Cα	53.8	50.5	55.7	53.4
Leu Cβ	40.1	43.3	39.5	40.7
Ser C=O		172.9	174.6	171.5
Ser Cα	56.3	55.2	59.2	56.6
Ser Cβ	62	63.1	60.7	62.1
p-Ser C=O				174.2
p-Ser Cα	54.8			56.8
p-Ser Cβ	64.3			63.9
Val C=O	173.7	171.8	174.9	174.6
Val Cα	59	58.4	65.5	60.5
Val Cβ	32.7	32.4	28.7	31.2
Arg Cγ	25.1			25.1
Arg Cδ	41.7			41.7
Arg Cϵ	157 - 159			157.9

$^{1}H \rightarrow {}^{31}P$ cross-polarization NMR data also provided important structural information about caddisfly silk. In liquid state NMR, molecular motion is sufficiently fast to average out chemical shielding information. However in solid samples where molecular motion is limited, the chemical shielding tensor is not averaged over the spatial dimensions and can therefore yield important information on the local environment about a nucleus. Understanding the phosphorus environment in caddisfly silk would be substantially helpful towards characterizing the phosphorylated $(SX)_4$ motifs. Here we use solid-state NMR techniques to extract environment-dependent Chemical Shift Anisotropy (CSA) information for the ^{31}P nuclei found in caddisfly silk. Using $^{1}H \rightarrow {}^{31}P$ cross-polarization NMR with and without magic angle spinning, CSA parameters were extracted from caddisfly silk and from four preparations of phosphorylated serine (Figure 2.7 and Table 2.2) using the Herzfeld-Berger convention [35]. The data are shown in blue, and the resulting fits in red. The first and most evident finding is that caddisfly silk observes a negative skew parameter; the CSA is asymmetric favoring the right. This is consistent with trends observed by C. Gardiennet et al. in which the phosphate on L-O-Phosphoserine is doubly ionized [49]. This point is exemplified when comparing the caddisfly spectra to the CSA pattern of protonated L-phosphoserine from Sigma Aldrich. The presence of cations near the phosphorus resonance can also affect the CSA pattern [50], so deprotonated phosphoserine was prepared in the presence of calcium, magnesium and sodium cations. Extracted CSA parameters, summarized in Table 2.2, reveal that divalent cations calcium and magnesium behave virtually identically in terms of their interaction with phosphoserine. Sodium appears to significantly increases the σ_{33} parameter and in turn the $\Delta\sigma$ and span values. Additionally, the isotropic ^{31}P chemical shift moves downfield in the presence of sodium when compared to the spectra with calcium or magnesium. Molecular level reasoning for the observed differences are not

clear; necessary computer simulations of the CSA have not yet been performed. Nevertheless, comparison of all determined CSA parameters shows that the phosphorus environment of caddisfly silk is most similar to that of phosphoserine in the presence of divalent cations. This observation is consistent with $(pSX)_4$ repeat motifs in divalent cation-phosphoserine β-sheet structures.

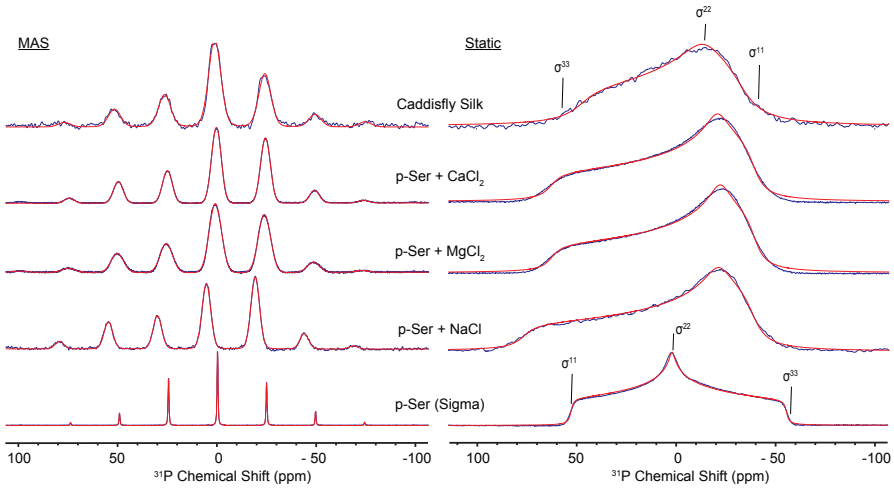

Figure 2.7: $^{1}H \rightarrow {}^{31}P$ solid-state NMR of caddisfly silk and of 4 different preparations of L-Phosphoserine. Chemical Shift Anisotropy parameters were extracted from both static and MAS spectra at 4 kHz spinning speed, and are summarized in Table 2.2. The data are shown in blue, and the resulting fits in red. By convention, σ^{11} and σ^{33} correspond to the directions with the least and most shielding, respectively. All spectra were fit to a single component powder pattern based on the Herzfeld Berger convention using DMFIT software [35, 36].

WAXD on Caddisfly Silk. The 2D wide-angle X-ray diffraction (WAXD) pattern on a vertically aligned caddisfly silk bundle is seen in Figure 2.8. The blue diffraction band shows increased intensity along the equatorial plane, an observation consistent with β-sheet nanocrystals aligned parallel to the fiber axis [51, 52]. Although not as intense as the diffraction patterns observed for spider and silkworm silks, which can be greater than 25% crystalline [52, 53, 54], the observed pattern for caddisfly silk suggests the presence of a significant crystalline component. The percent of silk fibroin protein in a crystalline conformation was estimated from the data, and

Table 2.2: ^{31}P Chemical Shift Anisotropy parameters have been extracted from each spectra in Figure 2.7 using DMFIT software [36]. The negative skew parameter is indicative of a phosphate carrying a -2 charge. σ^{33} parameter changes significantly for monovalent versus divalent cations. The CSA parameters obtained from caddisfly silk are most similar to those from phosphoserine in complex with divalent cations. Using the Herzfeld Berger convention, the span (span = The σ^{11} - The σ^{33}) describes the breadth of the spectrum, while the skew (skew = 3(σ^{22} - σ^{iso})/span) describes the axial symmetry of the CSA tensor [35]

Sample	Δ (ppm)	η	σ^{11} (ppm)	σ^{22} (ppm)	σ^{33} (ppm)	span (ppm)	skew	σ^{iso} (ppm)
Caddisfly, Static	50.01	0.39	-32.88	-13.48	51.84	84.72	-0.54	1.83
Caddisfly, MAS	58.36	0.54	-43.38	-11.9	59.89	103.27	-0.39	1.54
P-Ser + $CaCl_2$, Static	62.3	0.29	-39.11	-20.98	63.4	102.51	-0.65	1.10
P-Ser + $CaCl_2$, MAS	65.05	0.4	-44.91	-18.59	65.83	110.74	-0.52	0.78
P-Ser + $MgCl_2$, Static	62.26	0.28	-39.54	-22.23	62.51	102.05	-0.66	0.25
P-Ser + $MgCl_2$, MAS	64.34	0.38	-44.08	-19.4	64.77	108.85	-0.55	0.43
P-Ser + 2NaCl, Static	71.03	0.24	-38.64	-21.35	76.56	115.2	-0.7	5.52
P-Ser + 2NaCl, MAS	71.59	0.4	-44.41	-15.9	77.23	121.64	-0.53	5.64
P-Serine, Static	-55.35	0.92	52.86	2.02	-55.58	108.44	0.06	-0.23
P-Serine, MAS	-56.54	0.92	54.08	2.29	-56.63	110.71	0.06	-0.09

inter-plane distances were extracted. Radial integration finds that repeat spacings of 3.7 and 4.5 angstroms are observed in increased intensity along the equatorial plane (Figure 2.9). The peak positions were obtained by using four Gaussian fits, one at 3.7 angstroms, one at 4.5 angstroms and 2 broader Gaussians for the remainder of the data. If the repetitive unit cell of the crystalline region is orthorhombic, as assumed for spider and silkworm silks, we can assign the 4.5 angstrom reflection to inter-sheet spacings because it is analogous to the reflections observed from poly(A) nanocrystalline β-sheet regions in both spider and silkworm silks [51, 52, 55]. An additional equatorial reflection at 3.7 angstroms is seen in the caddisfly fiber diffraction pattern, however we cannot confidently identify its source. Interestingly, unpublished WAXD results from black widow egg sac fibers show a similar reflection near 3.7 angstroms that also has not been assigned. The crystallite unit in caddisfly silk seems to be

vastly different than those observed in other biological fibers, thus we are not entirely surprised that we cannot yet fully interpret and assign the diffraction pattern. We have current efforts to collect better, higher-resolution diffraction data on caddisfly silk, and are working on solving the dimensions of the repetitive unit cell. Nevertheless, in this present study it is sufficient to state that the equatorial reflections clearly demonstrate that caddisfly silk contains crystalline regions oriented with respect to the fiber axis.

The amount of crystallinity was estimated in two different ways. First, radial integration of 15 degrees on either side of the equator, the region assumed to be the component relating to crystallinity, is compared to radial integration occurring at 45 degrees from the equator and the meridian integration. Subtracting the total integration of the amorphous halo from the equatorial integration gives the component thought to be crystalline, yielding approximately 7-8% crystallinity (Supplemental Figure 1). Secondly, integration along an angle of 45 degrees, the equator, and the meridian yields differing intensities of the shoulder at 3.7 angstroms. The equatorial integration was selected to determine the peak position based on maximum intensity. A Gaussian fitting protocol was used to determine peak positions and intensity integrations iteratively until there were no changes. The peak positions were then held constant and the remaining integration areas were fit. These results show 7% crystallinity based on integration of the full WAXD pattern (Supplemental Figure 1). We note here that each silk fiber in the bundle could not be perfectly aligned vertically along the beam axis, thus 7-8% crystallinity is likely a low estimate; previous WAXD results estimated 12% crystallinity for caddisfly silk from the species *S. marmorata* [21]. Regardless, the absence of poly(A) or poly(GA) motifs from the H-fibroin primary protein sequence in caddisfly silk means that the observed crystallinity must come from some other hierarchical structure.

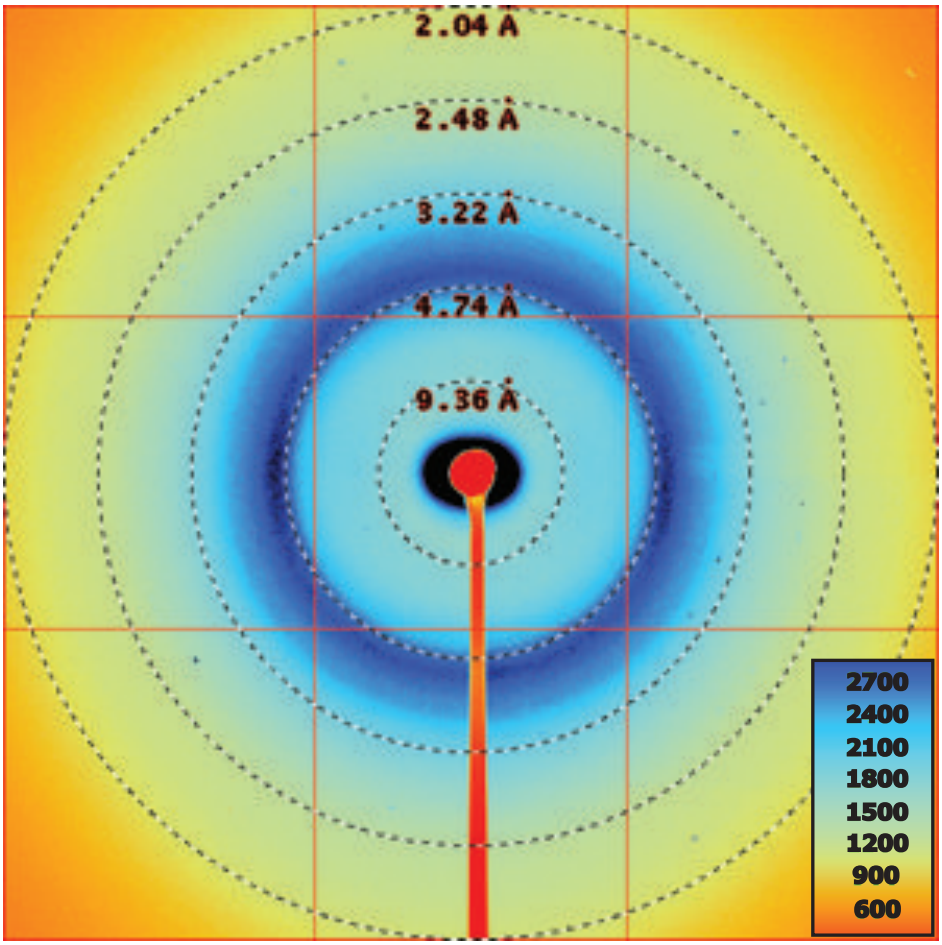

Figure 2.8: 2D Wide angle x-ray diffraction pattern of caddisfly silk recorded at 298 K. A beamstop, seen as a thick red area, was used to ensure that only scattered x-rays hit the detector. The beam stop and fiber axis are parallel (vertical). The sample was 300 mm from the detector, which was composed of 9 physically separated CCD panels. X-ray wavelength: 0.9787 Angstroms. The data seen is a result of five trial averages with an exposure time of 60 seconds each, after subtraction of 5 similar backgrounds.

Figure 2.10 shows an illustration of the proposed structural motif, in which negatively charged phosphorylated serine residues from $(pSX)_4$ repeat regions complex with divalent cations to form β-sheet structures in caddisfly silk [12]. A 2-dimensional sheet is formed when the repeats extend both above and below the illustration in Figure 2.10, stabilized by hydrophobic Van der Waals interactions between the larger valine and isoleucine side chains. If one additionally imagines standard backbone

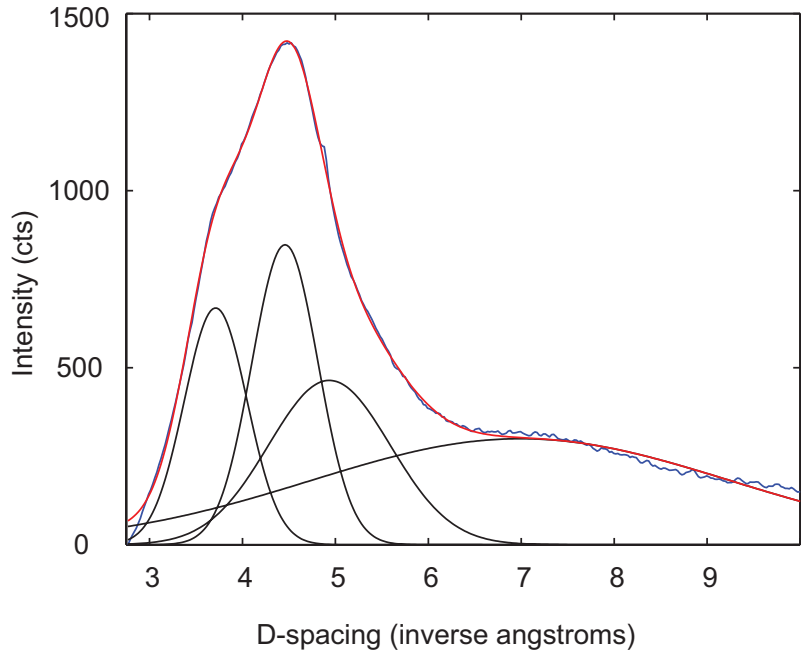

Figure 2.9: 1D radial integration profile of the full 2D WAXD pattern of caddisfly silk is converted to d-spacing to obtain real distances. The data is fit to four Gaussian fits to determine inter-sheet and inter-plane distances. Distances at 3.7 and 4.5 Angstroms show increased equatorial intensity and are associated with a crystalline component aligned parallel to the fiber axis.

hydrogen bonding with $(pSX)_4$ motifs both towards and away from the reader, 3-dimensional crystalline blocks are created. Phosphorylated $(SX)_4$ repeats in caddisfly silk therefore likely serve as a structural replacement for poly(A) and poly(GA) crystalline β-sheet structures found in spider and silkworm fibers.

Caddisfly silk is a very complicated and imperfectly understood material. We can only speculate if and how the described $(pSX)_4$ nanostructure contributes to the adhesive properties of the caddisfly silk fiber. The mechanisms with which the fibers adhere to debris underwater is not the subject of this paper, although electrostatic interactions between charged residues and surfaces may play an important role. While we argue that the phosphorylated $(SX)_4$ repeats in caddisfly silk are incorporated into nanocrystalline β-sheet regions within the silk fibers, perhaps some of these charged repeats remain available for surface binding.

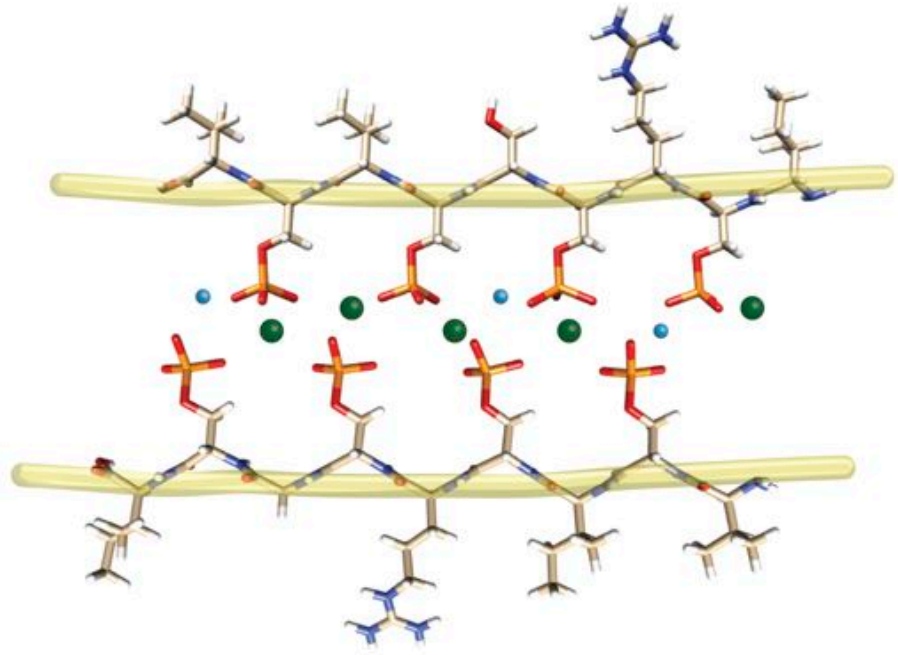

Figure 2.10: Proposed structural motif for phosphorylated $(SX)_4$ repeats found in caddisfly silk fibers [12]. In the model, alternating phosphorylated serine residues interact with divalent cations Ca^{2+} and Mg^{2+} to form rigid β-sheet structures. Backbone amide hydrogen bonding would also stabilize sheet formation into and out of the page, thus forming 3-dimensional blocks similar to the poly(Ala) and poly(Gly-Ala) crystalline blocks observed in spider and silkworm silks.

2.5 Conclusions

Phosphorylated $(SX)_4$ repeats in Trichopteran silks were recently suggested as a structural replacement for the β-sheet-forming poly(GA) motifs found in Lepidopteran silks [12]. Here we have presented solid-state NMR and WAXD results on caddisfly larval silk. X-ray diffraction data identifies a significant (at least 7-8%) crystalline component, with an inter-sheet distance of 4.5 angstroms. Solid-state NMR was used to probe the composition of both the crystalline and amorphous domains. Conformation-sensitive ^{13}C chemical shifts were identified from ^{13}C-^{13}C DARR and ^{1}H-^{31}P-^{13}C DCP NMR. Chemical shifts from many amino acids, including glycine, leucine, valine, serine and phosphoserine, are compared to the chemical shifts from

model peptides with known secondary structures. The data indicates that both valine and phosphoserine residues, commonly found in $(pSX)_4$ repeat regions, likely exist in β-sheet rich environments. The contrast between the ^{13}C CP-MAS and DD-MAS spectra on hydrated silk additionally suggests that phosphorylated serine exists in a less mobile environment than unmodified serine, further supporting the idea of rigid calcium-phosphoserine regions. Glycine and leucine residues however, often seen in GGX repeats, exist predominantly in a random or disordered conformation. ^{31}P Chemical Shift Anisotropy (CSA) data was extracted from caddisfly silk and from different preparations of L-O-Phosphoserine. The CSA parameters summarized in Table 2.2 support a structural motif in which divalent cations Ca^{2+} and Mg^{2+} complex with negatively charged phosphoserine residues.

2.6 Supplementary Material

The figures below were provided as supplementary material for chapter 2, which was published in Biomacromolecules in April of 2013 (Addison, J. B. (2013). *Biomacromolecules*, 14(4), 1140-1148.).

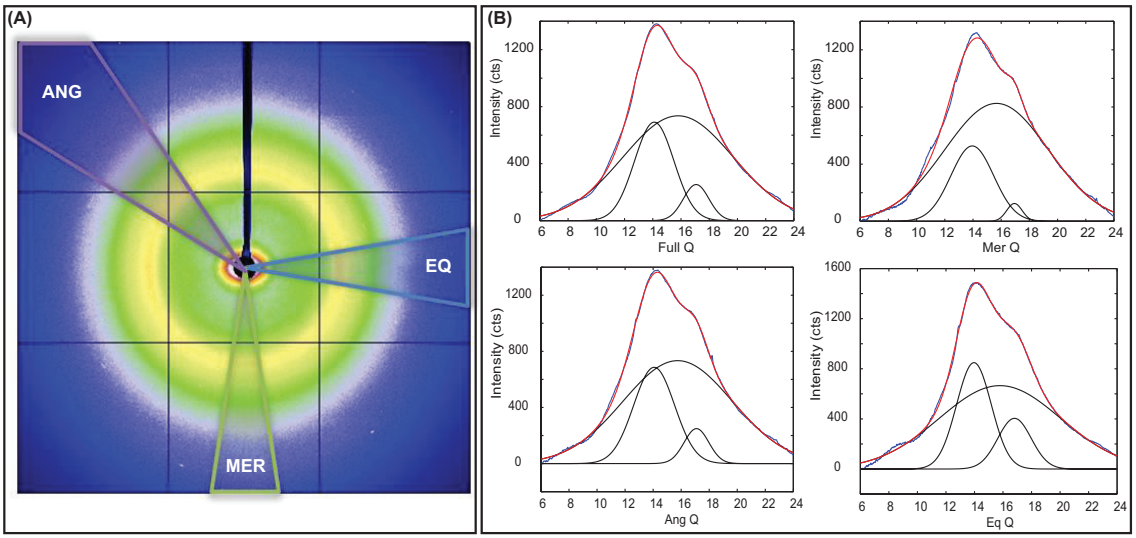

Figure 2.11: A: 2D wide angle X-ray diffraction pattern of caddisfly silk, with equatorial, meridian and 45 degree angle regions highlighted. B: Q integration plots of the full 2D diffraction pattern, and of the three highlighted regions. The peak positions were fixed 14.0, 15.8 and 16.8 in Q-space, and a Gaussian fitting protocol was used to fit each data set. It is clear that the peaks located at 14.0 and 16.8 Q-space, associated with distances of 4.5 and 3.7 inverse angstroms, respectively, are observed in increased intensity in the equatorial region. The differences in peak area in the three regions were used to estimate percent crystallinity at ∼7-8%.

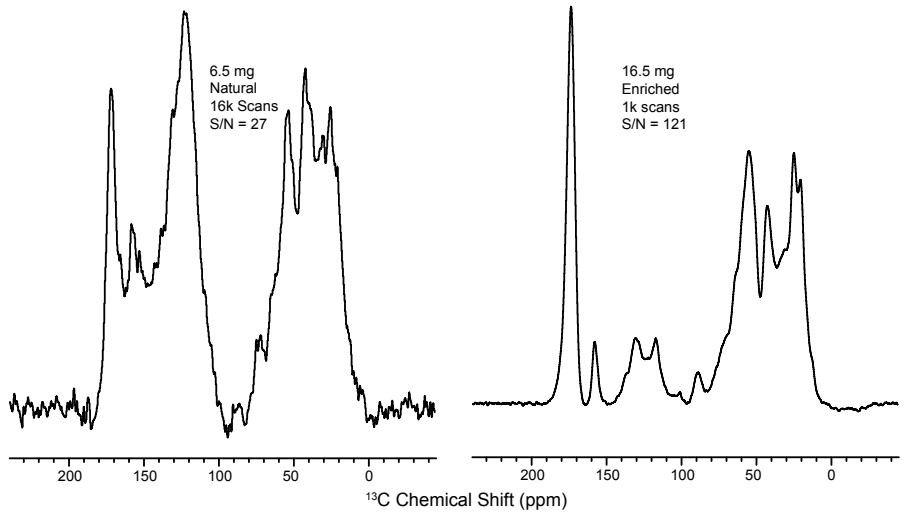

Figure 2.12: ^{1}H-^{13}C CP-MAS of naturally-abundant caddisfly silk (left) and ^{13}C, ^{15}N isotopically enriched caddisfly silk (right). The signal-to-noise ratios were estimated for each spectrum. By adjusting for differences in sample weight and number of scan averages, the percent enrichment was estimated at 6-8%. The large broad peak near 130 ppm in the natural spectrum is due to background from the rotor.

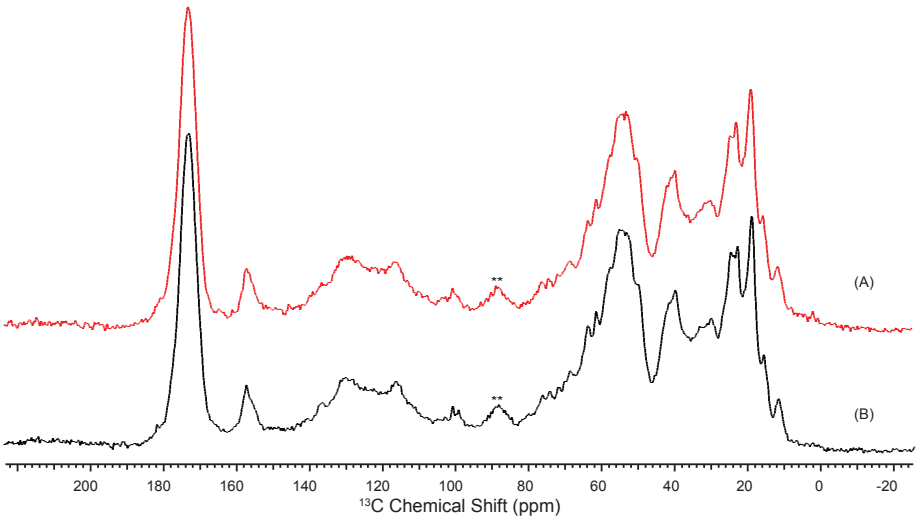

Figure 2.13: ^{1}H-^{13}C CP-MAS NMR spectra of isotopically-enriched hydrated caddisfly silk before drying the silk under nitrogen gas (A), and after re-hydrating the same sample (B). Spectra were taken with a Varian 400 MHz Wide-Bore spectrometer using a 3.2 mm solid state probe configured in HCN triple resonance mode under 8.5 kHz MAS. Carbonyl spinning side bands are indicated with a double asterisk. Experimental conditions were identical: 4096 transients, 5 second recycle delay, 1 ms CP contact time, and 100 kHz TPPM proton decoupling during acquisiton. 25 Hz exponential line broadening was applied to each spectra before Fourier Transformation. The spectra are identical (within experimental error), indicating that drying and re-hydrating the silk has no significant effect on the structural nature of the silk.

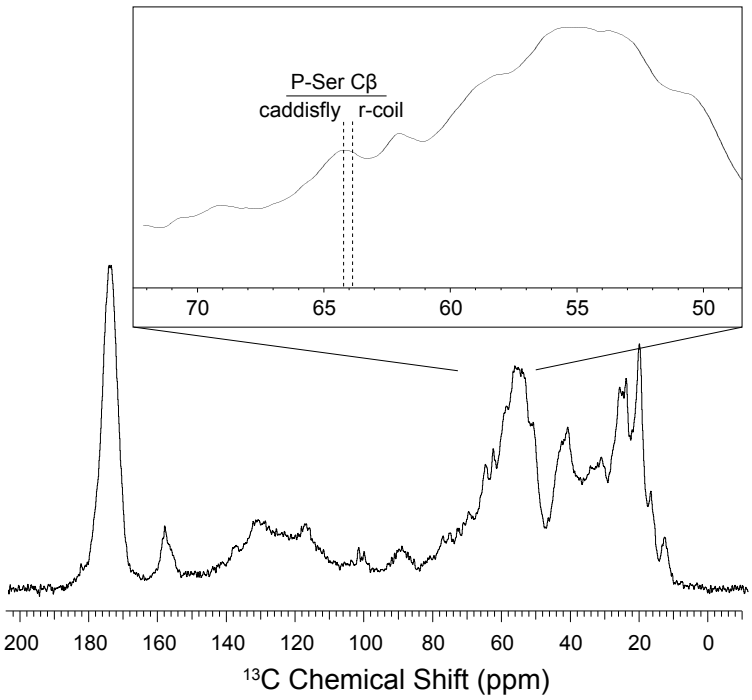

Figure 2.14: ^{1}H-^{13}C CP-MAS NMR spectra of isotopically-enriched hydrated caddisfly silk. The region near the phosphoserine resonance is expanded to illustrate that the p-Ser Cβ resonance of caddisfly silk is shifted downfield with respect to a random coil chemical shift.

REFERENCES

[1] K M Kjer, R J Blahnik, and R W Holzenthal. Phylogeny of caddisflies (Insecta, Trichoptera). *Zoologica Scripta*, 31(1):83–91, 2002.

[2] J C Morse. Phylogeny of trichoptera. *Annual review of entomology*, 42(1):427–450, 1997.

[3] Gary LaFontaine. *Caddisflies*. The Lyons Press, April 1989.

[4] Glenn B Wiggins. *The caddisfly family Phryganeidae (Trichoptera)*. University of Toronto Press Incorporated, 1998.

[5] Russell J Stewart, Ching Shuen Wang, and Hui Shao. Complex coacervates as a foundation for synthetic underwater adhesives. *Advances in Colloid and Interface Science*, 167:85–93, 2011.

[6] Carrie E Brubaker and Phillip B Messersmith. The Present and Future of Biologically Inspired Adhesive Interfaces and Materials. *Langmuir*, 28(4):2200–2205, January 2012.

[7] Kensuke Shimura, Aiko Kikuchi, Kohei Ohtomo, Yōtarō Katagata, and Akio Hyodo. Studies on Silk Fibroin of Bombyx mori. I. Fractionation of Fibroin Prepared from the Posterior Silk Gland. *The Journal of Biochemistry*, 80(4):693–702, 1976.

[8] N Yonemura, F Sehnal, and K Mita. Protein composition of silk filaments spun under water by caddisfly larvae. *Biomacromolecules*, 7(12):3370–3378, 2006.

[9] Naoyuki Yonemura, Kazuei Mita, Toshiki Tamura, and František Sehnal. Conservation of Silk Genes in Trichoptera and Lepidoptera. *Journal of molecular evolution*, 68(6):641–653, May 2009.

[10] M S Engster. Studies on silk secretion in the trichoptera (F. Limnephilidae). *Cell and Tissue Research*, 169(1):77–92, June 1976.

[11] F Sehnal and M Zurovec. Construction of silk fiber core in Lepidoptera. *Biomacromolecules*, 5(3):666–674, 2004.

[12] R J Stewart and C S Wang. Adaptation of Caddisfly Larval Silks to Aquatic Habitats by Phosphorylation of H-Fibroin Serines. *Biomacromolecules*, 11(4):969–974, 2010.

[13] Richard E Marsh, Robert B Corey, and Linus Pauling. An investigation of the structure of silk fibroin. *Biochimica et Biophysica Acta*, 16:1–34, January 1955.

[14] Osman Rathore and Dotsevi Y Sogah. Self-assembly of β-sheets into nanostructures by poly (alanine) segments incorporated in multiblock copolymers inspired by spider silk. *J. Am. Chem. Soc*, 123(22):5231–5239, 2001.

[15] A Simmons, E Ray, and LW Jelinski. Solid-state 13C NMR of Nephila clavipes dragline silk establishes structure and identity of crystalline regions. *Macromolecules*, 27(18):5235–5237, 1994.

[16] Wei-Qiang Chen, Helga Priewalder, Julius Paul Pradeep John, and Gert Lubec. Silk cocoon of Bombyx mori: Proteins and posttranslational modifications - heavy phosphorylation and evidence for lysine-mediated cross links. *PROTEOMICS*, 10(3):369–379, February 2010.

[17] Nicholas N Ashton, Daniel S Taggart, and Russell J Stewart. Silk tape nanostructure and silk gland anatomy of trichoptera. *Biopolymers*, 97(6):432–445, 2012.

[18] G H Altman, F Diaz, C Jakuba, T Calabro, R L Horan, J Chen, H Lu, J Richmond, and D L Kaplan. Silk-based biomaterials. *Biomaterials*, 24(3):401–416, 2003.

[19] B Lotz and F C Cesari. Chemical-Structure and the Crystalline-Structures of Bombyx-Mori Silk Fibroin. *Biochimie*, 61(2):205–214, 1979.

[20] M Tsukada, MMR Khan, E Inoue, and G Kimura. Physical properties and structure of aquatic silk fiber from Stenopsyche marmorata 10.1016/j.ijbiomac.2009.10.003 : International Journal of Biological Macromolecules — ScienceDirect.com. *International Journal of Biological Macromolecules*, 46:54–58, 2010.

[21] Y Wang, K Sanai, H Wen, and T Zhao. Characterization of unique heavy chain fibroin filaments spun underwater by the caddisfly Stenopsyche marmorata (Trichoptera; Stenopsychidae). *Molecular biology reports*, 37:2885–2892.

[22] M S Creager, E B Butler, R V Lewis, J L Yarger, and G P Holland. Solid-state NMR evidence for elastin-like β-turn structure in spider dragline silk. *Chemical Communications*, 46(36):6714–6716, 2010.

[23] R W Williams, A Chang, D Juretić, and S Loughran. Secondary structure predictions and medium range interactions. *Biochimica et Biophysica Acta*, 916(2):200–204, 1987.

[24] Jan Johansson, Charlotte Nerelius, Hanna Willander, and Jenny Presto. Conformational preferences of non-polar amino acid residues: An additional factor in amyloid formation. *Biochemical and biophysical research communications*, 402(3):515–518, November 2010.

[25] Janusz W. Strzelecki, Joanna Strzelecka, Karolina Mikulska, Mariusz Tszydel, Aleksander Balter, and Wieslaw Nowak. Nanomechanics of new materials - AFM and computer modelling studies of trichoptera silk. *Central European Journal of Physics*, 9(2):482–491, 2011.

[26] Emma Lang, Gyorgyi I Szendrei, Ilona Elekes, Virginia M-Y Lee, and Laszlo Otvos Jr. Reversible β-pleated sheet formation of a phosphorylated synthetic τ peptide. *Biochemical and biophysical research communications*, 182(1):63–69, January 1992.

[27] M Hollosi, L Urge, A Perczel, J Kajtar, I Teplan, J Otvos, and G D Fasman. Metal Ion-Induced Conformational-Changes of Phosphorylated Fragments of Human Neurofilament (Nf-M) Protein. *Journal of Molecular Biology*, 223(3):673–682, 1992.

[28] S Holly, I Laczko, G D Fasman, and M Hollosi. FT-IR Spectroscopy Indicates That Ca2+-Binding to Phosphorylated C-Terminal Fragments of the Midsized Neurofilament Protein Subunit Results in [beta]-Sheet Formation and [beta]-Aggregation. *Biochemical and biophysical research communications*, 197(2):755–762, 1993.

[29] Andrew E Bennett, Chad M Rienstra, Michèle Auger, K V Lakshmi, and Robert G Griffin. Heteronuclear decoupling in rotating solids. *The Journal of Chemical Physics*, 103(16):6951, 1995.

[30] K Takegoshi, S Nakamura, and T Terao. 13C–1H dipolar-assisted rotational resonance in magic-angle spinning NMR. *Chemical Physics Letters*, 344(5):631–637, 2001.

[31] K Takegoshi, S Nakamura, and T Terao. C–H dipolar-driven C–C recoupling without C rf irradiation in nuclear magnetic resonance of rotating solids. *The Journal of Chemical Physics*, 118(5):2325–2341, 2003.

[32] J Schaefer, R A McKay, and E O Stejskal. Double-Cross-Polarization Nmr of Solids. *Journal of Magnetic Resonance*, 34(2):443–447, 1979.

[33] E O Stejskal, Jacob Schaefer, and R A McKay. Analysis of double cross-polarization rates in solid proteins. *Journal of Magnetic Resonance (1969)*, 57(3):471–485, May 1984.

[34] Wlodzimierz Ciesielski, Hassan Kassassir, and Marek J Potrzebowski. A practical guide for the setup of a 1H–31P–13C double cross-polarization (DCP) experiment. *Solid State Nuclear Magnetic Resonance*, 39(3-4):151–157, May 2011.

[35] J Herzfeld and A E Berger. Sideband Intensities in Nmr-Spectra of Samples Spinning at the Magic Angle. *Journal of Chemical Physics*, 73(12):6021–6030, 1980.

[36] D Massiot, F Fayon, M Capron, I King, S Le Calvé, B Alonso, J O Durand, B Bujoli, Z Gan, and G Hoatson. Modelling oneand twodimensional solidstate NMR spectra. *Magnetic Resonance in Chemistry*, 40(1):70–76, 2002.

[37] J G Hardy and T R Scheibel. Production and processing of spider silk proteins. *Journal of Polymer Science Part A: Polymer Chemistry*, 47(16):3957–3963, 2009.

[38] Z Yang, O Liivak, A Seidel, G LaVerde, DB Zax, and LW Jelinski. Supercontraction and backbone dynamics in spider silk: 13C and 2H NMR studies. *J. Am. Chem. Soc*, 122(37):9019–9025, 2000.

[39] Gregory P Holland, Janelle E Jenkins, Melinda S Creager, Randolph V Lewis, and Jeffery L Yarger. Solid-state NMR investigation of major and minor ampullate spider silk in the native and hydrated states. *Biomacromolecules*, 9(2):651–657, 2008.

[40] Akira Shoji, Takuo Ozaki, Hazime Saito, Ryoko Tabeta, and Isao Ando. Conformational characterization of solid polypeptides by carbon-13 NMR recorded by the cross polarization-magic angle spinning method: conformation-dependent carbon-13 chemical shifts of oligo- and poly(γ-benzyl L-glutamates) and sequential copolymers of γ-benzyl and γ-methyl L-glutamates and qualitative evaluation of side-chain orientation. *Macromolecules*, 17(8):1472–1479, August 1984.

[41] T Asakura. 13C CP/MAS NMR study on structural heterogeneity in Bombyx mori silk fiber and their generation by stretching. *Protein Science*, 11:2706–2713, 2002.

[42] Hans R Kricheldorf and Detlef Mueller. Secondary structure of peptides. 3. Carbon-13 NMR cross polarization/magic angle spinning spectroscopic characterization of solid polypeptides. *Macromolecules*, 16(4):615–623, July 1983.

[43] DS Wishart, CG Bigam, A Holm, RS Hodges, and BD Sykes. 1 H, 13 C and 15 N random coil NMR chemical shifts of the common amino acids. I. Investigations of nearest-neighbor effects. *Journal of biomolecular NMR*, 5(1):67–81, 1995.

[44] Ewa A Bienkiewicz and Kevin J Lumb. Journal of Biomolecular NMR, Volume 15, Number 3 - SpringerLink. *Journal of biomolecular NMR*, 15(3):203–206, 1999.

[45] Tetsuo Asakura, Mingying Yang, Taiji Kawase, and Yasumoto Nakazawa. 13C Solid-State NMR Study of Structural Heterogeneity in Peptides Containing Both Polyalanine and Repeated GGA Sequences as a Local Structural Model of NephilaclavipesDragline Silk (Spidroin 1). *Macromolecules*, 38(8):3356–3363, April 2005.

[46] J D van Beek. The molecular structure of spider dragline silk: Folding and orientation of the protein backbone. *Proceedings of the National Academy of Sciences*, 99(16):10266–10271, July 2002.

[47] Gregory P Holland, Melinda S Creager, Janelle E Jenkins, Randolph V Lewis, and Jeffery L Yarger. Determining Secondary Structure in Spider Dragline Silk by Carbon Carbon Correlation Solid-State NMR Spectroscopy. *J. Am. Chem. Soc*, 130(30):9871–9877, 2008.

[48] M S Creager, T Izdebski, A E Brooks, and R V Lewis. Elucidating Metabolic Pathways for Amino Acid Incorporation Into Dragline Spider Silk using 13C Enrichment and Solid State NMR. *Comparative Biochemistry and Physiology-Part A: Molecular & Integrative Physiology*, 2011.

[49] Carole Gardiennet-Doucet, Xavier Assfeld, Bernard Henry, and Piotr Tekely. Revealing Successive Steps of Deprotonation of l- Phosphoserine through 13C and 31P Chemical Shielding Tensor Fingerprints. *The Journal of Physical Chemistry A*, 110(29):9137–9144, July 2006.

[50] T M Duncan and D C Douglas. On the 31P chemical shift anisotropy in condensed phosphates. *Chemical Physics*, 87(3):339–349, July 1984.

[51] J O Warwicker. Comparative studies of fibroins. II. The crystal structures of various fibroins. *Journal of Molecular Biology*, 2(6):350–362, December 1960.

[52] Sujatha Sampath, Thomas Isdebski, Janelle E Jenkins, Joel V Ayon, Robert W Henning, Joseph P R O Orgel, Olga Antipoa, and Jeffery L Yarger. X-ray diffraction study of nanocrystalline and amorphous structure within major and minor ampullate dragline spider silks. *Soft Matter*, 8(25):6713–6722, 2012.

[53] Yi Liu and Zhengzhong Shao. Elasticity of spider silks. *Biomacromolecules*, 9:1782–1786, 2008.

[54] Xiao Hu, David Kaplan, and Peggy Cebe. Determining Beta-Sheet Crystallinity in Fibrous Proteins by Thermal Analysis and Infrared Spectroscopy. *Macromolecules*, 39(18):6161–6170, September 2006.

[55] C Riekel, C Bränden, C Craig, C Ferrero, F Heidelbach, and M Müller. Aspects of X-ray diffraction on single spider fibers. *International Journal of Biological Macromolecules*, 24(2-3):179–186, March 1999.

Chapter 3

REVERSIBLE ASSEMBLY OF β-SHEET NANOCRYSTALS WITHIN CADDISFLY SILK

3.1 Abstract

NMR and XRD experiments reveal the structural importance of divalent cation-phosphate complexes in the formation of β-sheet nanocrystals from phosphorylated serine-rich regions within aquatic silk from caddisfly larvae of the species *H. consimilis*. Wide Angle X-ray Diffraction data on native caddisfly silk shows that the silk contains a significant crystalline component with a repetitive orthorhombic unit cell aligned along the fiber axis with dimensions 5.9 x 23.2 x 17.3 Å. These nanocrystalline domains depend on multivalent cations, which can be removed through chelation with EDTA. A comparison of WAXD data before and after EDTA treatment reveals that the reflections corresponding to the nanocrystalline regions decrease in integrated peak area by 15-25% while the amorphous background reflections increased in area by 20%, indicating a partial loss in crystallinity. ^{31}P solid-state NMR data on native caddisfly silk also shows that the phosphorylated serene-rich motifs transform from a rigid environment to one that is highly mobile and water-solvated after treatment with EDTA. The removal of divalent cations through exchange and chelation has therefore caused a collapse of the β-sheet structure. However, NMR results show that the rigid phosphorus environment is mostly recovered after the silk is retreated with calcium. The ^{31}P spin-lattice (T_1) relaxation times were measured at 7.6 $\pm$ 3.1 and 1 $\pm$ 0.5 seconds for this calcium-recovered sample and the native silk sample, respectively. The shorter ^{31}P T_1 relaxation times measured for the native silk sample

are attributed to the presence of paramagnetic iron that is striped away during EDTA chelation treatment and replaced with diamagnetic calcium.

3.2 Introduction

Caddisfly larvae (order Trichoptera) utilize aquatic silk fibers to stitch together available debris into elaborate underwater structures [1, 2]. Although closely related to Lepidopteran insects, including the domesticated silkworm *Bombyx mori* [3, 4], caddisfly fibers do not contain runs of poly(Ala) or poly(Gly-Ala). These repetitive motifs form rigid β-sheet regions in spider and silkworm silks, contributing greatly to the fibers impressive mechanical properties [5, 6, 7, 8]. Instead of alanine-rich repetitive motifs, caddisfly fibers contain phosphorylated $(SX)_4$ repeat regions in the H-fibroin primary protein sequence [9, 10]. This phosphate-rich motif is highlighted in red in Figure 3.1, which shows a portion of the caddisfly H-fibroin protein sequence labeled the D-repeat. Caddisfly silk fibers also contain a significant crystalline component [11, 12, 13, 14], thus it was recently suggested that phosphorylated $(SX)_4$ repeats form insoluble β-sheet structures through Ca^{2+} - phosphoserine complexes [15]. Such regions may serve as a structural replacement for β-sheet forming poly(Ala) or poly(Gly-Ala) domains in spider and silkworm silks.

D Repeat:
VSISRSVSIERIVTPGVYTKISRSSSVSVEGG

Figure 3.1: Extended D-repeat from the H-fibroin protein sequence from the species *Hesperophylax sp.* [16]. Phosphorylated $(SX)_4$ regions are shown in red, and a conserved, underlined proline-glycine turn is seen after both motifs. Calcium magnesium and iron cations are thought to stabilize these phosphorylated serine-rich motifs to form rigid β-sheet structures within caddisfly larval silks.

There is strong conceptual and experimental support for this hypothesis that has been laid out in previous works [15, 17, 14]. To summarize: The nanocrystalline

regions must arise from some sheet-forming motifs other than poly(Ala) or poly(Gly-Ala), and $(pSX)_4$ repeats fit the mold. A conserved proline-glycine motif, often seen in β-turn structures [18], exists shortly after every $(pSX)_4$ repeat region in the H-fibroin protein sequence (underlined in Figure 3.1) [9, 10]. The X residue in the $(SX)_4$ motif is often valine or isoleucine, which both have high tendencies to form β-sheet structures [19, 20]. Elemental analysis reveals significant levels of multivalent cations including calcium, magnesium and iron [15, 21]. Computer simulations of $(pSX)_4$ repeats shows a dramatic increase in strength when calcium cations are present [22]. Multi-phosphorylated peptides have previously been shown to form β-sheets when calcium cations are present; this mechanism may be related to neurofilament tangle formation in Alzheimer's patients [23, 24, 25]. Our recent ^{13}C and ^{31}P solid-state NMR data on caddisfly larval silk showed that valine and phosphoserine residues from phosphorylated $(SX)_4$ motifs exist in β-sheet structures, and that caddisfly silk contains a rigid phosphorus environment that is likely stabilized by divalent cations [14]. Moreover, it was recently shown that both the tensile properties of individual caddisfly fibers and the overall β-sheet content of the silk are diminished after removing cations through EDTA chelation [16].

While a strong interaction between negatively charged phosphates with di- and trivalent cations is no surprise, its prevalence within caddisfly larval silk is very unique within silk-based biopolymers. In this work, we further demonstrate that multivalent cations are absolutely essential to the structural integrity of caddisfly silk. NMR and XRD results show the reversible deformation and formation of β-sheet nanostructures within the phosphorylated serine-rich regions of caddisfly silk, through depletion or exposure of divalent cations, respectively.

3.3 Materials and Methods

Silk collection. Native caddisfly silk was obtained from larvae of the species *Hesperophylax consimilis* from the upper Red Butte creek in Salt Lake county Utah. The insects were removed from their original stone cases and were given blocks of polytetrafluoroethylene (PTFE) as fodder to construct new cases. After 3 days they were removed from PTFE cases and were placed back into their original stone cases for feeding. Silk was separated from the PTFE cases using fine forceps and stored in tap water at 4 °C. This process was repeated multiple times to obtain sufficient sample for solid-state NMR (SSNMR)

Preparation of phosphoserine - cation salts. Samples were prepared by dissolving L-O-Phosphoserine (Sigma Aldrich) in deionized water, adding equimolar amounts of cation-chloride salts, and adjusting the pH to 8.3 using dilute NaOH. The solution was then flash frozen and lyophilized. The cation mixture sample containing paramagnetic iron (Figure 3.6E) was prepared using a 10:6:3:1 ratio of phosphoseine:Ca^{2+}:Mg^{2+}:Fe^{3+}, a ratio similar to that observed in native caddisfly silk.[15]

Scanning Electron Microscopy. Both native and exchanged silk samples were placed onto conductive carbon tape, then gold coated using a Denton vacuum sputter coater desk II for 180 seconds at a deposition rate of 5 nm/min. The SEM was performed using a XL30 Environmental SEM-FEG built by FEI. The secondary electron (SE) detector was used for imaging. Measurements were collected under a vacuum pressure of less than 9 x 10^{-5} mbar and with a beam current of 5.00 kV.

Wide Angle X-ray Diffraction. Caddisfly larval silk was mounted onto a cardboard washer for WAXD measurements, and a small amount of super glue was used to secure the fibers to the washer at either end. The WAXD experiments were car-

ried out at the 14-BM-C beam line at Advanced Photon Source at Argonne National Laboratory using a beam energy of 12.6 KeV. The exposure time was fixed at 60 seconds for each of 5 averaged exposures, and the 9 panel CCD array detector was placed at a distance of 450 mm in both cases. The detector used was the ADSC Quantum-315 with a beam size of approximately 130 x 340 μm (FWHM). The sample was aligned such that the fibers were parallel to the axis of the beamstop. Cerium dioxide (CeO_2) was used as a calibrant in the FIT2D x-ray processing software to analyze the 2D diffraction patterns. Ethylenediaminetetraacetic acid (EDTA), a known metal-ion chelator, was then utilized to remove cations from the silk fibers through chelation. Identical XRD experimental conditions were used for both the native and EDTA-exchanged silk samples. To prepare the exchanged sample, the native sample was carefully treated with a cation-exchange solution containing 10 mM Tris pH 8.1, 2 mM EDTA, 10 mM NaCl for 6 hours. Agitation was kept to a minimum so that fiber alignment was not disrupted by turbulence.

Cation exchange treatment. For NMR studies, a bundle of native caddisfly silk fibers was introduced to a solution containing 10 mM Tris pH 8.1, 2 mM EDTA, and 10 mM NaCl. This solution was stirred overnight with a magnetic stir bar to ensure complete EDTA treatment. After NMR data collection, this sample was similarly treated with a solution containing 10 mM Tris pH 8.1 and 10 mM $CaCl_2$. The sample was stirred with a magnetic stir bar overnight, and silk was recovered for solid-state NMR experiments.

^{31}P Solid State NMR. ^{31}P solid-state NMR experiments were conducted on a 400 MHz Varian wide-bore instrument equipped with a 3.2 mm triple resonance MAS probe. All samples were spun at the magic angle at 4 kHz. ^{31}P chemical shifts were referenced externally to crystalline ammonium phosphate at 0.8 ppm, and the same reference sample was used to optimize $^{1}H \rightarrow {}^{31}P$ Cross Polarization under Magic

Angle Spinning (CP-MAS) conditions. For CP experiments, typical experimental conditions used were an initial 2.6 μs proton $\pi/2$ pulse, a 1 ms ramped ($\sim$10%) spin-lock pulse on both the ^{1}H and ^{31}P channels near 80 kHz, a 100 kHz spectral width, 10 ms acquisition time, a 5 second relaxation delay, and either 2048 or 4096 scan averages. Direct Detection under Magic Angle Spinning (DD-MAS) experiments on caddisfly silk samples utilized a 4.1 μs $\pi/2$ pulse, 10 ms acquisition time, 100 kHz spectral width, a 5 second relaxation delay, and 2048 scan averages. All experiments were collected using 100 kHz TPPM [26] proton decoupling during acquisition.

^{31}P T_1 measurements. The ^{31}P T_1 relaxation times were measured for native and exchanged caddisfly silks (Figure 3.4) and for phosphoserine in the presence of various cations (Figure 3.5) using the progressive saturation method [27]. Typical experimental parameters used were a 4.1 μs $\pi/2$ pulse, 10 ms acquisition time, 100 kHz spectral width, a minimum of 8 scans, and a 4 kHz MAS spin rate. Two-pulse phase-modulated [26] (TPPM) proton decoupling at 100 kHz was applied during acquisition. The recycle delay was varied to obtain a buildup curve dependent on T_1 relaxation properties. To obtain T_1 relaxation time constants, spectra from each recycle delay were baseline corrected, and the center-band of the chemical shift anisotropy (CSA) powder pattern was integrated and normalized. Normalized peak areas were plotted against recycle delay, and the curve was fit to the equation

$M(t) = A1[1 - \exp(-t/T_1)] + A2$

where A1 is a normalization constant and A2 is the y-intercept necessary for obtaining good fits. All T_1 values are listed in Table 3.1, and errors are reported as the 95% confidence intervals from the fits.

3.4 Results and Discussion

Caddisfly silk from the species *Hesperophylax consimilis* was studied with wide angle X-ray diffraction (WAXD) and solid-state NMR techniques, and the importance of multivalent cations within the silks was investigated. EDTA was introduced to caddisfly silk to remove divalent cations from the fibers. Figure 3.2 shows SEM micrographs of caddisfly silk, demonstrating the effects of removing divalent cations. The natural silks from the species *H. consimilis* are a fusion of two fibrils into flat, ribbon-like fibers. Surface detail seen in Figure 3.2B shows that the fibers are composed of approximately 120 nm nanofibrils aligned along the fiber axis. When the silk is treated with a cation-exchange solution (10 mM Tris pH 8.1, 2 mM EDTA, 10 mM NaCl), the fiber morphology is completely destroyed. Instead of 5-10 μm-wide ribbons, the silk becomes warped, inconsistent, and the nanofibrils are exposed and disorganized (Figure 3.2C and 3.2D).

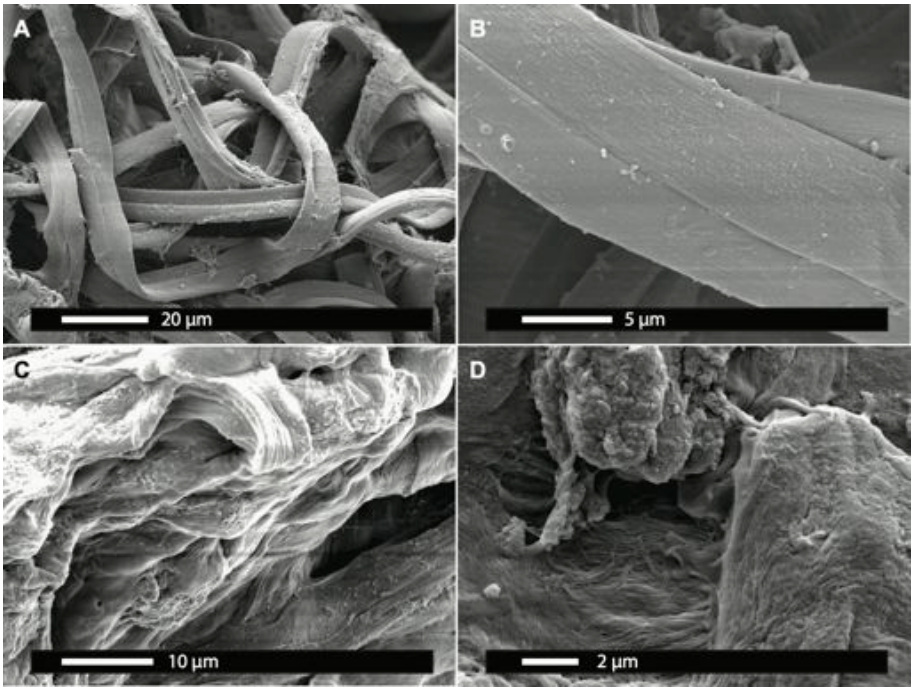

Figure 3.2: Scanning Electron Microscopy (SEM) images of natural caddisfly silk (A, B) and silk treated with EDTA (C, D). The fibers are destroyed when Ca^{2+} is removed through EDTA chelation, exposing the small (≈120 nm) nanofibrils [22, 17]. The images were collected on gold-coated samples using a XL30 Environmental SEM-FEG built by FEI.

The substantial changes to the fiber appearance seen in the SEM images occur upon removal of divalent cations via EDTA chelation. These cations are potentially being removed from phosphoserine-cation complexes, thus we probed any structural changes caused by EDTA treatment through Wide Angle X-ray Diffraction (WAXD). Many of the reflections have been assigned using an orthorhombic unit cell; here the peaks labeled 1, 2, 3 and 4 correspond to (123), (004), (120) and (100) reflections, respectively. The d-spacings associated with each peak are indicated in Figure 3.3B. The assignments yield a repetitive orthorhombic unit cell aligned along the fiber axis, of dimensions 5.9 x 23.2 x 17.3 Å.

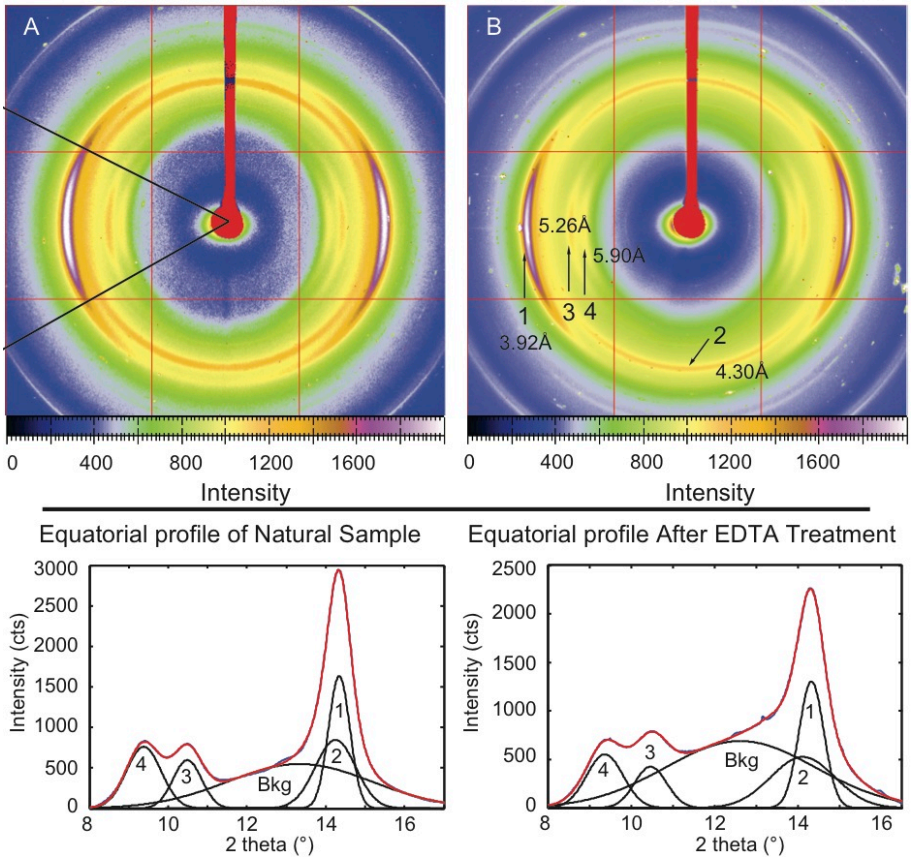

Figure 3.3: Wide Angle X-ray Diffraction (WAXD) profiles of axially-aligned caddisfly silk before (A) and after (B) EDTA treatment. Integrations from the equatorial wedges (indicated in 3A) are shown below each profile, and the data was fit to four gaussian peaks (1-4) and one background peak. After EDTA treatment, the intensity of the amorphous background peak is increased while peaks 1, 2 and 4 are reduced. The data shows a decrease in crystallinity after cation removal through EDTA chelation.

This crystalline unit is not caused by the traditional poly(Ala) or poly(Gly-Ala) found in spider and silkworm fibers; instead they arise from phosphorylated-serine rich motifs stabilized by calcium, magnesium and iron cations [15, 14]. To further investigate any structural changes upon removal of cations from the silk, the native caddisfly silk sample used for Figure 3.3A was carefully treated with a cation exchange buffer (10 mM Tris pH 8.1, 2 mM EDTA, 10 mM NaCl) for 6 hours. Agitation was minimal as to not alter the sample alignment. The sample was rinsed and air dried, and the WAXD experiment was then recollected (Figure 3.3B). Both the

2D diffraction pattern and the equatorial 2 theta integration profiles clearly show an increase in background and a decrease in aligned repetitive reflections. The amorphous background signal, seen as the large broad lines, increased in integrated peak area after cation removal by 20%. Similarly, the diffraction peaks associated with axially-aligned repetitive β-sheet units decrease in intensity after EDTA treatment; the peak areas for each of the three equatorial reflections 1, 3 and 4 are diminished by 15-25%. The WAXD data clearly indicates that removal of divalent cations from caddisfly silk disrupts the repetitive β-sheet structures. The percent crystallinity was calculated for both the native and treated samples using methods described by Grubb et al. [28], resulting in 18 and 16% crystalline, respectively. We associate the drop in crystallinity with a partial disruption of the cation - phosphoserine nanocrystalline β-sheets within caddisfly larval silks. While only a minor change in crystallinity, we note that the sample agitation was kept to a minimum, so a full disruption of the β-sheets is not expected.

A more complete EDTA treatment was performed on non-oriented caddisfly silk bundles, and changes in phosphorus environments were probed with ^{31}P NMR. Initially, both ^{31}P DD-MAS and CP-MAS spectra were collected on caddisfly silk in its natural, hydrated state. The ^{31}P solid state NMR data provides clear evidence for rigid phosphate environments. Both the DD-MAS and CP-MAS spectra in Figure 3.4A and 3.4B show broad powder patterns with an isotropic chemical shift (σ^{iso}) at 1.5 ppm. The ^{31}P chemical shift anisotropy (CSA) pattern mapped out by the spinning side bands exhibits a negative skew parameter (skew = -0.4), which is characteristic of a rigid phosphate carrying a $^{-}2$ charge [29, 30]. One might expect charged phosphoserine residues to be highly mobile and water-solvated, however the observation of a strong ^{1}H $\rightarrow$ ^{31}P cross polarization signal implies that the phosphates are surrounded by a rigid proton dipolar-coupling network.

Rigid phosphoserine environments are found in caddisfly silk even when the fibers are wet, however this is lost upon EDTA-treatment. Both direct and CP spectra were recollected (Figure 3.4C and 3.4D) after treating the silk with the cation exchange buffer. The lack of signal from the CP-MAS spectrum implies that ^{31}P nuclei are no longer in strong dipolar contact with rigid protons. The direct ^{31}P spectra has collapsed to a single isotropic resonance as opposed to a broad powder pattern, indicating that molecular motion is now sufficiently fast to average away the chemical shielding tensor. The isotropic phosphorus chemical shift in the direct spectra now falls at 3.1 ppm, shifted downfield from the natural silk as indicated by the dotted line. This noticeable shift is consistent with our recently published data collected on phosphoserine-cation salts; the isotropic ^{31}P chemical shift from phosphoserine moves downfield when sodium is present as opposed to either calcium or magnesium [14]. Furthermore, the observations of a dramatically increased signal and the clearly sharpened line shape in the direct spectra are again indicative of a mobile environment. Therefore upon EDTA-mediated removal of divalent cations from caddisfly silk, a rigid phosphoserine environment is replaced by one that is highly mobile and solvent-exposed.

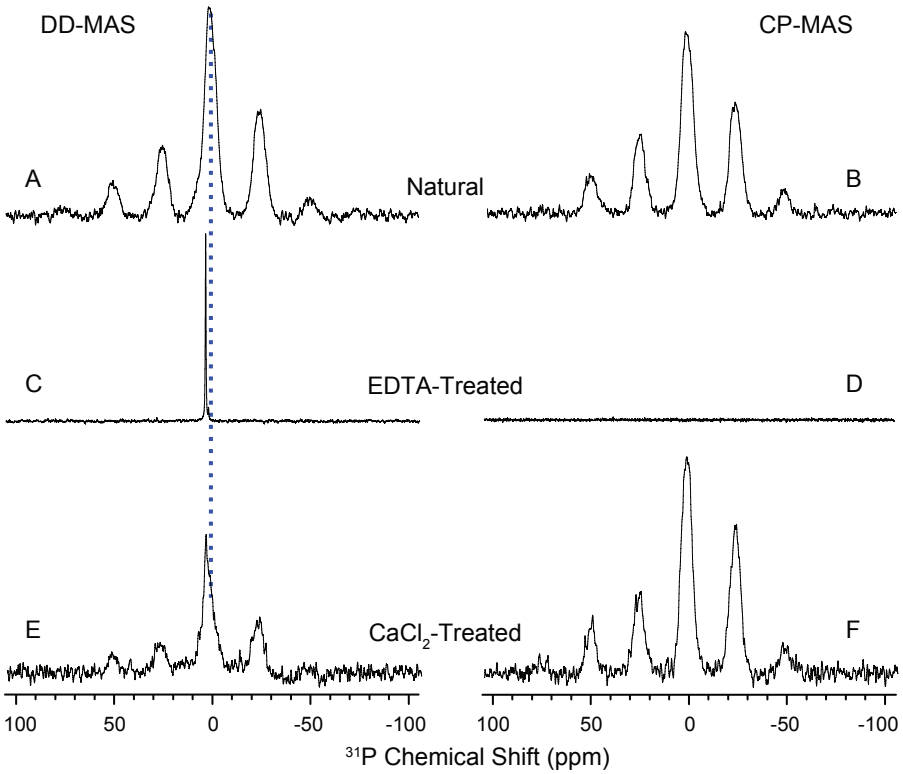

Figure 3.4: ^{31}P DD-MAS and CP-MAS NMR data on natural (A, B), EDTA-treated (C, D) and $CaCl_2$-treated (E, F) caddisfly silk fibers. Direct spectra were acquired using 2048 scan averages and a 5 second recycle delay, while CP spectra were collected using 2048 (B and F) or 4096 (D) scan averages, a 1 ms CP contact time and a 5 second recycle delay.

Both our WAXD and NMR data on native versus exchanged caddisfly silk are in excellent agreement with recently published mechanical and FTIR results [16]. When individual silk fibers were treated with EDTA and multivalent cations are replaced with Na^+, the fiber's tensile properties stiffness, strength, and energy-dissipating hysteresis are all destroyed. The loss of mechanical properties is directly correlated to a decrease in overall β-sheet content within the silk, as evident in a drop in intensity of the β-sheet component of Amide I band in the FTIR spectra after EDTA treatment. Amazingly, the original fiber mechanical properties and the overall β-sheet content are both reestablished after calcium cations are reintroduced to the material.

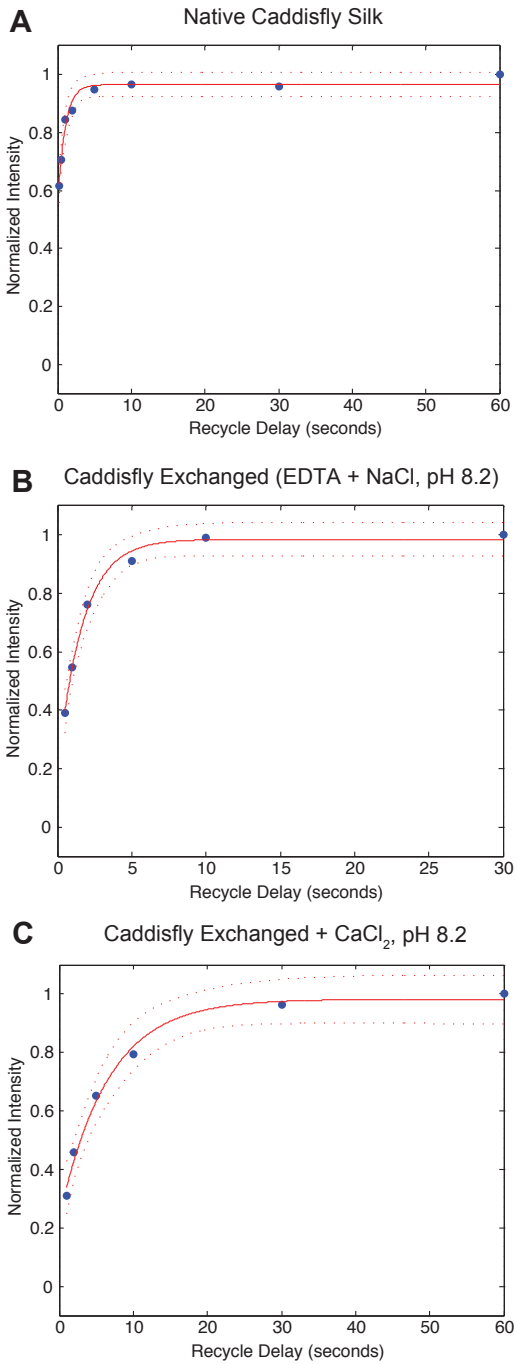

Figure 3.5: ^{31}P T_1 relaxation curves for native caddisfly silk (A), silk after removing cations with EDTA (B), and silk after reincorporation of Ca^{2+} (C). Data are shown in blue, the resulting fits with a solid red line, and the 95% confidence intervals with red dashed lines. The difference in T_1 relaxation rates between native silk and Ca^{2+} exchanged silk is due to the removal of paramagnetic iron from the native sample.

Table 3.1: T_1 relaxation times for native and exchanged caddisfly silks, and for phosphoserine in the presence of various cations. *Sample prepared with a 10:6:3:1 ratio of pSer:Ca^{2+}:Mg^{2+}:Fe^{3+}

Sample	T_1 (seconds)
Caddisfly native	1 ± 0.5
Caddisfly EDTA/NaCl	1.7 ± 0.7
Caddisfly $CaCl_2$	7.6 ± 3.1
pSer + 2LiCl	88 ± 8
pSer + 2NaCl	61 ± 3
pSer + $MgCl_2$	54 ± 5
pSer + $CaCl_2$	69 ± 6
pSer + Mixture*	7.5 ± 2.5

Our NMR results also show that one can reestablish rigid calcium - phosphoserine β-sheet regions from cation-depleted caddisfly silk after reintroducing calcium cations. The ^{31}P NMR data seen in Figure 3.4 reveals that when the exchanged silk was treated with a solution containing 10 mM $CaCl_2$, rigid phosphorus environments are partially recovered. Although the CP-MAS signal intensity is diminished in Figure 3.4F with respect to the natural silk spectra seen in Figure 3.4B, the broad powder pattern is clearly recovered. The chemical shift in the CP spectra moves from 3.1 ppm back to the original 1.5 ppm, again in agreement with a phosphoserine-divalent cation interaction [14]. The direct spectrum shows a faint sharp component at 3.1 ppm, similar to that observed for the EDTA-treated silk, however the signal intensity is dramatically decreased. Both spectra were collected on the same amount of sample and with the same NMR acquisition parameters, thus the loss in the direct ^{31}P signal intensity is explained by mobile phosphates being re-incorporated into rigid, water-

inaccessible calcium-phosphoserine complexes. Interestingly, the native silk exhibits both a strong and broad DD-MAS and CP-MAS signal (4A, 4B), but after removal of cations and reintroducing Ca^{2+}, this broad DD-MAS signal is weak as compared to the CP spectrum (3.4E, 3.4F). In fact for the native silk sample the direct signal is actually stronger than from the CP with the same relaxation delay (5 seconds) and same number of scan averages (2048), but is much weaker than the CP after calcium is reintroduced as the stabilizing cation. This difference is intriguing, and deserves an explanation. We attribute the difference between the direct spectra in (4A) and (4E) to differences in T_1 relaxation properties.

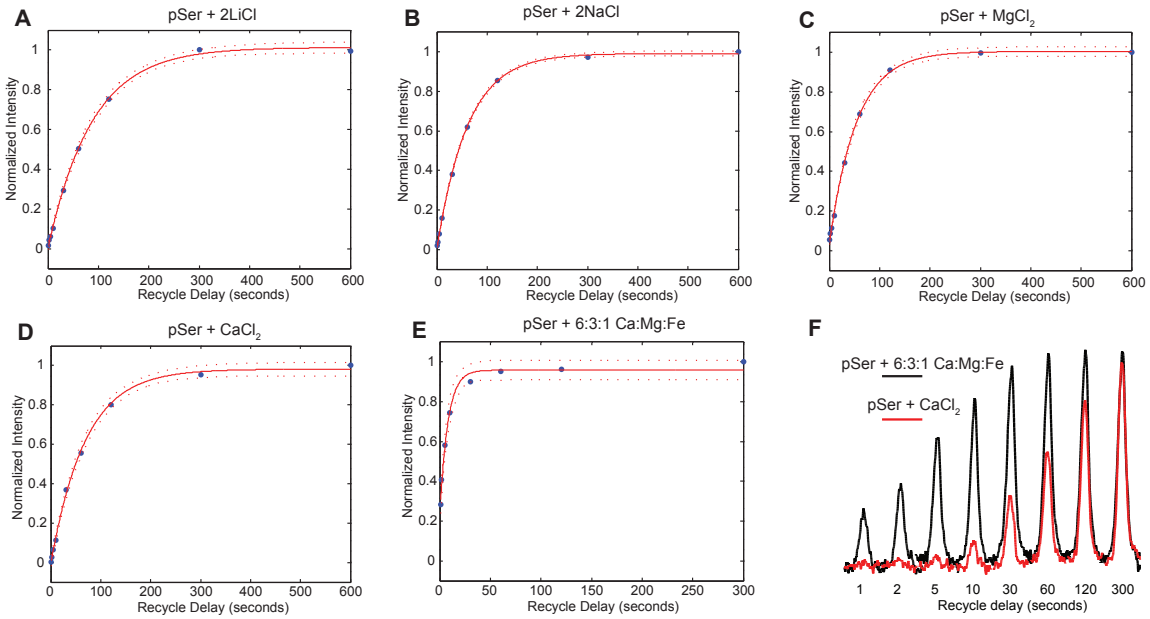

Figure 3.6: ^{31}P T_1 relaxation curves for phosphoserine in the presence of various cations. 6A - 6E show pSer with Li^+, Na^+, Mg^{2+}, Ca^{2+}, and the Fe^{3+} mixture, and figure 3.6F compares the ^{31}P signal buildup for pSer with Ca^{2+} (red) and for the Fe^{3+} mixture (black). Data are shown in blue, the resulting fits with a solid red line, and the 95% confidence intervals with red dashed lines. The 10-fold enhancement of relaxation rates when iron is present as opposed to absent is similar to that observed in native vs. exchanged caddisfly silk

To further investigate the difference in relaxation properties between the native and calcium-exchanged silk samples, spin-lattice relaxation times were measured using

the progressive saturation method [27], and trends were compared to model systems of phosphoserine in the presence of various cations. The ^{31}P T_1 relaxation time for native and calcium-exchanged caddisfly silks were measured at 1 ± 0.5 seconds and 7.6 ± 3.1 seconds, respectively (Figure 3.5, Table 3.1), confirming that the weakened signal observed in Figure 3.4E as compared to 3.4A is simply a result of incomplete spin-lattice relaxation. We propose that the likely explanation for this curious difference is that native caddisfly silk contains paramagnetic Fe^{3+} [15], enhancing ^{31}P T_1 relaxation rates. This paramagnetic effect is lost when cations are stripped from the silk with EDTA. To test this hypothesis, we measured T_1 relaxation rates of phosphoserine in the presence of various cations: lithium, sodium, magnesium, calcium, and a mixture containing a 10:6:3:1 ratio of pSer:Ca^{2+}:Mg^{2+}:Fe^{3+}. In this mixture the concentration of Fe^{3+} approximately mimics that observed in natural caddisfly silks [15]. The data is shown in Figure 3.6, and T_1 data is summarized in Table 3.1. We observe ^{31}P relaxation times in the range of 70 seconds for the phosphoserine samples when iron is not present, which is very common for rigid phosphate materials [31, 32]. However in the mixture, the phosphorus spin-lattice relaxation time is reduced by about 10 fold (Figure 3.6, Table 3.1). While the relaxation rates are certainly different between the hydrated silk materials and the powder phosphoserine model systems, it is the difference between samples with and without paramagnetic iron that is important. While this paramagnetic effect is likely just a coincidence and does not directly benefit the properties of silk, this observation provides additional support that multivalent cations are being removed from the silk fibers with EDTA. This result further highlights the importance of these cations within caddisfly larval silks.

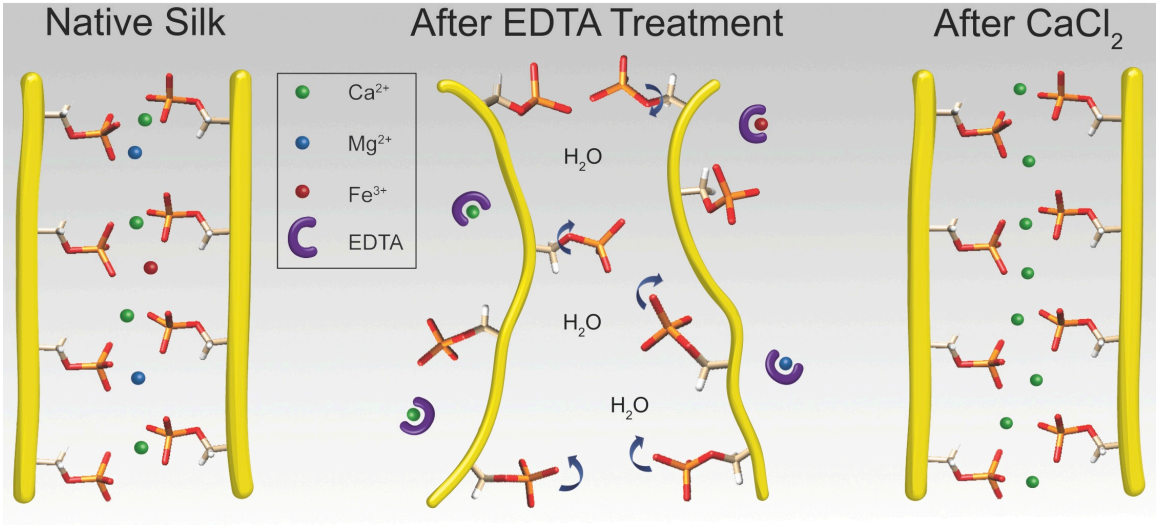

Figure 3.7: The rigid cation-phosphate regions from $(pSX)_4$ repeat motifs in native caddisfly silk (A) are stripped of cations through EDTA chelation. Multiple negatively charged phosphates now reside in close proximity. Water is able to penetrate into these regions and solvate the phosphates, increasing molecular motion to a near liquids-like dynamic regime (B). However when calcium cations are reintroduced to the silk, a rigid phosphorous environment is recovered as phosphorylated $(SX)_4$ repeat regions collapse back into calcium-stabilized β-sheet nanocrystalline structures (C). The phosphoserine side chains are visible, and the protein backbone is represented by yellow tubes.

3.5 Conclusions

Figure 3.7 provides a summary of our findings. ^{31}P solid state NMR data reveals that when cations are removed from caddisfly silks through EDTA chelation, rigid phosphate environments transform into solvated, highly mobile regions. When calcium is re-introduced to the fibers, rigid calcium-phosphoserine complexes are partially recovered. A paramagnetic effect caused by the presence of Fe^{3+} cations within the silk was lost after EDTA treatment, adding further support to the idea that removal of multivalent cations from the silk fibers is responsible for the structural changes observed after EDTA treatment. Additionally, WAXD results show that removal of divalent cations disrupts repetitive β-sheet nanocrystallites within the silk. The data highlights the structural necessity of di- and trivalent cations in caddis-

fly larval silks, and strongly supports a structural motif in which repetitive $(pSX)_4$ interact with calcium magnesium and iron cations to form rigid β-sheet structures [15].

REFERENCES

[1] Gary LaFontaine. *Caddisflies*. The Lyons Press, April 1989.

[2] Glenn B Wiggins. *The caddisfly family Phryganeidae (Trichoptera)*. University of Toronto Press Incorporated, 1998.

[3] J C Morse. Phylogeny of trichoptera. *Annual review of entomology*, 42(1):427–450, 1997.

[4] K M Kjer, R J Blahnik, and R W Holzenthal. Phylogeny of caddisflies (Insecta, Trichoptera). *Zoologica Scripta*, 31(1):83–91, 2002.

[5] Richard E Marsh, Robert B Corey, and Linus Pauling. An investigation of the structure of silk fibroin. *Biochimica et Biophysica Acta*, 16:1–34, January 1955.

[6] Osman Rathore and Dotsevi Y Sogah. Self-assembly of β-sheets into nanostructures by poly (alanine) segments incorporated in multiblock copolymers inspired by spider silk. *J. Am. Chem. Soc*, 123(22):5231–5239, 2001.

[7] O Rabotyagova and P Cebe. Role of Polyalanine Domains in βSheet Formation in Spider Silk Block Copolymers. *Macromolecular Bioscience*, 10:49–59, 2010.

[8] G P Holland, J E Jenkins, M S Creager, R V Lewis, and J L Yarger. Quantifying the fraction of glycine and alanine in β-sheet and helical conformations in spider dragline silk using solid-state NMR. *Chemical Communications*, (43):5568–5570, 2008.

[9] N Yonemura, F Sehnal, and K Mita. Protein composition of silk filaments spun under water by caddisfly larvae. *Biomacromolecules*, 7(12):3370–3378, 2006.

[10] Naoyuki Yonemura, Kazuei Mita, Toshiki Tamura, and František Sehnal. Conservation of Silk Genes in Trichoptera and Lepidoptera. *Journal of molecular evolution*, 68(6):641–653, May 2009.

[11] M S Engster. Studies on silk secretion in the trichoptera (F. Limnephilidae). *Cell and Tissue Research*, 169(1):77–92, June 1976.

[12] M Tsukada, MMR Khan, E Inoue, and G Kimura. Physical properties and structure of aquatic silk fiber from Stenopsyche marmorata 10.1016/j.ijbiomac.2009.10.003 : International Journal of Biological Macromolecules — ScienceDirect.com. *International Journal of Biological Macromolecules*, 46:54–58, 2010.

[13] Y Wang, K Sanai, H Wen, T Zhao, and M Nakagaki. Characterization of unique heavy chain fibroin filaments spun underwater by the caddisfly Stenopsyche marmorata (Trichoptera; Stenopsychidae). *Molecular biology reports*, 37(6):2885–2892, 2010.

[14] J Bennett Addison, Nicholas N Ashton, Warner S Weber, Russell J Stewart, Gregory P Holland, and Jeffery L Yarger. β-Sheet Nanocrystalline Domains Formed from Phosphorylated Serine-Rich Motifs in Caddisfly Larval Silk: A Solid State NMR and XRD Study. *Biomacromolecules*, 14(4):1140–1148, April 2013.

[15] R J Stewart and C S Wang. Adaptation of Caddisfly Larval Silks to Aquatic Habitats by Phosphorylation of H-Fibroin Serines. *Biomacromolecules*, 11(4):969–974, 2010.

[16] Nicholas N Ashton, Daniel R Roe, Robert B Weiss, Thomas E Cheatham, III, and Russell J Stewart. Self-Tensioning Aquatic Caddisfly Silk: Ca 2+-Dependent Structure, Strength, and Load Cycle Hysteresis. *Biomacromolecules*, 14(10):3668–3681, October 2013.

[17] Nicholas N Ashton, Daniel S Taggart, and Russell J Stewart. Silk tape nanostructure and silk gland anatomy of trichoptera. *Biopolymers*, 97(6):432–445, 2012.

[18] M S Creager, E B Butler, R V Lewis, J L Yarger, and G P Holland. Solid-state NMR evidence for elastin-like β-turn structure in spider dragline silk. *Chemical Communications*, 46(36):6714–6716, 2010.

[19] R W Williams, A Chang, D Juretić, and S Loughran. Secondary structure predictions and medium range interactions. *Biochimica et Biophysica Acta*, 916(2):200–204, 1987.

[20] Jan Johansson, Charlotte Nerelius, Hanna Willander, and Jenny Presto. Conformational preferences of non-polar amino acid residues: An additional factor in amyloid formation. *Biochemical and biophysical research communications*, 402(3):515–518, November 2010.

[21] Russell J Stewart, Ching Shuen Wang, and Hui Shao. Complex coacervates as a foundation for synthetic underwater adhesives. *Advances in Colloid and Interface Science*, 167:85–93, 2011.

[22] Janusz W. Strzelecki, Joanna Strzelecka, Karolina Mikulska, Mariusz Tszydel, Aleksander Balter, and Wieslaw Nowak. Nanomechanics of new materials - AFM and computer modelling studies of trichoptera silk. *Central European Journal of Physics*, 9(2):482–491, 2011.

[23] Emma Lang, Gyorgyi I Szendrei, Ilona Elekes, Virginia M-Y Lee, and Laszlo Otvos Jr. Reversible β-pleated sheet formation of a phosphorylated synthetic τ peptide. *Biochemical and biophysical research communications*, 182(1):63–69, January 1992.

[24] M Hollosi, L Urge, A Perczel, J Kajtar, I Teplan, J Otvos, and G D Fasman. Metal Ion-Induced Conformational-Changes of Phosphorylated Fragments of Human Neurofilament (Nf-M) Protein. *Journal of Molecular Biology*, 223(3):673–682, 1992.

[25] S Holly, I Laczko, G D Fasman, and M Hollosi. FT-IR Spectroscopy Indicates That Ca2+-Binding to Phosphorylated C-Terminal Fragments of the Midsized Neurofilament Protein Subunit Results in [beta]-Sheet Formation and [beta]-Aggregation. *Biochemical and biophysical research communications*, 197(2):755–762, 1993.

[26] Andrew E Bennett, Chad M Rienstra, Michèle Auger, K V Lakshmi, and Robert G Griffin. Heteronuclear decoupling in rotating solids. *The Journal of Chemical Physics*, 103(16):6951, 1995.

[27] E Fukushima and SBW Roeder. *Experimental Pulse Nmr: A Nuts and Bolts Approach*. Westview Press, 1983.

[28] DT Grubb and LW Jelinski. Fiber morphology of spider silk: the effects of tensile deformation. *Macromolecules*, 30(10):2860–2867, 1997.

[29] Carole Gardiennet-Doucet, Xavier Assfeld, Bernard Henry, and Piotr Tekely. Revealing Successive Steps of Deprotonation of l- Phosphoserine through 13C and 31P Chemical Shielding Tensor Fingerprints. *The Journal of Physical Chemistry A*, 110(29):9137–9144, July 2006.

[30] Carole Gardiennet, Bernard Henry, Paul Kuad, Bernard Spiess, and Piotr Tekely. Straightforward detection of the secondary ionisation of the phosphate group and pK determinations by high-resolution solid-state 31P NMR. *Chemical communications (Cambridge, England)*, (2):180–182, January 2005.

[31] Christian Jäger, Thea Welzel, Wolfgang Meyer-Zaika, and Matthias Epple. A solid-state NMR investigation of the structure of nanocrystalline hydroxyapatite. *Magnetic Resonance in Chemistry*, 44(6):573–580, 2006.

[32] Xavier Marchandise, Patrick Belgrand, and André-Pierre Legrand. Solid-State 31P NMR Spectroscopy of Bone and Bone Substitutes. *Magnetic Resonance in Medicine*, 28(1):1–8, November 1992.

Chapter 4

STRUCTURAL CHARACTERIZATION OF NANOFIBER SILK PRODUCED BY EMBIOPTERANS (WEBSPINNERS)

4.1 Abstract

Embiopterans produce silken galleries and sheets using exceptionally fine silk fibers in which they live and breed. In this study, we use electron microscopy (EM), Fourier-transform infrared (FT-IR) spectroscopy, wide angle x-ray diffraction (WAXD) and solid-state nuclear magnetic resonance (ssNMR) techniques to elucidate the molecular level protein structure of webspinner (embiid) silks. Silks from two species *Antipaluria urichi* and *Aposthonia ceylonica* are studied in this work. Electron microscopy images show that the fibers are about 90-100 nm in diameter, making webspinner silks among the finest of all known animal silks. Structural studies reveal that the silk protein core is dominated by β-sheet structures, and that the protein core is coated with a hydrophobic alkane-rich surface coating. FTIR spectra of native embiid silk shows characteristic alkane CH_2 stretchings near 2800-2900 cm^{-1}, which decrease approximately 50% after washing the silk with 2:1 $CHCl_3$:MeOH. Furthermore, ^{13}C ssNMR data shows a significant CH_2 resonance that is strongly affected by the presence of water, supporting the idea that the silk fibers are coated with a hydrocarbon-rich layer. Such a layer is likely used to protect the colonies from rain. FTIR data also suggests that embiid silks are dominated by β-sheet secondary structures similar to spider and silkworm silk fibers. NMR data confirms the presence of β-sheet nanostructures dominated by serine-rich repetitive regions. A deconvolution of the serine Cβ NMR resonance reveals that approximately 70% of all seryl residues exist in a

β-sheet structure. This is consistent with WAXD results that suggest webspinner silks are 70% crystalline, which is the highest crystalline fraction reported for any animal silks. The work presented here provides a molecular level structural picture of silk fibers produced by webspinners.

4.2 Introduction

Embioptera (often called webspinners or embiids) produce silken galleries and sheets using exceptionally fine silk fibers in which they live and breed [1, 2]. Embiopterans are unusual insects because they are soft-bodied and flexible even as adults, and to a great extent, rely on silk instead of a tough exoskeleton for protection. Juvenile-form adult females, maternal care, and a colonial life that is defined by shared silk characterize this taxonomic order of insects. They spin silk produced in glands in the basal segment of their front feet (Figure 4.1D) [1]. They step around the head and body as silk issues forth from multiple silk ejectors (for examples of spin step kinematics see Edgerly et al., 2012) [3]. Immatures, as well as adults, spin silk into domiciles that serve as retreats and egg chambers and into covered route-ways that lead to food. The two focal species in this study, *Antipaluria urichi* (Family Clothodidae) and *Aposthonia ceylonica* (Family Oligotomidae), are arboreal and tropical, living on tree bark where they graze on epiphytic algae and lichens within the relative safety of the silk (Figure 4.1A). Arboreal species share silk, affording them protection from predators, especially ants, which typically walk over silk apparently without recognizing that valuable prey lay beneath.

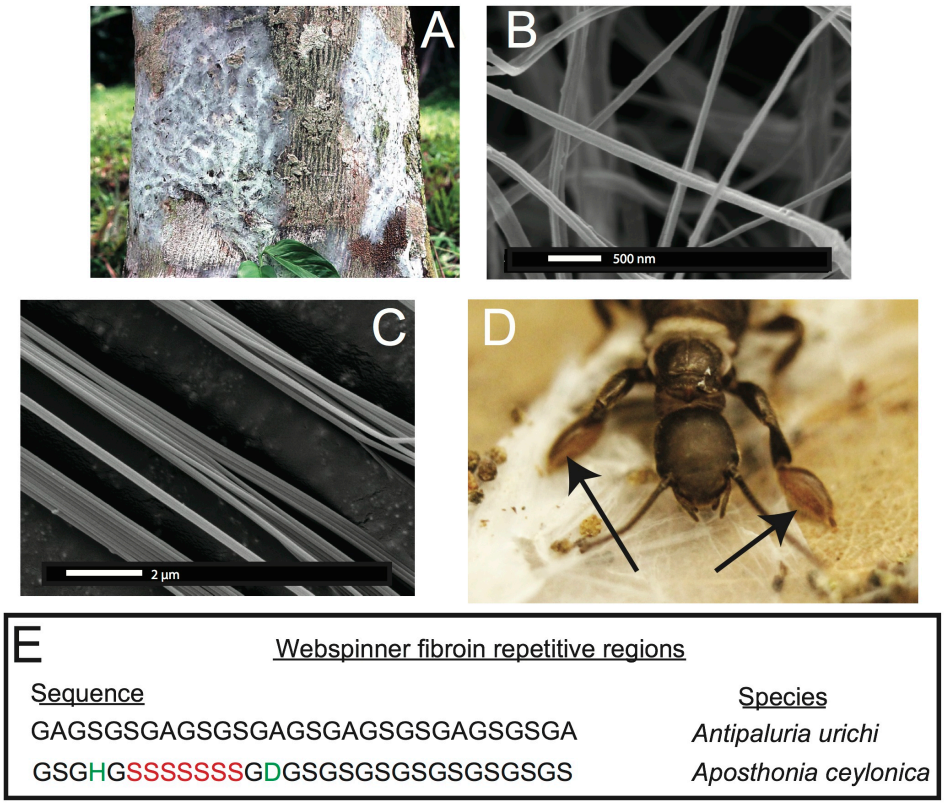

Figure 4.1: (A - D) Optical and SEM images of arboreal embidoptera insect silk from the species *Antiplauria urichi*. The insects spin silken sheets and tunnels that protect and harbor the colonies (A) using exceptionally fine (∼90 nm) fibers (B, C) from their tarsus (forearms), indicated with arrows in (D). Adult insects are approximately 1.6 cm in length. A representation of the repetitive protein regions from both species is shown in (E). Sequences from *Antiplauria urichi* and *Aposthonia ceylonica* silks were obtained from GenBank [FJ361212] and [EU170437], respectively

.

Webspinner silks are among the thinnest of all known silk-based biopolymers, but previous reports of fiber diameters are conflicting. Okada et al. [4] found from SEM images that silks from the Australian webspinner *Aposthonia gurneyi* have fibers with a mean diameter of only 65 nm, while polarized optical microscopy data by Collin et al. [5, 6] found fiber diameters in the range of 500 nm for multiple embiopteran species. This discrepancy is curious, and is addressed in this work.

While the embiopteran taxonomy and behavior have been well studied [1, 3, 7,

8, 2, 9], very little is known about the molecular-level structure of their silks. Significant insight was gained through cDNA sequencing of the primary silk protein sequence from multiple embiopteran species including *An. urichi* and *Ap. ceylonica*, which are the subjects of this study [6, 10]. Representations of the full (approximately 70 kDa) primary protein sequence for both species are seen in Figure 4.1E. Like other silk-based biopolymers [11, 12, 13], webspinner silks are composed of highly repetitive protein sequences in which glycine, serine, and alanine are heavily represented [4, 6, 10]. Although there exists very little experimental data characterizing webspinner silks, the obvious similarities between the embiopteran protein sequence and other well-characterized fibroin biopolymers allows us to make predictions. Silkworm and spider silks are also composed of highly repetitive proteins that contain runs of poly(GA) and poly(A) [14, 15]. It is well known that these repeat motifs form water-inaccessable antiparallel β-sheet structures that are aligned along the fiber axis, and these rigid, nanocrystalline β-sheets are thought to be responsible for the impressive mechanical strengths of both spider and silkworm silks [16, 17, 18]. When one looks at the cDNA sequences for many embiid silks [10], similarities are observed but alanine appears to have been mostly replaced by serine. Instead of runs of poly(GA), embiopteran primary protein sequences are dominated by runs of poly(GS) or GAGSGS repeats. Instead of runs of poly(A), some webspinner silks contain runs of poly(S). Serine has a higher propensity to adopt a β-sheet environment than alanine because of its ability to form side chain intra-sheet hydrogen bonds [19, 20, 21], therefore similar nanocrystalline β-sheet structures are fully expected from poly(GS), GAGSGS and poly(S) repeats found in embiopteran silks. Indeed, previous Fourier transform infrared spectroscopy studies on embiopteran silks have suggested that the fibers are dominated by β-sheet secondary structures within the protein core, presumably arising from said repetitive protein motifs [6, 10, 5, 4].

These β-sheet structures within webspinner silks are potentially nanocrystalline and well aligned with respect to the fiber axis, similarly to other well-characterized silks. The percentage of the total fiber content that is nanocrystalline varies significantly among animal silks. Studies on spider dragline silk fibers show that the crystallinity content ranges from about 30% (*Nephila clavipes*) to 40% (*Latrodectus hesperus*), [22, 23] while fibers from the domesticated silkworm are typically higher, in the range of 40-60% crystallinity [24, 25]. The crystalline fractions arise mainly from repeated sequences, thus the primary protein sequence for webspinner silks should yield predictive power; protein secondary structure within spider dragline silk fibers has been shown to correlate quantitatively with silk primary protein sequences [26, 23]. With the exception of short C-terminal domains, the protein sequences of many embiopteran silks are virtually entirely composed of repetitive motifs, which likely adopt a β-sheet structure. For example, if all of the repeat domains within embidopteran silk from the species *An. urichi* adopt a β-sheet nanocrystalline structure, then the percent crystallinity may be upwards of 90%. If true, embidopteran silks are substantially higher in nanocrystalline content than other well characterized silk biopolymers. To the best of our knowledge, no attempt has been made to measure the nanocrystallite size, orientation or crystalline fraction of any webspinner silks, which we address in this work through Wide Angle X-ray Diffraction (WAXD) techniques.

We are interested in better understanding the hierarchical structure of webspinner silks. Considering the many similarities in primary protein composition, it would not be surprising if the hierarchical structure of webspinner silk is similar to that of other well-characterized silks. The current skin-core model for spider dragline silks, for example, is a fibrous protein core that is encapsulated by a thin protective lipid-like coating [27]. As discussed, the protein core of spider dragline silk is composed of nanocrystalline β-sheet structures with dimensions of a few nanometers aligned

along the fiber axis, separated by loosely-organized sheet, helical or randomly-oriented domains [28, 29, 30, 31]. This protein core is surrounded by a thin protective coating that is rich in long chain lipids and alkanes [32, 33, 34]. Very little work has been performed characterizing this outer protective coating on spider silks, although Schulz et al. [34] conducted a thorough GC-MS analysis of the lipid and hydrocarbon content in silk from the orb weaver spider *Nephila clavipes*, revealing the presence of mostly long chain alkanes and methoxyalkanes of chain length between C_{28} and C_{34}. The role of the lipid or alkane-rich surface coating is unclear, but it likely serves to both waterproof the silk fibers and maintain moisture within the silk core [32]. Based on observations in the field and on laboratory colonies, embiopteran silken galleries are remarkably water-repellant, thus it is feasible that along with a β-sheet dominated protein core webspinner silk fibers possess a similar lipid or alkane-rich surface coating that serves a waterproofing purpose. Water-repellency would appear an especially adaptive trait for *An. urichi*, a tropical rainforest species from Trinidad and Tobago. Their colonies live on tree bark where they feed on epiphytic algae and lichens from within the protective covering of their silk. Rainfall is heavy, often torrential, and yet water appears to flow over the surface of the silk, leaving the insects dry beneath. *Ap. ceylonica* species are subtropical and tropical as well and are likely exposed to similar environmental conditions as the Trinidadian species. The availability of these two species in laboratory cultures and of published work on their silk provided us with an opportunity to further investigate the functional and structural aspects of embiopteran silk.

Interestingly, a few other silk-producing insects are known to contain a significant lipid content [35, 36]. It is often challenging to characterize a surface coating on spider silks with NMR techniques because this layer is thin relative to the overall fiber size and therefore hard to detect. The exceptionally fine fiber diameters of embiid silks provides us with a unique opportunity to observe and characterize any

surface coating in addition to the protein core because of the higher surface area to volume ratio. In this present study, we use SEM, TEM, FT-IR, WAXD and solid-state NMR techniques to help elucidate both molecular-level protein structure within the silk fiber core, and to interrogate the alkane-rich surface coating surrounding the silk fibers.

4.3 Materials and Methods

Silk collection Cultures of approximately 50 *An. urichi* and *Ap. ceylonica* were established in separate plastic terrariums with dry oak leaves used as substrate. The insects were fed fresh romaine lettuce leaves every few days. The colony was misted with tap water every few days to maintain moisture and humidity within the domicile. The insects would spin silken sheets and tunnels, and the clean areas of these freshly spun networks were removed from the terrarium. Any visible debris (fragmented oak leaves, pebbles, dirt and waste) were removed from the silk using a pair of fine forceps under a dissecting microscope.

Fourier Transformed Infrared Spectroscopy FT-IR analyses were performed using a Thermo Nicolet 6700 spectrometer equipped with an attenuated total reflectance (Smart Orbit ATR) accessory. For each sample, silk bundles were pressed onto a diamond window of the ATR attachment, and 64 scan averages were collected after 128 background scans.

Scanning Electron Microscopy Cleaned webspinner silks were secured to conductive carbon tape, then were gold coated using a Denton vacuum sputter coater for 3 minutes at a deposition rate of 5 nm/min. The SEM was performed using a XL30 Environmental SEM-FEG built by FEI. The secondary electron (SE) detector was used for imaging. Images were collected under a vacuum pressure of less than

9 x 10^{-5} mbar and with a beam current of 5 kV. SEM images were processed using Gwyddion version 2.31 to measure fiber diameters from multiple images [37].

Transmission Electron Microscopy Cleaned webspinner silk samples were immersed in 0.5% aqueous uranyl acetate and incubated 30 min at room temperature. An untreated control group was run in parallel and incubated in deionized water only. Both groups were washed with 3 consecutive changes of deionized water and allowed to air-dry overnight. Samples were then incubated in 3 consecutive changes of Spurrs epoxy resin over several hours, flat-embedded on Teflon-coated glass slides, and polymerized at 60°C for 24 hrs. Segments containing multiple fibers were cut from the thin resin layer and re-embedded in flat polymer molds to obtain the desired cross-sectional orientation for microtomy. Sections were cut at 70 nm thickness with a diamond knife on a Leica Ultracut-R microtome. Images were generated on a Philips CM12 TEM operated at 80kV and captured with a Gatan model 791 CCD camera. TEM images were processed using Gwyddion version 2.31 to measure fiber diameters [37].

Wide Angle X-ray Diffraction Embiid silk fibers were aligned parallel across a cardboard washer using a small amount of super glue at either end. Wide-angle x-ray diffraction measurements were collected at the Advanced Photon Source located at Argonne National Laboratory, Argonne IL, USA on the BioCars 14BM-C beamline which has x-ray wavelength of 0.9787 Å(12.668 keV) and a beam size of 130 x 340 μm (FWHM). The samples were mounted on a goniometer 300 mm from the ADSC Quantum-315 9-panel CCD array detector with the fibers offset a small angle from the beamstop to better view the meridian reflections. The exposure time was 60 seconds for each of ten images averaged and 5 background images were taken with the same parameters to remove air scattering. Images were then processed using Fit2D x-ray processing software and calibrated with cerium dioxide (CeO_2).

Peptide Preparation A peptide model, GSGHGSSSSSSSGDGSGSGSGSGSGS-GSGA, was synthesized using Fmoc-chemistry to mimic webspinner silk of the species *Ap. ceylonica*. A fully automated microwave-assisted peptide synthesizer (Liberty 1 by CEM) was used to prepare the peptide on the 0.1 mmol scale. The crude peptide was cleaved from the resin (preloaded Alanine-Wang resin from AAPPTEC) for 4 hours using a standard cleavage cocktail (95:2.5:2.5 TFA:TIS:H_2O). The crude peptide was precipitated out of TFA using cold diethyl ether, and after several ether washes, the crude peptide was dried, dissolved in 6M LiBr, and dialyzed against water at 4 °C for 4 days. Any water-insoluble peptide was centrifuged out, and solubilized peptide was recovered by lyophlization. This lyophilized peptide represents *Ap. ceylonica* silks in a random-coil structure. Some of this peptide was dissolved in Formic acid and carefully pipetted onto a clean glass surface. The peptide crystallized into a β-sheet structure upon slow evaporation of Formic Acid. Peptides were then characterized using NMR spectroscopy.

Solid-State NMR. ^{13}C solid-state NMR experiments were conducted on a 400 MHz Varian wide-bore instrument equipped with a 1.6 mm triple resonance MAS probe. Samples were spun at the magic angle at 30 kHz. ^{13}C chemical shifts were referenced externally to TMS by setting the downfield adamantane resonance to 38.56 ppm. ^{1}H $\rightarrow$ ^{13}C Cross Polarization under Magic Angle Spinning (CP-MAS) conditions were optimized using U-[^{13}C, ^{15}N] glycine. For CP experiments, typical experimental conditions used were an initial 2 μs proton $\pi/2$ pulse, a 1 ms ramped ($\sim$15%) spin-lock pulse at a maximum of 150 kHz on the ^{1}H channel, and a square contact pulse set to the -1 spinning side band of the Hartmann-Hahn profile on the ^{13}C channel. A 100 kHz spectral width was used with 20 ms acquisition time, a 5 second relaxation delay, and 10240 scan averages. Direct Detection under Magic Angle Spinning (DD-MAS) experiments on hydrated embiid silk samples used a 2.5 μs $\pi/2$ pulse, 20 ms

acquisition time, 100 kHz spectral width, a 1 second relaxation delay, and 40960 scan averages. All CP and DD-MAS experiments were collected using 150 kHz TPPM [38] proton decoupling during acquisition. To collect data on hydrated samples, silks were first soaked in DI water for at least 30 minutes then blotted with a Kim-Wipe to remove excess water.

4.4 Results and Discussion

Fiber Diameters

Silk from the embiopteran species *Antipaluria urichi* and *Aposthonia ceylonica* were studied using SEM, TEM, FT-IR, WAXD and NMR spectroscopy to characterize the molecular-level protein structure as well as a hydrophobic surface coating rich in long-chain lipids and alkanes. Figure 4.1 shows both optical and SEM images of insects and silk produced from *An. urichi*. The insects produce silk out of their tarsal organs, or forelimbs, creating very thin sheets of silk protecting the colonies. An example of a silk in a natural, arboreal setting can be seen in Figure 4.1A. Fiber diameters from *An. urichi* were determined using SEM and TEM microscopy. Previous work by Collin et al. [6, 5] reported fiber diameters in the range of 500 - 800 nm. However, the authors used polarized light microscopy techniques and thus could not resolve fibers below the optical resolution limit. Figure 4.1C shows how one could easily be fooled; it is likely that the authors were observing bundles of webspinner silks and were unable to resolve fine detail. Figure 4.2 shows a histogram of *An. urichi* fiber diameter measurements made from 68 isolated fibers over multiple SEM images and 82 fibers from TEM images. The fibers for SEM imaging had been coated with a layer of gold approximately 15 nm thick, thus 30 nm was subtracted from each edge to edge measurement. The average size was 93 $\pm$ 15 nm (one standard deviation), which is more consistent with the 65 nm fibers reported for a different webspinner

species [4]. For TEM imaging, fiber bundles were stained by submerging in an aqueous solution containing 0.5% uranyl acetate for 30 minutes prior to resin embedment. The average fiber diameter over 82 measurements from 3 separate TEM images was 100 ± 15 nm. This is slightly larger than the 93 nm average result from SEM images, but we note that these fibers were soaked in an aqueous-based uranyl acetate stain prior to resin embedment and thus we are potentially observing a slight swelling of the fibers due to water absorption. This observation brings doubt into the validity of previous mechanical testing results on embiid silks. Webspinner silks show elasticity similar to spider silks (15-40% extensibility), but silk strengths were reported at only about 150 MPa [5, 6]. If correct, this is many times weaker than spider dragline fibers and silkworm silk. As a silk used primarily for structural and protective purposes and not for absorbing impact, it would be surprising if webspinner fibers possess similar gigapascal-level strengths as spider dragline fibers. Nevertheless, embiopteran silk galleries must be strong enough to both deter predators, which often walk on top of the silk.

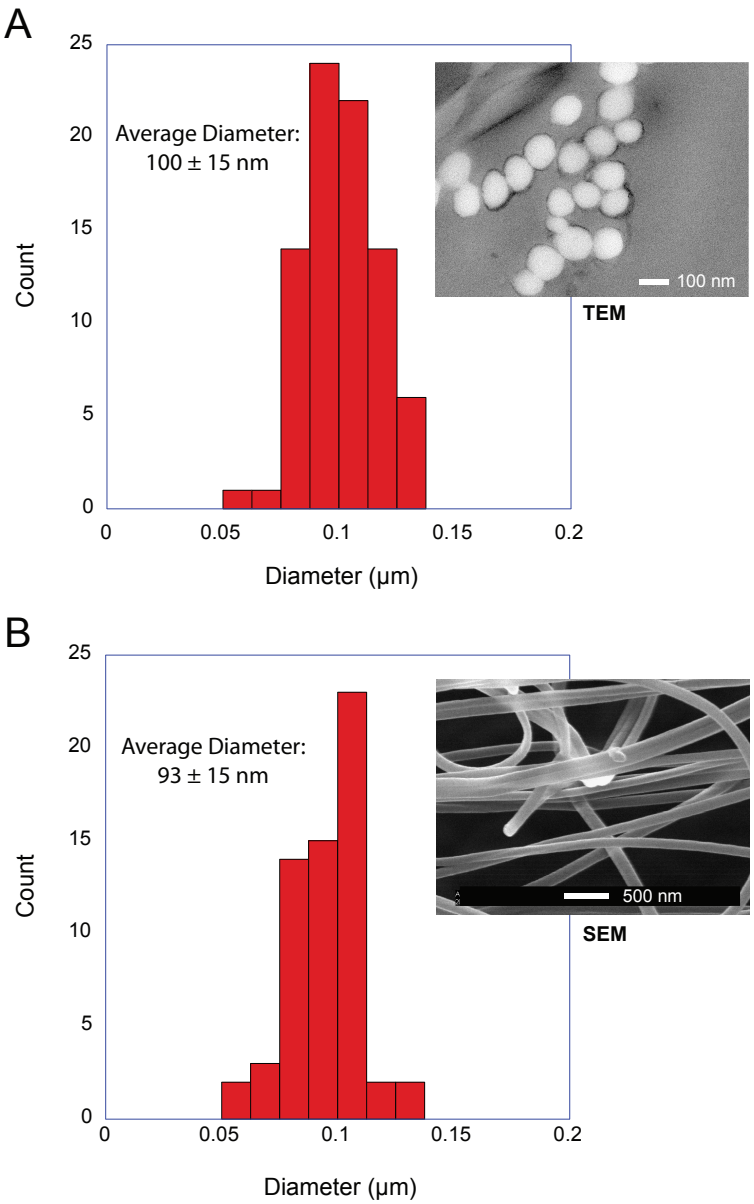

Figure 4.2: Fiber diameter distribution for silk obtained from adult female *Antipaluria urichi* using electron microscopy. 82 and 68 separate measurements were combined from multiple TEM (A) and SEM (B) images, respectively. The results indicate that *An. urichi* silk fibers are approximately 90 - 100 nm in diameter.

To the best of our knowledge, the only available mechanical data obtained on silk produced by webspinner insects is unreliable due to improper fiber diameter measurements. Therefore in an attempt to better estimate embiid fiber tensile properties, we

collected tensile stress-strain curves on silk bundles prepared for *An. urichi*. Samples were prepared by carefully brushing an E-shaped cardboard card across the tarsus of adult female insects of *An. urichi*. Fibers were superglued to each of the three anchor points on the E. Stress-strain curves were obtained by stretching one side of the E-shaped card at a rate of 1% per second, while the other unstretched side was analyzed using SEM to approximately obtain the number of fibers present. Additional experimental details and results are included as supplemental material. Results suggest that webspinner silks are significantly stronger than previously thought; we observed an average of 500 MPa mean ultimate stress and about 30% extensibility over 14 measurements. Due to the small fiber diameters and extreme difficulty in obtaining consistent samples, this result should only be interpreted as a rough estimate.

Infrared Spectroscopy: Surface coating and protein core

An additional key feature of embiopteran silken galleries is the ability to prevent water from penetrating into the silk networks. While composed primarily of protein, their silk is exceptionally hydrophobic; silken sheets protecting colonies do not appear to allow water to penetrate into the domiciles. If the surface of the silks were composed of glycine, alanine and serine-rich protein, one might expect water to easily penetrate a thin layer of silk. The hydrophobic nature of the silk suggests some form of lipid or alkane-rich surface coating similar to the water repelling layer found on spider silks [32, 33, 27]. Our results provide evidence for such a surface coating. FT-IR data and NMR data both show the presence of alkanes even after washing the silk with the detergent sodium dodecyl sulfate (SDS), indicating that the surface layer must be significantly longer than C_{12} as to not be removed by SDS. Indeed, initial GC-MS analysis of a $CHCl_3$:MeOH extraction from *An. urichi* silk shows the presence of straight and branched-chain alkanes of at least length C_{34}, and likely even longer (supporting information). FT-IR spectra seen in Figure 4.3 on native webspinner

silks show characteristic alkane CH_2 symmetric and asymmetric stretch absorbances at 2850 and 2920 cm^{-1}, respectively [39]. We attribute this to alkane CH_2 absorbance from the hydrocarbon-rich surface coating on the silk. Previous FT-IR studies on embiopteran silks also show a large CH_2 absorbance, but it was not assigned [4]. The native silk samples were then treated with 2:1 mixture of $CHCl_3$:MeOH overnight in attempt to remove any surface lipid or alkane-rich layer, and FT-IR analysis was then repeated on the treated silk samples. The amide I and amide III bands did not change suggesting that the protein structure remained unaffected (supporting information), but the alkane CH_2 stretchings dropped approximately 50% in intensity after extraction (Figure 4.3B). This result clearly shows the presence of a lipid or alkane-rich surface coating. It also becomes clear that the surface coating is not covalently attached to the protein core, so perhaps this surface layer is co-secreted along with the protein fiber.

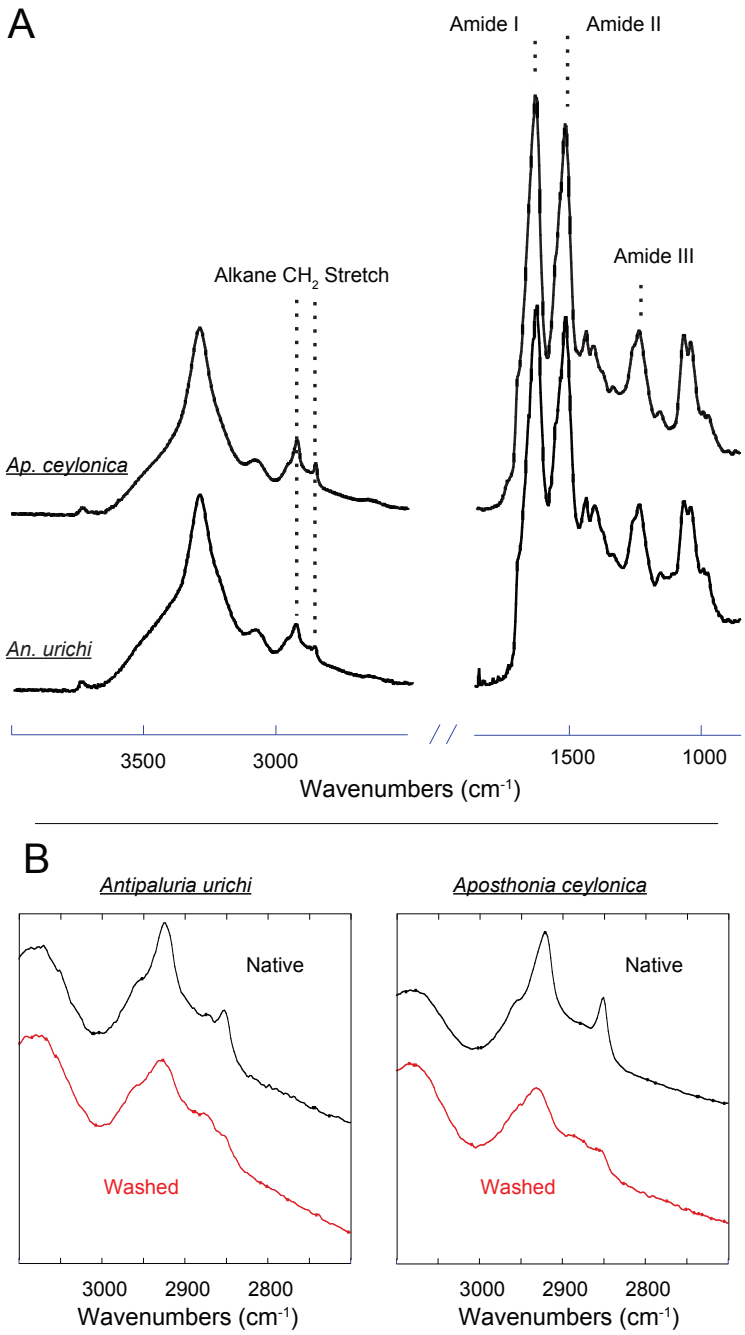

Figure 4.3: A: FT-IR spectra of native *Antipaluria urichi* and *Aposthonia ceylonica* silk bundles. The strong amide I and II absorbances at 1625 and 1514 cm^{-1}, respectively, suggest that the protein core is predominantly β-sheet. B: Native webspinner silks (black) are compared to silks that were washed with 2:1 $CHCl_3$:MeOH for 24 hours (red). Amide I, II and III bands remain unchanged (data not shown), but the alkane CH_2 symmetric and asymmetric stretches at 2850 and 2920 wavenumbers, respectively, drop approximately 50% in intensity after treatment. This is associated with the removal of a lipid or alkane-rich surface coating on the silk fibers.

The protein core structure was also analyzed using infrared spectroscopy. FT-IR is an extremely common technique used to study protein secondary structure of silk-based biopolymers; some examples include silks produced from silkworm [40, 41, 42, 43], spiders [42, 44] caddisfly larvae [45], silverfish [46], lacewing [36], and webspinners [4, 5]. The amide I, II and amide III absorbances are commonly used to infer protein secondary structure. There seems to be a general consensus in the literature regarding the amide I band, but significant debate in assigning secondary structures to components of the amide III band. For example, the amide III β-sheet and random coil absorbances were assigned at 1263 and 1230 cm^{-1} respectively for silkworm silk from *Bombyx mori* [40], but are assigned to 1222 and 1242 cm^{-1} for silkworm silk from *An. pernyi*. It is possible that the inversion of peak location is a result of different repetitive motifs; *Bombyx mori* silk is dominated by poly(GA) and GAGAGS units while *An. pernyi* contains runs of poly(A) similar to spider silks. In support, careful secondary structure assignments to the amide III band for poly(A)-rich spider silks agree well with *An. pernyi* but not with *Bombyx mori* [42]. Thus the primary protein sequence has a major impact on FT-IR absorption peak positions, as does fiber strain and overall secondary structure [47]. Considering significant variation in peak position, width, and shape, we think that a quantitative deconvolution of FT-IR absorbance bands will not give convincing results. Qualitative and especially comparative analysis of IR absorbance profiles, however, can be extremely powerful. Figure 4.4 shows that the FT-IR absorbance profile of *An. urichi* is virtually identical to that of *Ap. ceylonica*. The strong amide I absorbance maximum at 1627 wavenumbers is identical to reports from Okada et al. [4] on webspinner silk from the congener *Ap. gurneyi*, which is similarly dominated by poly(GS) and poly(S) motifs. For comparison, the amide I band for β-sheet-rich silkworm silk is found at 1615 cm^{-1} (supporting information). The shift towards higher frequency absorbance for webspinner silk rel-

ative to silkworm silk could be attributed to a larger random coil component, as is often done in the literature through peak deconvolution. While this is a possibility, we think it is more likely that the shift in frequency is a result of differing primary protein sequences rather than a lower β-sheet fraction, especially when considering the high expected crystalline fraction for webspinner silks. Amide I absorbances from random-coil structures are typically found near 1650 cm^{-1} while β-sheet structures show absorbances at lower frequencies (1620 cm^{-1}) [48]. Additionally, the shoulder absorbance at 1695 cm^{-1} is regularly assigned to β-sheet protein structures [48, 40], thus it is quite clear that like silkworm silks, webspinner silk fibers are dominated by β-sheet structures, and are remarkably similar across species.

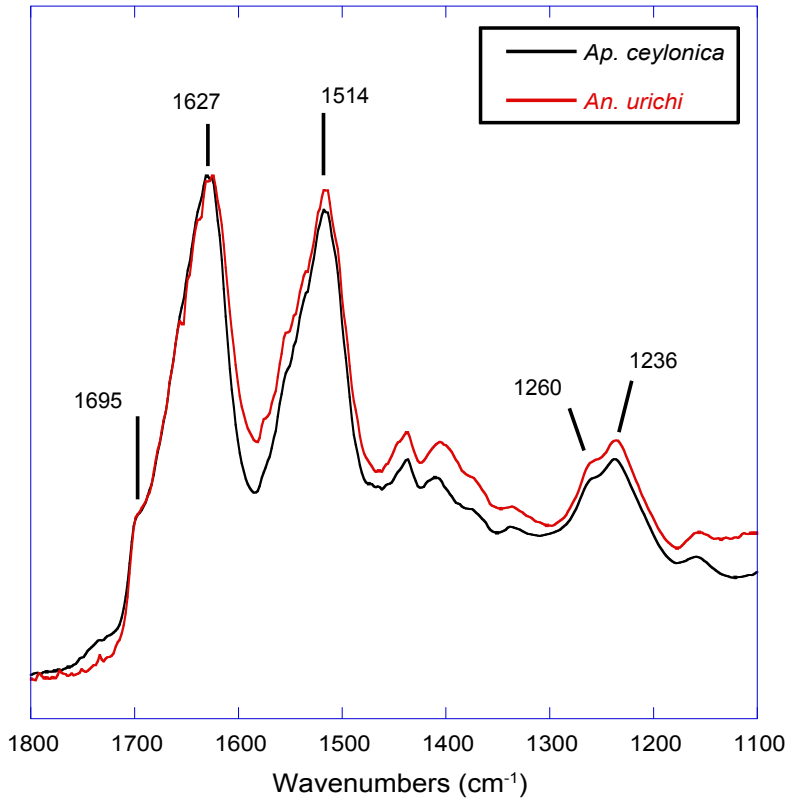

Figure 4.4: FT-IR absorbance profiles comparing webspinner silks from the species *Antipaluria urichi* (red) and *Aposthonia ceylonica* (black). Spectra are virtually identical, emphasizing their remarkable similarity in structure.

Wide Angle X-ray Diffraction

Characterization of webspinner silk from *An. urichi* by wide-angle x-ray diffraction (WAXD) indicates an amorphous fraction with diffuse scattering and a crystalline fraction comprised of nanocrystalline β-sheet structures. The diffraction pattern observed for axially-aligned webspinner silk from *An. urichi* shown in Figure 4.5A closely resembles our previously published spider silk patterns, confirming the presence of regular nanocrystalline β-sheet structures within the silk protein core [49, 22]. Careful analysis of the WAXD profile gives crystallite size, orientation of the nanocrystallite with respect to the fiber axis, and the overall percent crystallinity of the fiber. The 12 highest intensity unique reflections were identified and assigned to an orthorhombic unit cell of dimensions a = 6.6 $\mathring{A}$, b = 9.6 $\mathring{A}$, c = 19.2 $\mathring{A}$. Each reflection was fit as an individual component in d spacing using an iterative Gaussian fitting protocol until it converged. The radial broadening of the crystalline reflections, as demonstrated by the full width at half max (FWHM) in 2θ space (Figure 4.5C, 4.5D), was used to calculate the average crystallite size along the a, b, and, c axes using Scherrers formula. This resulted in crystallite dimensions of 3, 4, and 5 nm in the a, b, and c axes, respectively [24]. Azimuthal broadening of the crystalline reflections is indicative of variance in alignment of the crystalline fraction with respect to the fiber axis. Hermans orientation factor of the crystalline fraction, f_c, was calculated to be 0.93, from the FWHM of radial integration at 4.3 $\mathring{A}^{-1}$ where $f_c = (3(\cos^2\phi)\text{-}1)/2$ and ϕ is the angle between the c axis of the nanocrystallite and the fiber axis. Difficulty manually aligning the silk fibers during sample preparation leads to fiber misalignment, which means this is a low estimate of the actual nanocrystallite orientation within the fiber. The overall crystalline fraction can be estimated as a fraction of the area represented by radial integration 15° on either side of the equator for the equatorial (200) and (120) crystalline peaks relative to the area represented by the integrated intensity

of the full diffraction pattern resulting in 69% crystallinity. This high crystallinity content is likely due to the high fraction of repetitive motifs and significant serine content, both of which correlate to increased β-sheet content in the silk protein core.

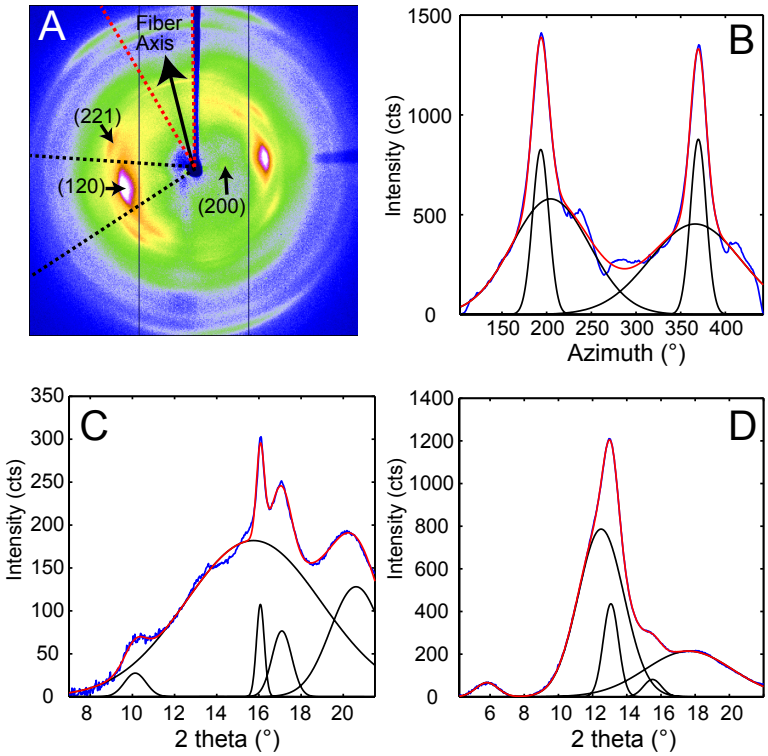

Figure 4.5: Summary of Wide Angle X-ray Diffraction (WAXD) data. (A) 2D WAXD pattern of axially aligned webspinner silk from *Antipaluria urichi*. The fiber axis relative to the beamstop shadow (vertical) is indicated with the arrow. Equatorial reflections (120) and (200) are associated with nanocrystalline β-sheets, and the (221) reflection is associated with the amorphous component. (B) 1D azimuthal intensity profile of narrow ring around the (120) reflection (4.3 $\mathring{A}^{-1}$) starting at the beamstop and continuing counter-clockwise. (C) 1D radial intensity profile of the meridian wedge, indicated with red dashed lines in (A). (D) 1D radial intensity profile of the equatorial wedge, indicated with black dashed lines in (A).

Solid-State NMR

To get a more complete understanding of both the silk protein core and the encapsulating surface coating, we used solid-state NMR techniques on both native and $CHCl_3$:MeOH-washed silks in their dry and hydrated states. Solid-state NMR is a very powerful tool for characterizing biopolymers; it has been widely utilized to eluci-

date molecular-level environments of repeat motifs such as poly(GA) and poly(A) in silkworm and spider silks, respectively. For embiid silks from both species discussed in this work, glycine and serine are the most dominant amino acids represented at approximately 45% and 36%, respectively [10]. The ^{13}C chemical shift of glycine Cα is not very sensitive to secondary structure, however both the alanine and serine Cα and especially Cβ chemical shifts are influenced dramatically by local conformation [50, 51]. ^{13}C chemical shifts have been used extensively to identify secondary structures within silk-based biopolymers, and can be applied here to elucidate molecular level environments within embiid silks. Cleaned, native silk from *Ap. ceylonica* and *An. urichi* were studied with ^{13}C solid-state NMR spectroscopy. ^{13}C resonances for the three most abundant amino acids are assigned, and secondary structures are indicated (Figures 4.6, 4.7). We are limited in the amount of information we can extract from ^{13}C data on naturally-abundant samples, but we can still draw many strong conclusions. For one, serine exists predominantly in β-sheet structures based on the ^{13}C chemical shifts observed for serine Cβ (Figure 4.6). As indicated in Figure 4.6, the serine Cβ resonances in the CP-MAS spectra lie at 64.5 ppm, a shift consistent with serine in a β-sheet environment. Serine from GAGSGS and poly(S) repeat motifs are most likely responsible for this observation. We also can see a minor shoulder at 62 ppm that is assigned to serine containing regions in a randomly-oriented environment.

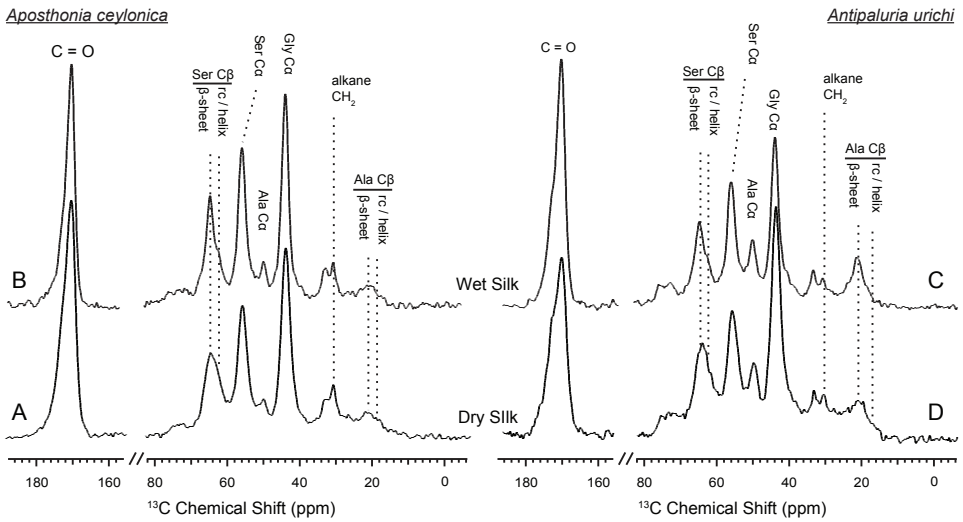

Figure 4.6: ^{1}H - ^{13}C CP-MAS NMR spectra on wet (top) and dry (bottom) embiid silks from *Aposthonia ceylonica* (left) and *Antipaluria urichi* (right). The three most common amino acids have been assigned, and secondary structures are indicated for serine and alanine Cβ resonances. An alkane CH_2 peak is clearly present in both silks. Silk from both species appears structurally very similar, although *An. urichi* contains significantly more alanine than *Ap. ceylonica*.

Further confirmation of the secondary structural assignments where made by comparing $^{1}H \rightarrow {}^{13}C$ CP-MAS NMR data of peptides mimicking webspinner repetitive motifs that were either trapped in a random-coil confirmation or crystallized into a β-sheet structure from formic acid (Figure 4.8). To mimic webspinner silk in a random-coil structure, a 30 AA peptide representing the protein sequence of *Ap. ceylonica* silk (illustrated in Figure 4.1E) was synthesized using solid-phase peptide synthesis, dissolved in 6M LiBr, dialyzed against DI water for 4 days, and then lyophilized. The peptide was then dissolved in formic acid and slowly dried, inducing a β-sheet structure. This method is commonly used to capture silkworm model peptides in both random-coil and β-sheet conformations [52, 53]. $^{1}H \rightarrow {}^{13}C$ CP-MAS data was collected on both peptides (4.8A). Using DMFIT software [54], the spectra for random-coil and β-sheet model peptides were independently fit to extract precise ^{13}C chemical shifts, peak widths, and % Gaussian vs. % Lorentzian line shapes. This

information was then used to deconvolute NMR spectra for native silks to approximate β-sheet content; only peak amplitudes were allowed to vary when fitting native webspinner silk data. Deconvolution of NMR data obtained for *Ap. ceylonica* (4.8B) and *An. urichi* (data not shown) silks indicate that serine Cβ, the residue most isolated and most sensitive to secondary structure, is approximately 70% β-sheet and 30% random-coil for both species. This estimation is consistent with both our FT-IR and our XRD data in that FT-IR absorbance profiles for the two species suggest that the silk protein structures are virtually identical and are dominated by β-sheet structures, and that analysis of XRD results reveal that *An. urichi* silk is 70% crystalline. The alanine Cβ resonance shows a similar story in both silks, although it is more clear for *An. urichi* silk fibers where alanine is better represented (4.6C, 4.6D). Alanine, found almost exclusively in GAGSGS repeat motifs from *An. urichi* silk, clearly exists predominantly in β-sheet structures.

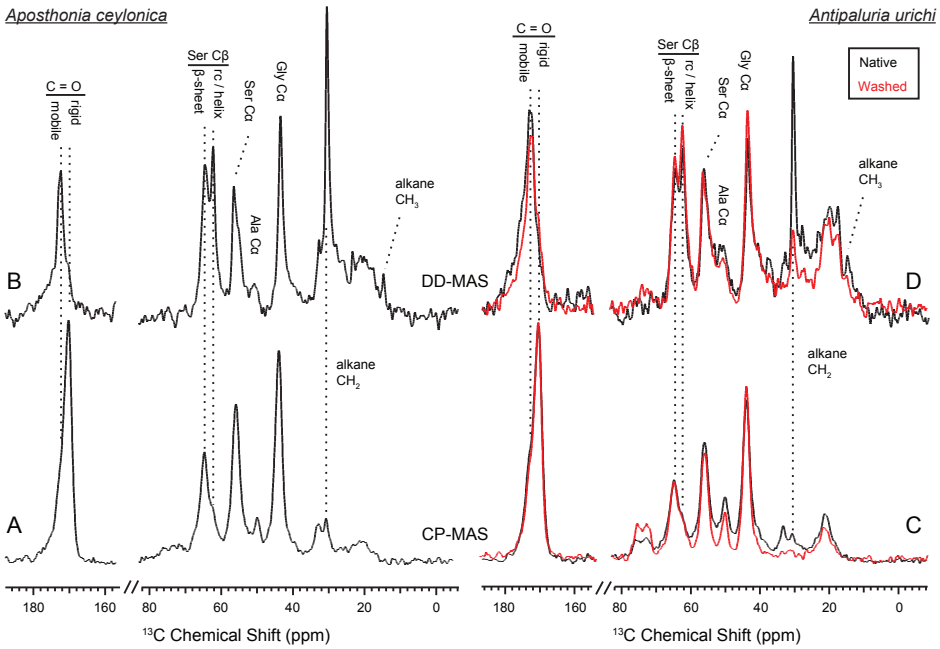

Figure 4.7: ^{1}H - ^{13}C CP-MAS (bottom) and DD-MAS (top) NMR on wet embiid silks from *Aposthonia ceylonica* (left) and *Antipaluria urichi* (right). Data from native silks is seen in black, while experiments performed on *An. urichi* silk that was extracted with 2:1 $CHCl_3$:MeOH is overlaid in red. Peaks observed in the direct spectra are significantly plasticized by water, while those observed in the CP spectra are from more rigid regions. The CH_2 alkane resonance is clearly affected by water, suggesting its presence on the fiber surface. A new CH_3 peak is seen in the direct spectra at 14 ppm, which we assign to terminal or branded alkane methyl groups from the surface coating.

The contrast between CP and DD-MAS spectra in Figure 4.7 is very useful to highlight rigid versus mobile regions of hydrated silks [55, 56, 57, 58]. Domains of the silk that are affected by water will typically have shortened ^{13}C T_1 and longer T_2 relaxation times due to increased molecular motion, thus are easily seen as sharp peaks in the direct spectra. The DD-MAS experiment uses a fast (1 second) recycle delay so that ^{13}C resonances from rigid regions of the silk with long T_1 relaxation properties become saturated and therefore are not observed. While the majority of serine adopts a β-sheet structure within the silks, a new sharp resonance emerges in the direct spectra from both species at 62.2 ppm. This peak corresponds to serine Cβ in a random coil or loose helical environment. Serine is found almost exclusively in

poly(GS), poly(GAGSGS) or poly(S) repetitive motifs in both silks, therefore not all seryl residues from these repeats exist in a β-sheet structure. A native silk gallery will naturally repel water due to its hydrophobic coating, but in this case we encouraged hydration of the fibers by completely submerging the silk samples in water. Perhaps when the silk becomes forcibly hydrated, poly(GS) and GAGSGS repeats from *Ap. ceylonica* and *An. urichi* silks are stable in both conformations, or can exchange between sheet-like and randomly-oriented structures on a slow timescale. Alanine resonances are weak from *Ap. ceylonica* silks, but we also observe a sharp peak emerge at 17.5 ppm for alanine Cβ from *An. urichi* silk in the direct spectra. Similar to the random coil serine Cβ peak evident by the sharp peak at 62.2 ppm, a portion of alanine also appears to adopt a random coil environment. Alanine from *An. urichi* silks comes from GAGSGS repeat domains, further supporting the idea that such repeats are found in both sheet-like and random structures when hydrated. For comparison, *Bombyx mori* silkworm silk is dominated by similar GAGAGS repeat domains, however a parallel experiment conducted on these fibers does not result in an emerging sharp helix or random-coil resonance upon fiber wetting. It appears then that when water penetrates into and solvates webspinner silk fibers, a higher fraction of silk protein becomes mobile as compared to similar regions of silkworm silk. Webspinner silk protein is much smaller than that of silkworm (70 kDa vs. 350 kDa). Perhaps for both silkworm and webspinner silks then, the dominant protein repeat units are embedded primarily in β-sheet nanostructures, but C- and N-terminal ends are less restricted. The shorter length of the webspinner protein and therefore higher percentage of protein near the C- and N-terminal domains may account for the apparent increase in random-coil protein content after fiber wetting.

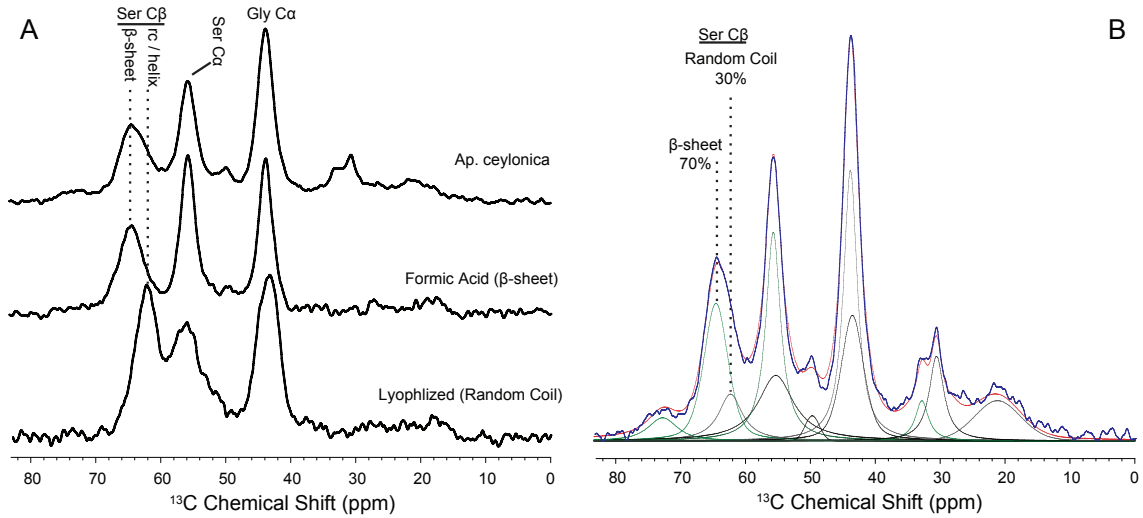

Figure 4.8: (A) ^{1}H - ^{13}C CP-MAS NMR data comparing native webspinner silk (*Aposthonia ceylonica*, top) to representative peptide models mimicking β-sheet (middle) or random-coil (bottom) conformations. (B) Using peak locations, widths and lineshapes obtained from data on peptide mimics in (A), native webspinner silk data was fit such that only peak amplitude was allowed to vary. The data is shown in blue, and the resulting fit in red. Results suggest that approximately 70% of seryl residues adopt a β-sheet structure, which is in strong agreement with WAXD results.

Figure 4.7 also yields information on the surface coating surrounding the silk fibers. For both *Ap. ceylonica* and *An. urichi* silks, one notices that the alkane CH_2 resonance is significantly pronounced in the direct spectra when the silk is wet. The alkane CH_2 resonance from both silks is both sharp and strong in the direct spectra, presumably because of fast molecular motion induced by the presence of water on the silk surface. Additionally, both *An. urichi* and *Ap. ceylonica* silks show a new sharp resonance in the direct spectra at 14 ppm, which we assign to terminal or branched alkane CH_3 groups on the silk surface. Similar to FT-IR results in Figure 4.3, NMR data shown in Figure 4.7 on *Ap. ceylonica* silk fibers reveal the severe reduction of alkane CH_2 and CH_3 signals after washing the fibers with a 2:1 mixture of $CHCl_3$:MeOH (red). We conclude that the surface coating surrounding the silk protein core is composed of long-chain lipids or alkanes that are non-covalently attached to the protein.

4.5 Conclusions

An in depth analysis has been performed on webspinner silks from *An. urichi* and *Ap. ceylonica*, and our findings, summarized in Figure 4.9, allow us to improve the current understanding of the molecular-level and hierarchical structure of embiopteran silk fibers. Our best electron microscopy results show that webspinner silks are 90-100 nm in diameter, making them among the thinnest known silk-based biopolymers. Both FT-IR and NMR results confirm what could be predicted by the repetitive primary protein sequences; the protein core is dominated by nanocrystalline β-sheet structures arising from glycine- and serine-rich repeat motifs. Wide angle x-ray diffraction results show that for *An. urichi* silk, and presumably other embiopteran silks, these nanocrystallites are highly ordered, are well aligned with respect to the fiber axis (low estimate: $f_c = 0.93$), and the crystallites are approximately 3 to 5 nm in dimension. Additionally, x-ray data show that webspinner silks possess an extremely high crystalline fraction at 69%. This is consistent with solid-state NMR results, which indicate that 70% of serine residues reside in nanocrystalline β-sheet structures. The silk is naturally water-repellent, but when the silk is water saturated, some regions of the protein, possibly the N- and C-termini of the relatively small (70 kDa) protein, become mobile and randomly-oriented. NMR and FT-IR data also provide evidence for a long-chain lipid or alkane-rich surface coating on webspinner silk fibers. Characteristic alkane infrared absorbances and ^{13}C resonances decrease 50% in intensity after treating the silk with 2:1 $CHCl_3$:MeOH, suggesting that this surface coating is non-covalently adhered to the protein core. The hydrophobic nature of silken galleries appears to serve to protect the insects from being dislodged from their arboreal dwellings during heavy rain. It also protects the interior of their domiciles and their bodies from extreme wetting, which has multiple negative conse-

quences including increased risk of suffocation and of fungal attack. During severe dry periods, the silk might also serve to limit desiccation of the insects sheltering inside. The basic hierarchical structure of webspinner silk fibers is illustrated in this study: the thin fiber core is composed of glycine and serine-rich repetitive protein motifs that primarily adopt a β-sheet nanostructure, and the protein core surrounded by a thin protective hydrophobic lipid or alkane-rich shell.

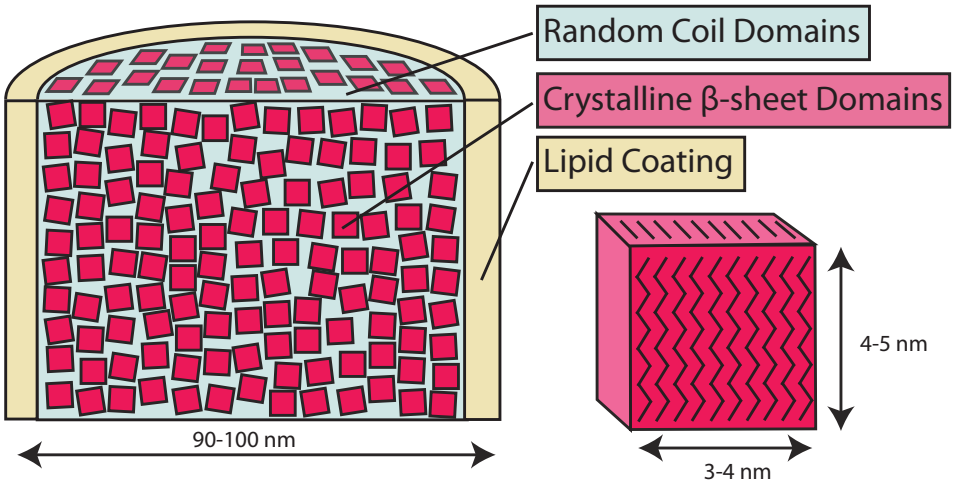

Figure 4.9: Conceptual model of webspinner silk based on experimental results. β-sheet nanocrystallites (red) are a few nanometers in dimension, are well-aligned with respect to the fiber axis, and they make up about 70% of the silk protein core. Separating these nanocrystalline regions are random or loosely-oriented domains (blue). The silk protein core is surrounded by a thin hydrophobic lipid or alkane-rich layer (yellow).

4.6 Supplemental Material

The figures below were provided as supplementary material for chapter 4, which was submitted for publication to RCS Advances. We chose not to feature the mechanical testing data in the main body of the publication because considering the difficulty in preparing consistent samples, we do not think the data gives much more information than a rough estimate. It was sufficient in our case to point out that webspinner silk fibers are stronger than previous studies had suggested. We encourage other interested researchers to improve on our initial results.

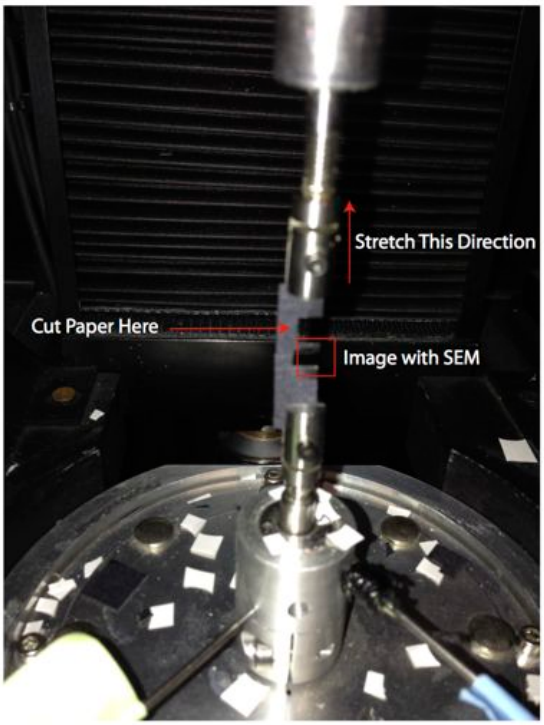

Figure 4.10: Tensile properties for webspinner silks of the species *Antipaluria urichi* were investigated in an attempt to improve on suspect results from previous works. Fourteen stress-strain curves were obtained using a Nano Bionix tensile tester (MTS System Corp, Akron, OH, USA). Samples were prepared on E-shaped cards by first anesthetizing an adult female insect with CO_2 gas, then pinning the insect on her back using strips of Parafilm. Then under a dissecting microscope, the tips of the E card were brushed against the tarsus a couple times until a silk bundle was visible to the naked eye. The silk was then secured to the 3 tips of the E with superglue (cyanoacrylate). E-shaped cards were mounted on the Nano Bionix apparatus seen above for tensile testing. The card was secured, and one side of the E paper card was cut with scissors prior to testing. The other half of the E contains an untested silk bundle that was imaged with SEM to estimate the number of fibers present in the tested sample. Fiber bundles were extended at a rate of 1% strain per second until complete failure, and force versus extension curves were obtained for all samples.

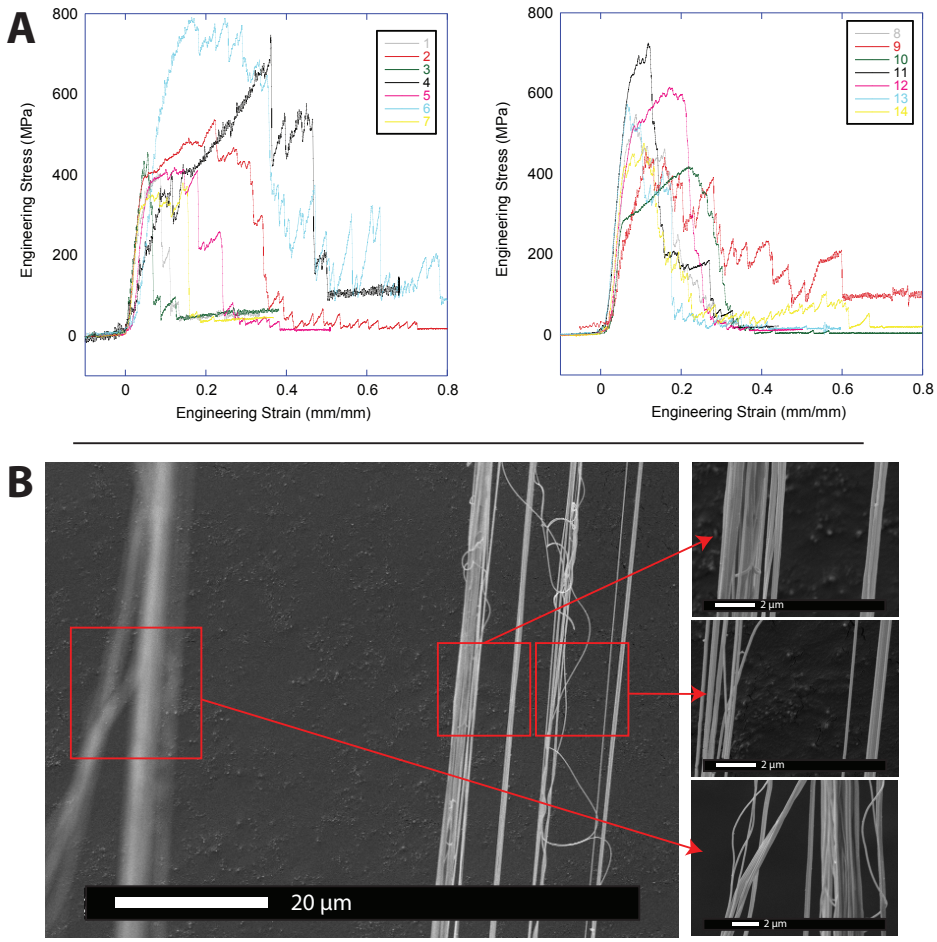

Figure 4.11: (A) 14 stress-strain curves obtained from webspinner silk bundles of the species *Antipaluria urichi*. Raw force data was converted to engineering stress after accounting for the total silk cross sectional area as estimated through SEM imaging of the non-stretched portion of each sample. (B) Example SEM image corresponding to trace 13. Approximately 120 fibers are present in this case. The mean ultimate stress for the 14 fibers is 500 MPa, revealing that the webspinner silk is significantly stronger than previously reported.

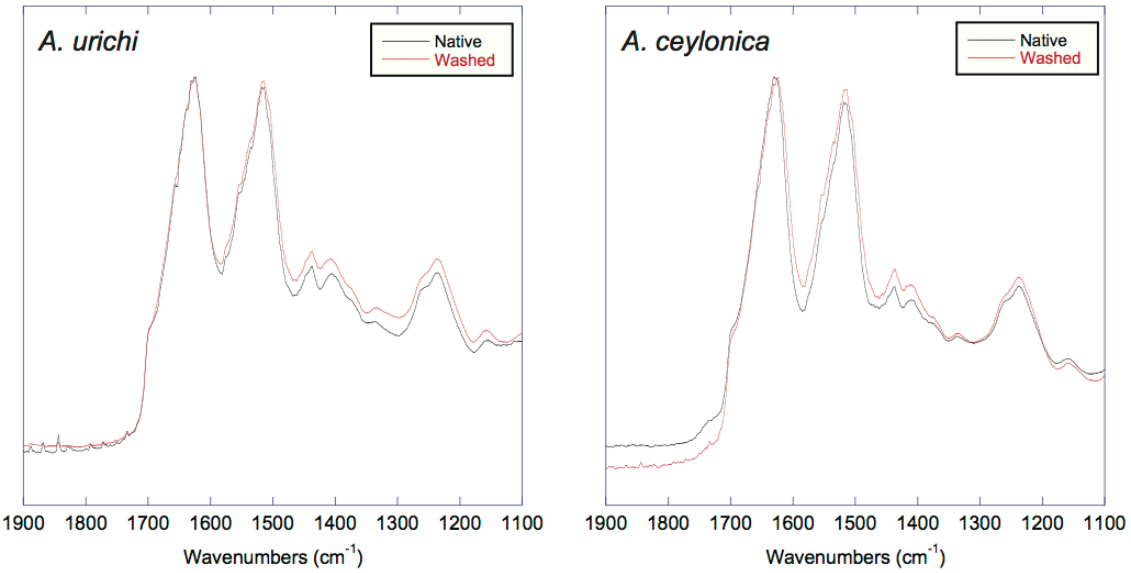

Figure 4.12: Comparison of the FT-IR absorbance profiles before (black) and after (red) washing webspinner silks with 2:1 $CHCl_3$:MeOH to remove the surface lipid or alkane-rich layer. The amide I, II, and III bands are all essentially identical after washing, which suggests that the silk protein structure remains unchanged.

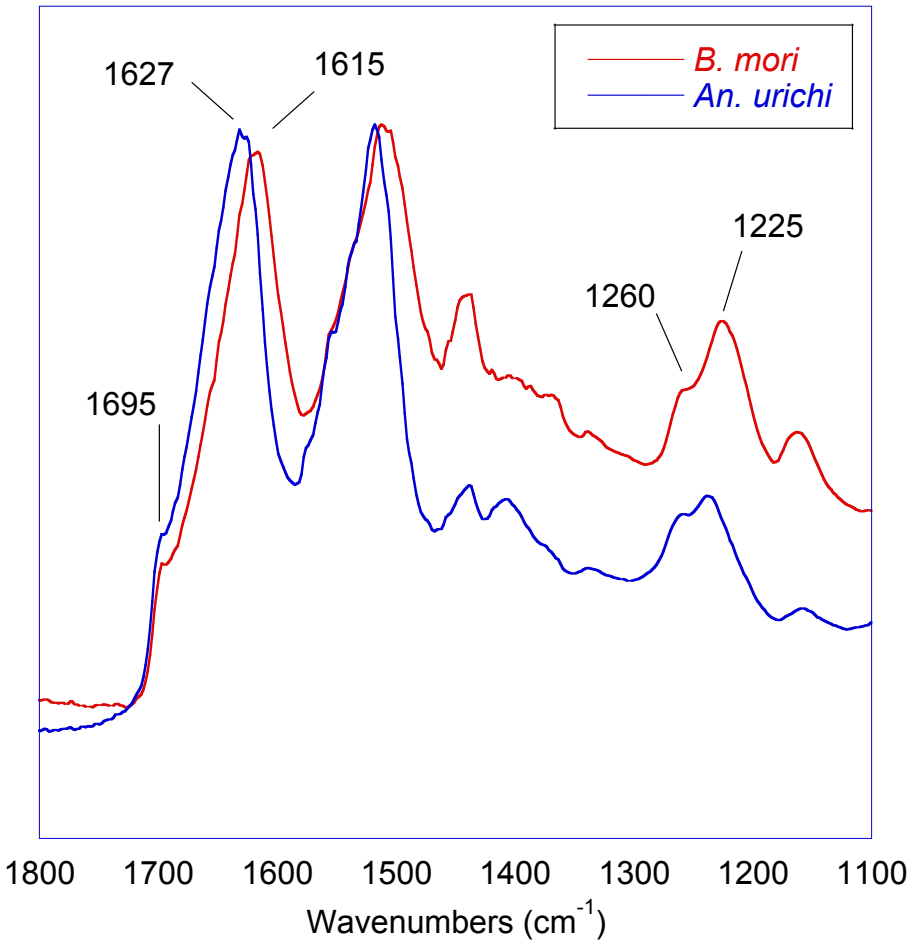

Figure 4.13: Comparison of the FTIR absorbance profiles of degummed *Bombyx mori* silkworm silk (red) with native *Antipaluria urichi* silk (blue). Both silks are protein-based biopolymers rich in GAGAGS (*B. mori*) or GAGSGS (*An. urichi*) repetitive motifs. The profile for *An. urichi* silk is similar to that of *B. mori* silkworm silk, but the amide I, II and III bands are shifted towards slightly higher frequencies. We believe that the shift in frequency is a result of differing primary protein sequences. It is clear that both silks are dominated by β-sheet secondary structures.

REFERENCES

[1] J S Edgerly, J A Davilla, and N Schoenfeld. Silk Spinning Behavior and Domicile Construction in Webspinners - Springer. *Journal of Insect Behavior*, 15(2):219–242, 2002.

[2] Janice S Edgerly. Life Beneath Silk Walls: A Review of the Primitively Social Embiidina. In J C Choe and B Crespi, editors, *The Evolution of Social Behavior in Insects and Arachnids*, pages 14–25. Cambridge University Press, 1997.

[3] J S Edgerly, S Büsse, and T Hörnschemeyer. Spinning behaviour and morphology of the spinning glands. *Zoologischer Anzeiger*, (251):297–306, 2012.

[4] Shoko Okada, Sarah Weisman, Holly E Trueman, Stephen T Mudie, Victoria S Haritos, and Tara D Sutherland. An Australian webspinner species makes the finest known insect silk fibers. *International Journal of Biological Macromolecules*, 43(3):271–275, October 2008.

[5] Matthew A Collin, Edina Camama, Brook O Swanson, Janice S Edgerly, and Cheryl Y Hayashi. Comparison of embiopteran silks reveals tensile and structural similarities across Taxa. *Biomacromolecules*, 10(8):2268–2274, August 2009.

[6] Matthew A Collin, Jessica E Garb, Janice S Edgerly, and Cheryl Y Hayashi. Characterization of silk spun by the embiopteran, Antipaluria urichi. *Insect biochemistry and ...*, 39:79–82, 2009.

[7] J S Edgerly, A TADIMALLA, and E P DAHLHOFF. Adaptation to thermal stress in lichen-eating webspinners (Embioptera): habitat choice, domicile construction and the potential role of heat shock proteins. *Functional Ecology*, 19(2):255–262, April 2005.

[8] Edward S Ross. Webspinners (Embiidina). In John L Capirena, editor, *Encyclopedia of Entomology*, pages 4169–4172. Springer Netherlands, 2008.

[9] Kelly B Miller, Cheryl Y Hayashi, Michael F Whiting, Gavin J Svenson, and Janice S Edgerly. The phylogeny and classification of Embioptera (Insecta). *Systematic Entomology*, 37(3):550–570, 2012.

[10] Matthew A Collin, Janice S Edgerly, and Cheryl Y Hayashi. Comparison of fibroin cDNAs from webspinning insects: insight into silk formation and function. *Zoology (Jena, Germany)*, 114(4):239–246, September 2011.

[11] Randolph V Lewis. Spider silk: ancient ideas for new biomaterials. *Chemical reviews*, 106(9):3762–3774, September 2006.

[12] G H Altman, F Diaz, C Jakuba, T Calabro, R L Horan, J Chen, H Lu, J Richmond, and D L Kaplan. Silk-based biomaterials. *Biomaterials*, 24(3):401–416, 2003.

[13] Tara D Sutherland, James H Young, Sarah Weisman, Cheryl Y Hayashi, and David J Merritt. Insect silk: one name, many materials. *Annual review of entomology*, 55:171–188, 2010.

[14] C Z Zhou, F Confalonieri, N Medina, Y Zivanovic, C Esnault, T Yang, M Jacquet, J Janin, M Duguet, R Perasso, and Z G Li. Fine organization of Bombyx mori fibroin heavy chain gene. *Nucleic Acids Research*, 28(12):2413–2419, June 2000.

[15] M Xu and R V Lewis. Structure of a protein superfiber: spider dragline silk. *Proceedings of the National Academy of Sciences of the United States of America*, 87(18):7120–7124, September 1990.

[16] Sinan Keten, Zhiping Xu, Britni Ihle, and Markus J Buehler. Nanoconfinement controls stiffness, strength and mechanical toughness of β-sheet crystals in silk. *Nature Materials*, 9(4):359–367, March 2010.

[17] Sinan Keten and Markus J Buehler. Atomistic model of the spider silk nanostructure. *Applied physics letters*, 96(15):153701, 2010.

[18] C Y Hayashi, N H Shipley, and R V Lewis. Hypotheses that correlate the sequence, structure, and mechanical properties of spider silk proteins. *International Journal of Biological Macromolecules*, 24(2-3):271–275, March 1999.

[19] Jan Johansson, Charlotte Nerelius, Hanna Willander, and Jenny Presto. Conformational preferences of non-polar amino acid residues: An additional factor in amyloid formation. *Biochemical and biophysical research communications*, 402(3):515–518, November 2010.

[20] R W Williams, A Chang, D Juretić, and S Loughran. Secondary structure predictions and medium range interactions. *Biochimica et Biophysica Acta*, 916(2):200–204, 1987.

[21] David L Minor, Jr and Peter S Kim. Measurement of the b-sheet-forming propensities of amino acids. *Nature*, 367(6464):660–663, 1994.

[22] Sujatha Sampath, Thomas Isdebski, Janelle E Jenkins, Joel V Ayon, Robert W Henning, Joseph P R O Orgel, Olga Antipoa, and Jeffery L Yarger. X-ray diffraction study of nanocrystalline and amorphous structure within major and minor ampullate dragline spider silks. *Soft Matter*, 8(25):6713–6722, 2012.

[23] Janelle E Jenkins, Sujatha Sampath, Emily Butler, Jihyun Kim, Robert W Henning, Gregory P Holland, and Jeffery L Yarger. Characterizing the secondary protein structure of black widow dragline silk using solid-state NMR and X-ray diffraction. *Biomacromolecules*, 14(10):3472–3483, October 2013.

[24] Ku Liang, Yu Gong, Jianlong Fu, Shi Yan, Yuanyuan Tan, Rong Du, Xueqing Xing, Guang Mo, Zhongjun Chen, Quan Cai, Dongbai Sun, and Zhonghua Wu. Microstructural change of degummed Bombyx mori silk: an in situ stretching wide-angle X-ray-scattering study. *International Journal of Biological Macromolecules*, 57:99–104, June 2013.

[25] Tetsuo Asakura, Juming Yao, Tsutomu Yamane, Kosuke Umemura, and Anne S Ulrich. Heterogeneous Structure of Silk Fibers from BombyxmoriResolved by 13C Solid-State NMR Spectroscopy. *J. Am. Chem. Soc*, 124(30):8794–8795, July 2002.

[26] Janelle E Jenkins, Melinda S Creager, Randolph V Lewis, Gregory P Holland, and Jeffery L Yarger. Quantitative Correlation between the protein primary sequences and secondary structures in spider dragline silks. *Biomacromolecules*, 11(1):192–200, 2009.

[27] Alexander Sponner, Wolfram Vater, Shamci Monajembashi, Eberhard Unger, Frank Grosse, and Klaus Weisshart. Composition and Hierarchical Organisation of a Spider Silk. *PLoS ONE*, 2(10):e998, October 2007.

[28] Gregory P Holland, Randolph V Lewis, and Jeffery L Yarger. WISE NMR characterization of nanoscale heterogeneity and mobility in supercontracted Nephila clavipes spider dragline silk. *J. Am. Chem. Soc*, 126(18):5867–5872, 2004.

[29] Z Yang, DT Grubb, and LW Jelinski. Small-angle X-ray scattering of spider dragline silk. *Macromolecules*, 30(26):8254–8261, 1997.

[30] DT Grubb and LW Jelinski. Fiber morphology of spider silk: the effects of tensile deformation. *Macromolecules*, 30(10):2860–2867, 1997.

[31] C Riekel, C Bränden, C Craig, C Ferrero, F Heidelbach, and M Müller. Aspects of X-ray diffraction on single spider fibers. *International Journal of Biological Macromolecules*, 24(2-3):179–186, March 1999.

[32] Fritz Vollrath, Thor Holtet, Hans C Thogersen, and Sebastian Frische. Structural organization of spider silk. *Proceedings of the Royal Society of London. Series B: Biological Sciences*, 263(1367):147–151, 1996.

[33] S Frische, Maunsbach, AB, and F Vollrath. Elongate cavities and skin-core structure in Nephila spider silk observed by electron microscopy. *Journal of Microscopy*, 189(1):64–70, 1998.

[34] Stefan Schulz. Composition of the silk lipids of the spider Nephila clavipes. *Lipids*, 36(6):637–647, June 2001.

[35] Eliane Victoriano, Daniela O Pinheiro, and Elisa A Gregório. Histochemical and ultrastructural evidence of lipid secretion by the silk gland of the sugarcane borer Diatraea saccharalis (Fabricius) (Lepidoptera: Crambidae). *Neotropical entomology*, 36(5):707–711, September 2007.

[36] Sarah Weisman, Holly E Trueman, Stephen T Mudie, Jeffrey S Church, Tara D Sutherland, and Victoria S Haritos. An Unlikely Silk: The Composite Material of Green Lacewing Cocoons. *Biomacromolecules*, 9(11):3065–3069, November 2008.

[37] David Nečas and Petr Klapetek. Gwyddion: an open-source software for SPM data analysis. *Central European Journal of Physics*, 10(1):181–188, November 2011.

[38] Andrew E Bennett, Chad M Rienstra, Michèle Auger, K V Lakshmi, and Robert G Griffin. Heteronuclear decoupling in rotating solids. *The Journal of Chemical Physics*, 103(16):6951, 1995.

[39] Ruthven N A H Lewis and Ronald N McElhaney. Fourier transform infrared spectroscopy in the study of lipid phase transitions in model and biological membranes: practical considerations. *Methods in molecular biology (Clifton, N.J.)*, 400:207–226, 2007.

[40] Maxime Boulet-Audet, Thierry Lefèvre, Thierry Buffeteau, and Michel Pézolet. Attenuated Total Reflection Infrared Spectroscopy: An Efficient Technique to Quantitatively Determine the Orientation and Conformation of Proteins in Single Silk Fibers. *Applied Spectroscopy*, 62(9):956–962, September 2008.

[41] Jianzhong Shao, Jinhuan Zheng, Jinqiang Liu, and C M Carr. Fourier transform Raman and Fourier transform infrared spectroscopy studies of silk fibroin. *Journal of applied polymer science*, 96(6):1999–2004, 2005.

[42] Shengjie Ling, Zeming Qi, David P Knight, Zhengzhong Shao, and Xin Chen. Synchrotron FTIR Microspectroscopy of Single Natural Silk Fibers. *Biomacromolecules*, 12(9):3344–3349, September 2011.

[43] Shengjie Ling, Zeming Qi, David P Knight, Yufang Huang, Lei Huang, Huan Zhou, Zhengzhong Shao, and Xin Chen. Insight into the Structure of Single Antheraea pernyi Silkworm Fibers Using Synchrotron FTIR Microspectroscopy. *Biomacromolecules*, 14(6):1885–1892, June 2013.

[44] Periklis Papadopoulos, Roxana Ene, Immanuel Weidner, and Friedrich Kremer. Similarities in the Structural Organization of Major and Minor Ampullate Spider Silk. *Macromolecular Rapid Communications*, 30(9-10):851–857, May 2009.

[45] Nicholas N Ashton, Daniel R Roe, Robert B Weiss, Thomas E Cheatham, III, and Russell J Stewart. Self-Tensioning Aquatic Caddisfly Silk: Ca 2+-Dependent Structure, Strength, and Load Cycle Hysteresis. *Biomacromolecules*, 14(10):3668–3681, October 2013.

[46] Andrew A Walker, Jeffrey S Church, Andrea L Woodhead, and Tara D Sutherland. Silverfish silk is formed by entanglement of randomly coiled protein chains. *Insect biochemistry and molecular biology*, 43(7):572–579, July 2013.

[47] P Papadopoulos, J Sölter, and F Kremer. Structure-property relationships in major ampullate spider silk as deduced from polarized FTIR spectroscopy. *The European physical journal. E, Soft matter*, 24(2):193–199, October 2007.

[48] Venyaminov SYu and N N Kalnin. Quantitative IR spectrophotometry of peptide compounds in water (H2O) solutions. II. Amide absorption bands of polypeptides and fibrous proteins in alpha-, beta-, and random coil conformations. *Biopolymers*, 30(13-14):1259–1271, 1990.

[49] J O Warwicker. Comparative studies of fibroins. II. The crystal structures of various fibroins. *Journal of Molecular Biology*, 2(6):350–362, December 1960.

[50] Hazime Saito. Conformationdependent 13C chemical shifts: A new means of conformational characterization as obtained by highresolution solidstate 13C NMR. *Magnetic Resonance in Chemistry*, 24(10):835–852, 1986.

[51] Akira Shoji, Takuo Ozaki, Hazime Saito, Ryoko Tabeta, and Isao Ando. Conformational characterization of solid polypeptides by carbon-13 NMR recorded by the cross polarization-magic angle spinning method: conformation-dependent carbon-13 chemical shifts of oligo- and poly(γ-benzyl L-glutamates) and sequential copolymers of γ-benzyl and γ-methyl L-glutamates and qualitative evaluation of side-chain orientation. *Macromolecules*, 17(8):1472–1479, August 1984.

[52] Tetsuo Asakura, Kohei Suita, Tsunenori Kameda, Sergii Afonin, and Anne S Ulrich. Structural role of tyrosine inBombyx mori silk fibroin, studied by solidstate NMR and molecular mechanics on a model peptide prepared as silk I and II. *Magnetic Resonance in Chemistry*, 42(2):258–266, January 2004.

[53] Tetsuo Asakura, Rena Sugino, Tatsushi Okumura, and Yasumoto Nakazawa. The role of irregular unit, GAAS, on the secondary structure of Bombyx mori silk fibroin studied with 13C CP/MAS NMR and wide-angle X-ray scattering. *Protein science : a publication of the Protein Society*, 11(8):1873–1877, August 2002.

[54] D Massiot, F Fayon, M Capron, I King, S Le Calvé, B Alonso, J O Durand, B Bujoli, Z Gan, and G Hoatson. Modelling oneand twodimensional solidstate NMR spectra. *Magnetic Resonance in Chemistry*, 40(1):70–76, 2002.

[55] Melinda S Creager, Janelle E Jenkins, Leigh A Thagard-Yeaman, Amanda E Brooks, Justin A Jones, Randolph V Lewis, Gregory P Holland, and Jeffery L Yarger. Solid-state NMR comparison of various spiders' dragline silk fiber. *Biomacromolecules*, 11(8):2039–2043, August 2010.

[56] Gregory P Holland, Janelle E Jenkins, Melinda S Creager, Randolph V Lewis, and Jeffery L Yarger. Solid-state NMR investigation of major and minor ampullate spider silk in the native and hydrated states. *Biomacromolecules*, 9(2):651–657, 2008.

[57] Z Yang, O Liivak, A Seidel, G LaVerde, DB Zax, and LW Jelinski. Supercontraction and backbone dynamics in spider silk: 13C and 2H NMR studies. *J. Am. Chem. Soc*, 122(37):9019–9025, 2000.

[58] J Bennett Addison, Nicholas N Ashton, Warner S Weber, Russell J Stewart, Gregory P Holland, and Jeffery L Yarger. β-Sheet Nanocrystalline Domains Formed from Phosphorylated Serine-Rich Motifs in Caddisfly Larval Silk: A Solid State NMR and XRD Study. *Biomacromolecules*, 14(4):1140–1148, April 2013.

Chapter 5

EMBIOPTERAN (WEBSPINNER) SILK DISPLAYS THE ROSE PETAL EFFECT: UNWRAPPING THE ADAPTIVE LAYERING FROM NANOSCALE TO MICROSTRUCTURE

5.1 Abstract

In this study, the existence, composition, and function of an outer lipid coating on the surface of embiopteran (also referred to as embiid or webspinner) silk from the tropical rainforest species *Antipaluria urichi* were investigated. The choreography of spinning was also described in detail to address observations that *A. urichi* adult females changed their spinning behavior depending on the specific microenvironment. Webspinner silk galleries are constructed using exceptionally fine protein-based silk fibers (90-100 nm in diameter) that overlap and crisscross to form sheets and tunnels. These interwoven sheets are therefore heterogeneous surfaces, and Scanning Electron Microscopy (SEM) images reveal both nano- and microstructural fine structure features. SEM and Fourier Transform Infrared Spectroscopy (FTIR) data revealed the presence of a lipid or alkane-rich coating on the surface of the silk fibers. This lipid coating was extracted from the fibers using organic solvents, and its general composition was characterized with Gas Chromatography Mass Spectroscopy (GC-MS). GC-MS results on lipid extracts from both 2:1 chloroform/methanol ($CHCl_3$/MeOH) and 1:1 dichloromethane/hexanes (DCM/hexanes) revealed the presence of straight and branched-chain alkanes and fatty-acids up to and above 36 carbons in length, and in addition some steroid species were also seen. The hydrophobicity and wettability of the silk, an important property of embiopteran silk shelters, were studied using

contact angle analysis of water droplets on silk sheets. The native sheets were found to have a property of hydrophobicity similar to that of a rose petal, namely that the surface is extremely hydrophobic (150° advancing contact angle) while also exhibiting a high contact angle hysteresis, resulting in the capacity to grip water droplets tightly to the surface of the silk sheet without actually wetting the silk itself. Washing of the silk with 1:1 DCM/hexanes to remove lipids from the surface of the silk fibers resulted in the silk sheets becoming permeable to water, confirming that the lipid coating is critical to the silk's hydrophobic properties. Observation of *A. urichi* adult female stepping patterns shows that the insect adjusts her silk spinning behavior depending on the specific microenvironment. When in the more open environment the webspinner spins more silk by using much more complex stepping patterns than when in an enclosed environment. Considering the significant reliance on the silk, we hypothesize that the peculiar stepping behavior when creating the outer surface of the gallery is an evolutionary adaptation that selected for a superhydrophobic heterogeneous surface with the appropriate micro- and nanostructural features to exhibit water adhesion properties similar to the rose petal.

5.2 Introduction

Embiopterans, also known as webspinners or embiids, are tropical insects that use silk to build shelters of interconnected tunnels called galleries, typically on tree bark in humid climates and in leaf litter in dry regions [1, 2]. The species studied herein, *Antipaluria urichi*, is of the family Clothodidae in the insect Order Embioptera, honoring Clothos, the youngest of the three Fates of Greek mythology, known as the spinner of the thread of life. The name aptly reflects the order-defining spinning behavior and particularly that of species in the family Clothodidae of which *Antipaluria urichi* of Trinidad and Tobago is a prime example. This rainforest species spins very thin (on

the order of 100 nm in diameter, see Chapter 4) protein-based silk fibers from their forelimbs, or tarsi, the basal surface of which is covered with hundreds of silk ejectors that are fed by subdermal silk glands, enabling the insect to spin hundreds of fibers at once into sheets [3, 2, 4]. Their silk sheets are especially thick and cloth-like, acting as covering for domiciles and feeding sites of epiphytic algae and lichens on the bark of tropical trees (Figure 5.1A). The adult female dedicates much of her time to spinning behavior, an investment that apparently assists offspring in their development for they grow faster in her presence. Maternal investment in silk spinning greatly increases after her young hatch providing protection from predators and from, as yet unquantified but likely, abiotic elements [5, 6, 7]. We know from observations in the field that by lifting up the cloth-like covering following a torrential rainfall typical of their habitat, one finds the dwelling place beneath dry and seemingly protected from pounding raindrops and stem flow that gushes over the colonys silk surface [8]. Laboratory cultures also remain dry when water is poured onto the silk. The galleries are in fact so water resistant that to access water to drink, *A. urichi* individuals bite a small hole beneath a standing drop of water that sits on the silk sheet and suck in the water (this behavior was captured on film in the third installment of the BBC series Life in the Undergrowth, The Silk Spinners, narrated by David Attenborough). They quickly patch these small drinking holes. Many galleries are situated vertically on a tree as shown in Figure 5.1A. One might expect water to roll off of this vertical, hydrophobic surface, but amazingly after a rainstorm some droplets of water remain adhered to the gallery, and are thus accessible to the insects. This phenomenon is illustrated in Figure 5.1B; an oak leaf with attached silk was removed from the laboratory terrarium and situated vertically against a black backdrop. Water droplets on the silk surface are nearly spherical in shape (high contact angle) yet remain adhered to the surface. For comparison, the same sized droplets spread out (low contact angle)

when they come into contact with the oak leaf. The protective qualities of this silk might also include prevention of desiccation of these soft bodied insects, which must survive dry seasons as well as wet. These observations suggested to us that the way water interacts with embiopteran silk represents an adaptation worth investigating the hierarchical nature of silk architecture: how the silk is laid down by the spinner, the microstructure and finally, the nanostructure.

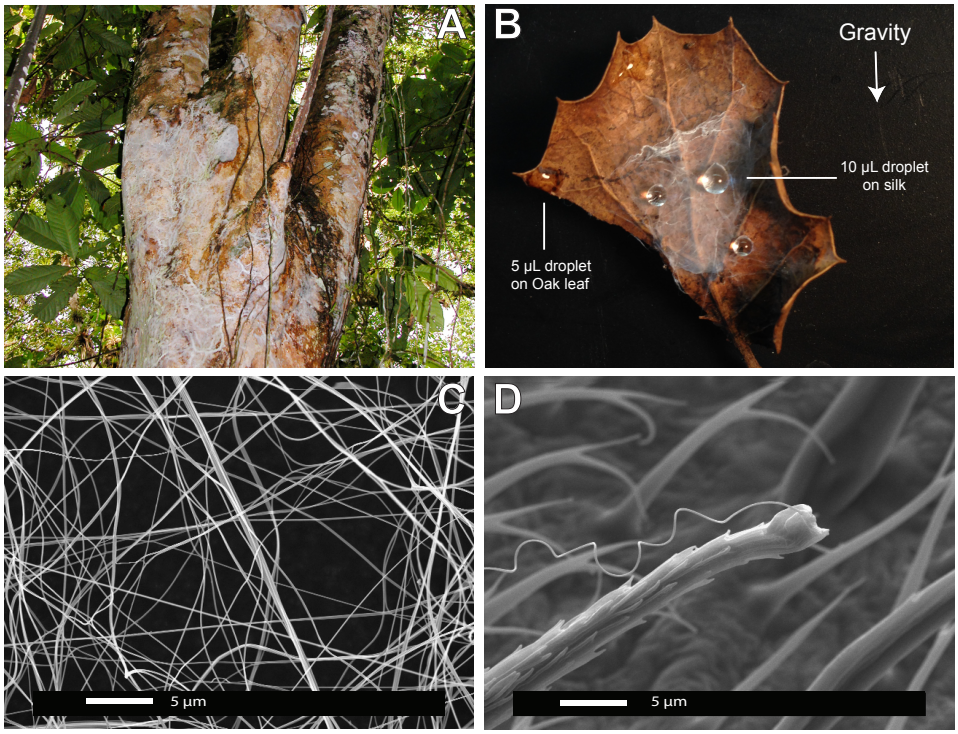

Figure 5.1: Optical (A, B) and SEM (C, D) images of *Antipaluria urichi* silk. (A) *A. urichi* silk gallery covering over 1 square meter is seen on tree bark in Trinidad. (B) A silk gallery attached to an oak leaf, held upright so that the axis of the leaf is perpendicular to the ground. Small drops are 5 μL, while the large drop is 10 μL. Droplets on the silk bead up yet remain pinned to the sheet against gravity, while droplets on the oak leaf spread out and drip down the surface of the leaf. (C) SEM image of webspinner silk, showing the nanoscale thickness (90-100 nm) of the fibers. (D) A single silk fiber being extruded from one of hundreds of silk ejectors on the tarsus of an *A. urichi* adult female.

The hydrophobic nature of the silk may arise from some form of lipid coating on the surface of the silk fibers. Previous studies have shown the presence of lipids in a

variety of arthropod silks [9, 10, 11, 12]. A gas chromatography mass spectrometry (GC-MS) analysis of derivatized lipid extracts from *Nephila clavipes* major dragline silks indicated that the lipid profile is mostly composed of long branched and straight chain alkane species with methyl ether, carboxylic acid , alcohol and diol headgroups [9]. Green lacewing cocoons also have been shown to contain a significant lipid content that is integrated into a matrix of silk protein fibers, serving as a waterproof barrier. GC-MS and thin layer chromatography (TLC) plate analysis showed the presence of both polar and nonpolar lipids, and some with carboxylic acid headgroups [10].

Previous studies on webspinner silks have focused mostly on initial characterizations of the amino acid sequence and secondary structure of the silk protein material [13, 14, 15]. While the amino acid sequence of the silk protein may vary slightly between taxa and species of Embioptera, the general trend is that webspinner silks are highly repetitive protein-based biopolymers comprised mostly of glycine, serine, and alanine. Fourier transform-infrared spectroscopy (FT-IR) measurements have suggested that the secondary structure of the silk fibroin is mostly β-sheet in structure Collin:2009je, Collin:2011il, Addison:gy. Our recent solid-state NMR and Wide-angle X-ray Diffraction results on *A. urichi* silks (see Chapter 4) revealed that approximately 70% of the protein fiber is composed of nanocrystalline β-sheet structures of a few nanometers in dimension that are well-aligned with respect the fiber axis. The high percentage of the silk fibers adopting a β-sheet structure likely accounts for the reasonably high (500 MPa mean ultimate stress) rigidity measured for the silk, which is a quality expected of a good structural material for building shelters.

The fine structure of webspinner silk galleries arising from the concerted stepping motions of the insect has a dramatic effect on the function of the silken sheets, and therefore may be an adaptation based on ecological necessities. We therefore seek to explore the fine details of *A. urichi* spinning behavior by filming adult females in

two different settings and by employing an event recorder designed to allow quantification of spinning during slow-speed replay. Our hypothesis, based on preliminary observations [2] is that when *A. urichi* are in the open, as on bark, they will express a complex spin routine that generates a framework for a domicile, followed by reinforcement of the emerging silk structure. If they are placed in a burrow-like arena that by its nature provides more protection for the insect, they should switch to a different routine to merely coat the arena walls with silk. There would not be a need for building a framework in this case. Quantifying spin steps will provide insight into how *A. urichi* creates structural details reported in other sections of this report. An alternative hypothesis is that their spinning behavior is stereotypical. If so, their spin style will be consistent irrespective of arena type. In either case, quantifying details of spinning will provide insight into how they create silk structures that appear to protect the occupants from flooding by tropical rain.

Thus, this present study is a combinatorial work that offers insight into both the molecular-level detail and macroscopic uses and production of these exceptional silk fibers. The existence, composition, and functional uses of a hydrophobic lipid-rich surface coating on *Antipaluria urichi* silk fibers are investigated for the first time. Additionally, to study a primary function of embiid silk, its hydrophobicity, the wettability of the silk gallery walls was measured via contact angle hysteresis. Finally, through carefully monitoring of *A. urichi* spinning behavior we investigated if their complex, concerted foot stepping behavior is stereotypical or is a result of adaptation to microhabitat.

5.3 Materials and Methods

Insect Rearing. *Antipaluria urichi* were collected from Trinidad and Tobago by researchers from Santa Clara University, reared in a plastic terrarium with dried Live

Oak leaves as substrate, and fed fresh lettuce leaves every few days. The terraria were covered with a fine mesh to prevent insects from escaping. Humidity was maintained by misting the sides of the container every few days.

Silk Spinning Behavior. Complete experimental details are given in the Supplementary material, but briefly: to induce spinning in the laboratory at Santa Clara University, five individuals were placed into either a narrow notch into a plywood block, covered with a transparent plastic lid, or into a bark-line plexiglass box Arena set-up is shown in Supplemental Figure 1. Behavioral acts were scored using Observer software (version 5, Noldus Information Technology, Wageningen, The Netherlands). Videos were replayed at 1/2 speed and the same investigator scored the behaviors to minimize investigator error.

Infrared Spectroscopy. Two samples of webspinner silk, each approximately 2 mg, were collected by taking sections of silk from the cleanest sections of the galleries in the terrarium. Any debris was removed manually under a microscope using fine tweezers. One sample was soaked in a 2:1 mixture of chloroform/methanol ($CHCl_3$/MeOH) for 12 hours, and subsequently rinsed with deionized water. The other sample was only rinsed with deionized water. Both samples were dried and then subsequently analyzed using a Nicolet 6700 FT-IR instrument with a Smart Orbit diamond Attenuated Total Reflectance (ATR) accessory, with spectra collected for 32 scans at a resolution of 2 cm^{-1}.

Electron Microscopy. Bundles of natural *A. urichi* silk and of $CHCl_3$/MeOH-washed silk were imaged with Scanning Electron Microscopy (SEM). Bundles were first secured to conductive carbon tape, and then were gold-coated using a Denton vacuum sputter coater desk II for 3 minutes at a deposition rate of 5 nm/min. The images were obtained using an XL30 Environmental SEM-FEG built by FEI. The secondary electron (SE) detector was used for imaging. Images were collected under a vacuum pressure of less than 9 x 10^{-5} mbar and with a beam current of 10 kV.

Gas Chromatography Mass Spectroscopy Analysis on Lipid Extractions The lipid extract was obtained by soaking 6 mg *A. urichi* silk in either 20 mL of 2:1 $CHCl_3$/MeOH or 1:1 dichloromethane/hexanes (DCM/hexanes) for 24 hours. Any undissolved material was removed manually or through centrifugation, and the remaining solvent was evaporated down to dryness with a stream of N_2 gas. The residue was then dissolved in 250 μL analytical grade dichloromethane for GC-MS. Silyl derivatization was performed by mixing 50 μL of the DCM/hexanes extract with 50 μl 99% N,O-Bis(trimethylsilyl) trifluoroacetamide (BSTFA) with 1% trimethylchlorosilane (TMCS) and heating in an oven at 65 °C for 3 hours. Methyl ester derivatization was carried out with methylnitronitrosoguanidine (MNNG) in water with potassium hydroxide to produce diazomethane to methylate 50 μL of the DCM/hexanes extract diluted in 1 mL of analytical grade DCM. The methylated extract was then evaporated down to 50 μL with N_2 gas. An alkane standard containing chains with lengths between 15 and 29 carbons in length, plus hexatriacontane, was prepared as well. For the analysis of the underivatized extracts, derivatized extracts, and the alkane standard, an Agilent 6890N/5973 inert GC-MS was used, operated in electron ionization mode using a HP-5MS column (30 mm x 0.250 mm x 0.25 μm) with splitless injection (10 psi) set at 300 °C. The helium carrier gas was set at a rate of 1.2 mL/min. The oven temperature was initially set to 65 °C for 10 min followed by an increase to 300 at 10°C/min and held for 20 minutes.

Contact Angle Hysteresis. Two debris-free sections of *A. urichi* silk galleries were collected from the terrarium and wrapped around glass slides. One of the silk-coated slides was soaked in 1:1 DCM/hexanes for 30 minutes and subsequently rinsed with water and allowed to dry. The other slide was simply rinsed with water and dried. A Krss Easy-Drop Contact Angle Goniometer was used to place 5 μL droplets of Millipore water on the silk surface and measure the advancing contact angles.

Water was added to the droplet in steps of 2.5 μL until an advancing contact angle maximum was reached. Five trials were performed for both the solvent-washed and unwashed samples and an average of the measurements was taken as the advancing contact angle.

5.4 Results and Discussion

Fiber Morphology and Surface Coating

Embiopteran silk from *Antipaluria urichi* was studied using SEM, FTIR, GC-MS, contact angle techniques, and by monitoring their spinning behavior. Electron Microscopy results highlight the organization and spacing of the exceptionally fine silk fibers that make up the protective, water-repellant silken galleries. Figure 5.1C shows an SEM image of *A. urichi* silk taken from the surface of a native colony kept in house. As can be seen by the scale bar in the image, individual silk fibers are approximately 90-100 nm in diameter. Previous reports have listed the diameter of webspinner silk fibers of various species as small as 65 nm from SEM and Small-angle X-ray Diffraction techniques [15], and as large as 800 nm from polarized-light microscopy techniques [13]. This discrepancy in the literature regarding the true thickness of webspinner silk fibers was attributed to the immature or young nymphs that presumably produced thinner fibers than adults [14], however our SEM image of a silk fiber extruding from an adult female webspinner ejector (Figure 5.1D) in addition to our recent fiber diameter measurements from SEM and TEM images (Chapter 4) should lay to bed any confusion. Embiopteran silk fibers are indeed on the order of 100 nm, making webspinner silks among the thinnest of all known animal silk biopolymers. The texture, nanostructure, and microstructure of a rough surface have been repeatedly shown to significantly influence the behavior of water when in contact with the surface [16, 17, 18]. Considering the necessity of embiopterans

to remain protected from heavy rainfall yet also retain access to water to drink, the texture and large-order organization of fibers comprising the silken galleries is of great interest. The SEM image seen in Figure 5.1C from *A. urichi* silk galleries reveals that silken sheets are composed of single fibers, bundles of a few fibers, and also bundles of many fibers that criss-cross and overlap in multiple directions. The fibers or collections of fibers appear relatively evenly spaced with gaps or open spaces between the fibers in the range of a few to tens of microns. In addition to the 100 nm thickness of individual fibers, there exists nanometer-scale texture of bundles of silk fibers as well as intersection points where fibers overlap. Thus, embiopteran silk galleries are textured surfaces with both microstructural and nanostructural features. In other words, the textured surface of webspinner silk sheets covers a range of features from as small as a few nanometers to as large as 10-20 microns. The effects of said features will be discussed in later sections.

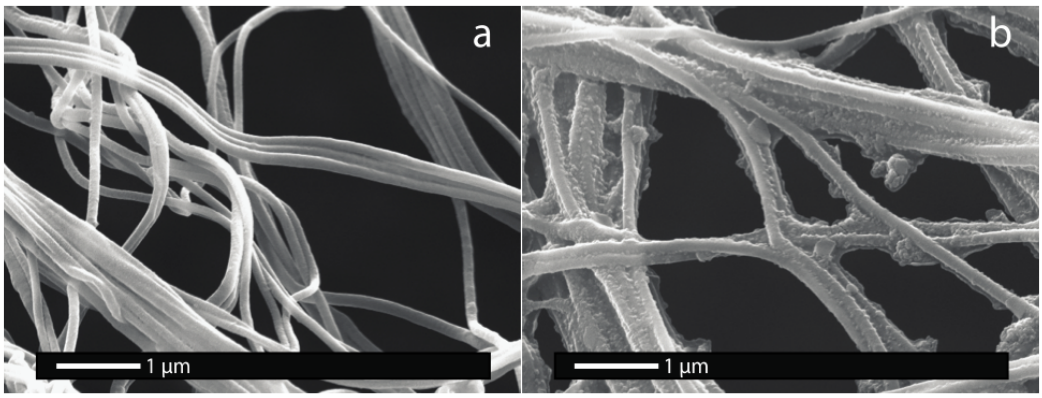

Figure 5.2: Scanning electron microscopy (SEM) image of natural silk. b) SEM image of silk washed with $CHCl_3$/MeOH. The natural silk has a smooth, uniform appearance with relatively even spacing between fibers or fiber bundles, while the washed silk has an uneven surface with small beads and clumps on the silks exterior. Additionally, the fibers are aggregated into larger bundles and less evenly spaced. The beaded, rough surface of the washed sample may be the result of undissolved lipid material remaining on the surface of the silk, and the clumping of fibers may be a result of the exposed fiber cores aggregating together in the presence of organic solvent.

The ability of protective silk galleries to repel water implies there may be some form of hydrophobic coating on the silk surface. Scanning electron microscopy (SEM) images of 2:1 chloroform/methanol ($CHCl_3$/MeOH)-washed and native *A. urichi* silk show changes in the morphology of the silk sheets upon washing (Figures 2A and 2B). The natural silk has a smooth, uniform appearance with relatively even spacing between fibers or fiber bundles, while the treated silk has an uneven surface with small beads or clumps on the silks exterior. Additionally, the fibers appear aggregated into larger bundles and are less evenly spaced. The beaded, rough surface of the washed sample may be the result of unremoved lipid material that remains on the surface of the silk, and the clumping of fibers may be a result of the exposed proteinaceous fiber cores aggregating together in the presence of the organic solvent. The apparent removal of an outer lipid coating with an organic solvent is consistent with the study by Sponner et al. [11] where a lipid coating on *Nephila clavipes* major dragline silk was removed by extraction with diethyl ether. In said study, TEM was used to image cross sections of *N. clavipes* dragline silk dyed with lipid-specific stains, showing the lipid layer on the surface of the silk and its subsequent removal after washing with ether. Unfortunately, the extremely thin fiber diameters of webspinner silks compared to spider silk has made obtaining similar stained cross sections of webspinner silk impractical.

The presence of lipids or alkanes on the silk surface was also investigated using Fourier-transform infrared spectroscopy. Figure 5.3 compares the FTIR spectra between 2600 and 3600 cm^{-1} of native *A. urichi* silk to silk that was washed with 2:1 $CHCl_3$/MeOH for 24 hours. Absorbances at 2922 cm^{-1} and 2850 cm^{-1} are associated with the sp^3 symmetric and asymmetric CH_2 stretching modes expected for alkanes [19]. Upon washing with $CHCl_3$/MeOH, the intensities of these peaks are greatly reduced while the remaining features in the spectrum (not shown) are unchanged. A

similar result was obtained by Weisman et al. [10] in the analysis of green lacewing cocoons, where it was observed that the peak intensities of $CHCl_3$/MeOH-washed cocoons were reduced by approximately 50% when compared to the spectra of natural cocoons. The observation that $CHCl_3$/MeOH appears to remove material from the surface of *A. urichi* silk fibers as seen from the SEM images in Figure 5.2, combined with the reduction in alkane CH_2 IR peak intensity after washing with $CHCl_3$/MeOH, suggests that the material being removed from the silk surface is an alkane or lipid-rich surface coating.

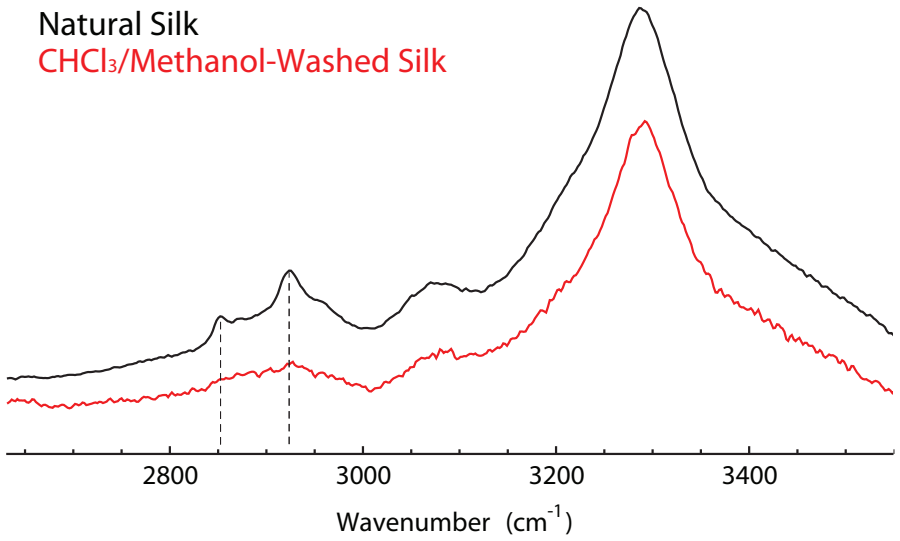

Figure 5.3: FT-IR spectra of natural silk (black) and $CHCl_3$/MeOH-washed silk (red) between the boundaries of 2600 and 3600 cm^{-1}. Peaks at 2922 cm^{-1} and 2850 cm^{-1} are associated with the sp^3 symmetric and asymmetric CH_2 stretching modes expected for lipids. Upon washing with $CHCl_3$/MeOH, the intensities of these peaks are greatly reduced while the remaining features in the spectrum (not shown) remain unchanged.

The source or mechanism of deposition of this lipid coating is not definitive, although it is likely that the lipid layer is co-extruded along with the silk as opposed to deposited onto the silk post-extraction. A study of the silk gland morphology of the Japanese embiopteran *Oligotoma japonica* showed that there exists two distinct materials within the lumen of each individual silk gland partitioned as a dominant

inner layer and a minor outer layer [3]. The outer material was labeled as sericin while the inner material was labeled as silk fibroin; this convention is consistent with the composition of *Bombyx mori* silkworm silk [20]. However, it is suggested from cDNA studies across the taxa of Embioptera that only one protein is used to produce webspinner silks [21]. It therefore seems likely that this outer layer is not a sericin-like second protein material but instead is the lipid coating being co-excreted with the silk protein. While we believe that co-secretion is a strong possibility for the source of the lipid material found on the surface of the silk, it is also possible that embiopterans also lay down cuticular lipids on their silk after spinning as a result of their exoskeletons coming into physical contact with the silk and rubbing off lipid material. It could also be that the lipids could come from both co-secretion and from the cuticle. A hypothesis of a combination of both secreted lipids and cuticular lipids being the origin of the lipids on the surface of silk fibers was suggested to explain the difference in lipid profiles between freshly drawn silk and silk obtained from harvested webs of *N. clavipes* [9].

GC-MS Analysis of Lipid Extracts

In order to characterize the lipid layer on the surface of embiopteran silk, two solvent systems, 2:1 $CHCl_3$/MeOH and 1:1 dichloromethane/hexanes (DCM/hexanes), were used to extract lipids from the silk for compositional analysis of the surface coating using GC-MS techniques. The lipid profile extracted from a biological sample is highly dependent on the extraction technique [22, 23]. It has been shown that for biological tissue samples, 2:1 $CHCl_3$/MeOH extracts more lipid material than other solvent systems [23]. $CHCl_3$/MeOH has also been used by previous studies of silk lipids [9, 10]. However, in studies of insect cuticular lipids, extraction with DCM/hexanes has been chosen because this system is better suited for extracting straight and branched-chain alkanes, and other very hydrophobic lipids found on in-

sect cuticles [24, 25]. Figure 5.4A shows the m/z = 99 ion chromatogram for the $CHCl_3$/MeOH extract of the silk, while Figure 5.4B shows the m/z = 99 ion chromatogram for the DCM/hexanes extract. The value m/z = 99 is characteristic of straight chain alkane ion fragments, corresponding to the undecanium cation, therefore the majority of the peaks in these two chromatograms are indicative of alkanes. The m/z = 99 chromatogram of a prepared alkane standard (in red) is included in each figure for comparison, with the latest eluting peak corresponding to a 36-carbon chain, and the span of earlier-eluting peaks corresponding to chains of 15-29 carbons in length.. In the chromatogram of the $CHCl_3$/MeOH extract (Figure 5.4A), two major classes of lipids are seen, distinguished by their elution times: an earlier-eluting group, corresponding to more polar and shorter chain lipid species, and a late-eluting group, corresponding to very long branched and straight chain lipids. The earlier-eluting group is absent in the DCM/hexanes extract (Figure 5.4B), while more species are present in the late-eluting group to such an extent that they broaden into a large hump. This broad hump is known in petrochemical analysis as an unresolved complex mixture (UCM) [26]. The hump is known to consist of a variety of straight and branched chain alkanes with varying branch substitution positions and lengths. We can characterize the UCM by where it elutes with respect to the elution times for the alkane standards. As it begins eluting near where icosane (20) elutes and extends past hexatriacontane (36), the lipid species in the *A. urichi* silk extract therefore span from around 20 carbons to beyond 36 in length, with various degrees of branching. While $CHCl_3$/MeOH extracts a wider profile of lipids including both short and long chain lipids, DCM/hexanes only selects for the fraction of the total lipid profile that contains the longest chain lipids. We are interested in identifying the presence of long-chain lipids and alkanes but not necessarily interested in a complete and quantitative analysis of the total lipid profile, thus we elected to derivatize only aliquots of

the DCM/hexanes extract, thereby focusing on the longer, more hydrophobic species in the DCM/hexanes extraction. Methyl ester derivatization of carboxylic acid headgroups in the extract enabled detection of lipid species with fatty acid headgroups, because peaks corresponding to species that could undergo methyl-ester derivatization had shifted in their elution times between the chromatograms of underivatized sample and the chromatograms of methyl-derivatized sample. This technique was also used by Weisman et al. [10] to observe the presence of fatty acids in the lipid extracts of green lacewing cocoon silk. Figure 5.4C shows the ion chromatogram at m/z = 143, corresponding to the heptanoic methyl ester cation, an ion fragment of long chain fatty acid methyl esters. Fatty acid esters up to 28 carbons in length could be resolved at relatively evenly spaced elution times, with hexadecanoic (16) and octadecanoic (18) acid esters being the highest in concentration and the icosanoic (20) acid ester being relatively absent. Fatty acids likely exist with carbon chains longer than 28, but the UCM hump makes them difficult to resolve. The mass spectrum of the second earliest-eluting peak in the m/z = 143 chromatogram is shown in Figure 5.4D, which identifies it as the methyl ester of octadecanoic acid. The molecular ion peak is observed at m/z = 298. Silyl ester derivatization of the DCM/hexanes extract also enabled detection of fatty acids in this same manner. Lipids with other headgroups such as alcohol and methyl ether groups were not able to be selected out from the chromatograms as was done for the fatty acids, however this does not necessarily mean that they are not present in the lipid profile of embiopteran silks. Considering the microgram amounts of extracted lipid material and the detection limits of the GC-MS instrument, if they are present, they exist at much lower concentrations. Based on the presence of straight chain and branched alkanes and long chain fatty acids observed in the GC-MS analysis from both the $CHCl_3$/MeOH and DCM/hexanes extractions, the profile of lipids encountered in embiopteran silk appears similar to the profile seen in the silk of the spider *N. clavipes* [9].

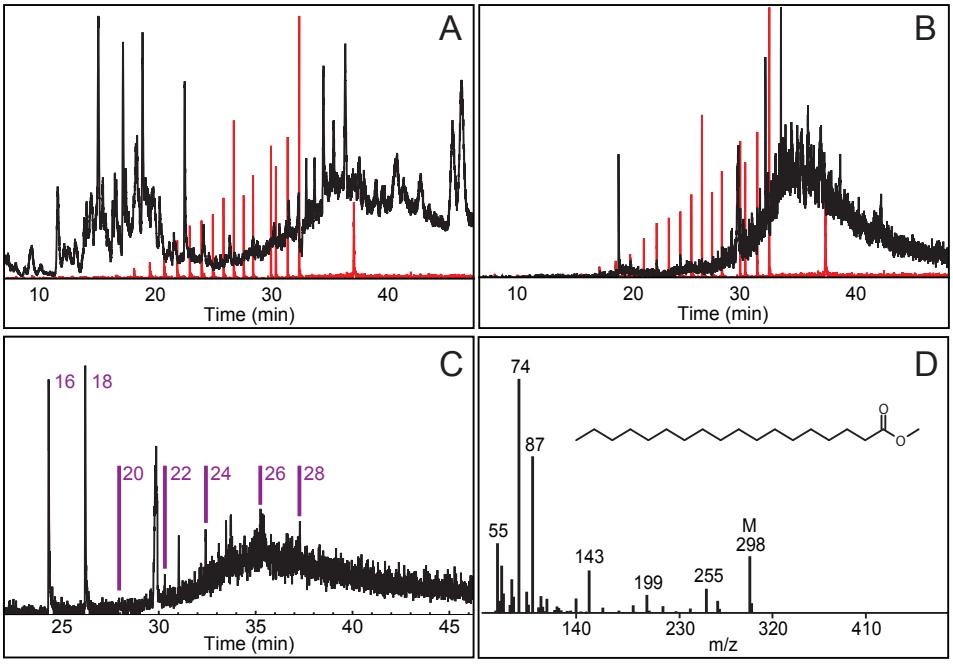

Figure 5.4: Normalized GCMS chromatograms of $CHCl_3$/MeOH (A) and DCM/hexanes (B, C) lipid extracts, with a mass spectrum of one of the lipid species (D). (A) Ion chromatogram at an m/z = 99 Da comparing the elution time of the lipid species extracted using $CHCl_3$/MeOH (black) to a standard mixture of alkanes (red). The highest alkane peak in the standard corresponds to a 36-carbon chain, and the span of earlier-eluting peaks corresponds to chains of 15-29 carbons in length. (B) Ion chromatogram at m/z = 99 Da comparing the elution time of the lipid species extracted using DCM/hexanes (black) to the same standard mixture of alkanes as in A (red). (C) Ion chromatogram of the methyl-ester derivatized lipid extract at m/z = 143. Labels on peaks indicate the length of the fatty acid chain in number of carbons. (D) Mass spectrum of the second-earliest eluting peak in C, identifying the lipid as the methyl ester of octadecanoic acid, with molecular ion peak of m/z = 298.

Also observed in the silyl ester derivatized extract at m/z = 255 were five distinctly resolved steroid silyl ester species, which is a characteristic ion fragment observed for derivatized steroid species [27]. It is possible that these steroid molecules are pheromone signals produced by embiopterans used for communication, as it is well known that many insects communicate by means of pheromones [28, 29], and is known that embiopterans are capable of other complex methods of communication such as the transmission of signals via vibration of their silk gallery walls [30, 31]. Another possibility is that these steroid molecules could exist as a functional component

of the lipid coating on the silk. Steroid incorporation in the surface coating could have the desirable effect of controlling the physical properties of the lipid coating, such as fluidity and mobility, so that the coated silk is not waxy and hard, yet still hydrophobic.

Contact Angle Hysteresis of Natural and Solvent-Washed Sheets

To analyze the behavior of water on the surface of webspinner silk galleries, we performed a study of the contact angle hysteresis for water on a sheet of silk using the sessile drop method [32]. Measurement of contact angles between liquid droplets and homogenous solid surfaces can provide information about the surface energy of the material by Youngs Equation [33, 34]. However, embiopteran silk sheets are heterogeneous, rough surfaces, and Youngs equation in the simplest sense cannot be used to model the system. Despite this, we are still able to characterize that rough surface to some degree through study of the hysteresis between the maximum and minimum contact angles observed after changing the volume of water in a droplet on a rough surface [35]. The maximum and minimum contact angles for a droplet on a surface are known as the advancing and receding contact angles, respectively. The macroscopic properties of the advancing and receding contact angles and the hysteresis between those depend greatly on both the surface chemistry and on microscopic morphology of the rough surface [16, 36, 36, 37].

Two famous examples of this found in nature are the lotus leaf and the rose petal. Both the lotus leaf and the rose petal are superhydrophobic surfaces (advancing contact angle greater than 150°) that contain micron-scale bumps, or pillars, which themselves are covered in nanoscale ridges. However, the behavior of a water droplet on these two surfaces is remarkably different; a droplet will roll off the surface of a lotus leaf with ease (low contact angle hysteresis), yet the same droplet will adhere to the rose petal (high contact angle hysteresis). These two phenomena are called

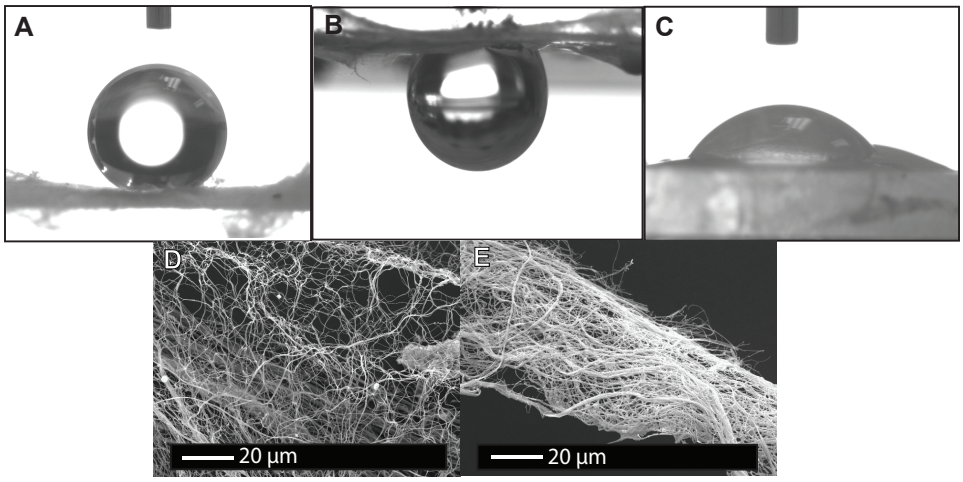

Figure 5.5: Contact angle hysteresis images (A,B,D) and and SEM images (C,E) of native and $CHCl_3$/MeOH washed webspinner silk sheets. (A) Droplet on native *A. urichi* silk, exhibiting a contact angle of 150.1°. (B) Droplet suspended upside down on natural silk, hanging against the force of gravity. (C) Droplet on $CHCl_3$/MeOH washed silk. Note the reduced contact angle of the droplet in contact with the silk, and as the droplet seeps through the silk to the glass slide below, the contact angle of water on the glass beneath can also be seen. (D) SEM image of natural silk. (E) SEM image of $CHCl_3$/MeOH-washed silk.

the lotus effect and the rose-petal effect, respectively. The difference between these two hydrophobic states is due to the degree to which the water droplet is capable of penetrating into the micro- and nanostructural features (for a nice discussion on the different superhydrophobic states and wetting schemes, see Bhushan and Nosonovsky, 2010) [37]. In the case of the lotus leaf, the geometry and spacing of the microscale pillars are such that a water droplet is incapable of penetrating and instead sits on top of both the micro- and nanostructures [38, 39], whereas the geometry and spacing of the pillars on the surface of the rose petal allow water to impregnate the microstructure but not into the nanostructure, effectively pinning the droplet in place [40].

Our contact angle measurements suggest that embiopteran silk sheets show similar macroscopic water-behavior properties to the rose petal, namely that the surface is superhydrophobic and shows a large hysteresis between advancing and receding

contact angles (Figure 5.5). The advancing contact angle between a water droplet and the surface of natural embiopteran silk sheets was determined to be 150 ± 0.1° averaged across five measurements (Figure 5.5A), indicating that the silk sheets are extremely hydrophobic. A value other than 0° was not obtained for the receding angle. As measurement of the receding contact angle using the sessile drop technique is a common problem for rough surfaces with high hysteresis, an attempt was made to determine the receding contact angle in the method suggested by Korhonen et al. [41], but even the very largest of droplets (75-100 μL) resulted in a receding angle of 0°. This result does not necessarily indicate that the contact angle hysteresis of the silk sheet truly spans between 150° and 0°, but rather that the receding angle is probably very small, making it very difficult to measure for this surface [34]. The high contact angle hysteresis is suggestive of water adhesion properties, and indeed Figure 5.5B shows an inverted 20 μL droplet adhering to the surface of the silk suspended against the force of gravity. Droplets up to a volume of 70 μL could be suspended in this manner. With this hydrophobic yet adhesive property, webspinner silk galleries are able to keep insects dry beneath while also maintaining access to drinking water.

The apparent rose-petal effect observed for webspinner silks is likely a result of a similar superhydrophobic state in which water is capable of penetrating into the sheets microstructure but not into the nanostructure [40, 37]. However in the case of *A. urichi* silk sheets, the micro- and nanostructure are not achieved through pillars with nanoscale ridges like the rose petal, but instead through the interwoven bundles of nanoscale silk fibers. As can be seen from Figure 5.5D, the micron-scale structure arises from the approximately 5-10 micron-wide gaps between silk fibers or bundles of fibers, and the nanostructure consists of the 90-100 nm thick fibers, the thin ridges between bundles of fibers, and intersection points of overlapping fibers. We believe it is these elements that form a microscopic hierarchical structure that creates the

macroscopic property of the rose-petal effect. It is also clear that the hydrophobic lipid coating is essential for the observed waterproofing property; after removal of the lipid coating through washing with DCM/hexanes, the silk sheet becomes completely permeable to water (Figure 5.5C). The reduced contact angle of the droplet post-wash is clear, and additionally one notices that the water has seeped through the silk sheet and is in contact with the glass surface beneath. Figure 5.5E shows the breakdown of the microscopic hierarchical structure post-wash, possibly due to exposed proteinaceous fiber cores clumping together, suggesting that the lipid layer is essential towards maintaining the microscopic fine structure.

Microenvironment and Choreography of Spinning

The structure and morphology of the silk galleries results in a protective shelter with qualities highly suited for the habitat and lifestyle of rainforest embiids. Most notably, the silk sheets must be strong and tough to deter predators, must have waterproofing properties to protect the colonies from the threat of drowning, and must have water-adhesive properties so that insects maintain access to drinking water without having to leave the safety of the colony. Therefore we believe it is likely that in addition to the tough β-sheet-rich proteinaceous core and the hydrophobic lipid surface coating on the silk fibers, the peculiar and specific silk-spinning motions of webspinners evolved as a means to create woven sheets that have a micro- and nanostructure optimal for exhibiting the beneficial rose-petal effect [2, 4]. Careful control of the micro- and nanostructural surface morphology of synthetic materials has allowed researchers and engineers to create superhydrophobic surfaces that show either low or high adhesion to water, thus replicating the lotus effect and the rose-petal effect, respectively [42, 43, 44, 17, 45]. We hypothesize that when spinning silk sheets, embiopterans are similarly capable of controlling the surface fine structure and morphology through their specific tarsal motions, and in turn the behavior of

water on the surface of the galleries. This hypothesis that embiopterans adjust their silk spinning behavior in response to habitat is supported by our observations of individual insects in controlled laboratory environments.

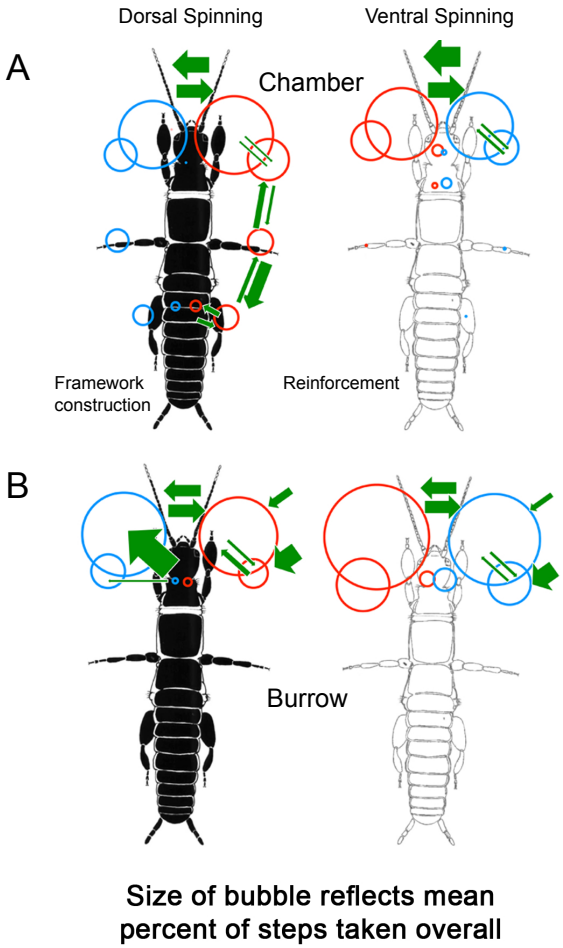

Figure 5.6: Kinematic diagrams of silk spinning behavior of *Antipaluria urichi* in a Chamber arena (A) or in a Burrow arena (B). The bubble size reflects the mean proportion of steps taken in a particular step position, represented by the position of the bubble around the body. The black image shows the insect spinning with her dorsum toward the camera as she sits on the bottom of the arena, whereas the outlined image shows her flipped over to face the camera, and the emerging silk covering (or the lid if in the burrow). If they are stepping in a position, the arrow shows the mean probability of going from that position to the next. Arrows pointing at a bubble indicate probability of repeating a step. Transitions on only one side are shown because they are approximately the same of the other side.

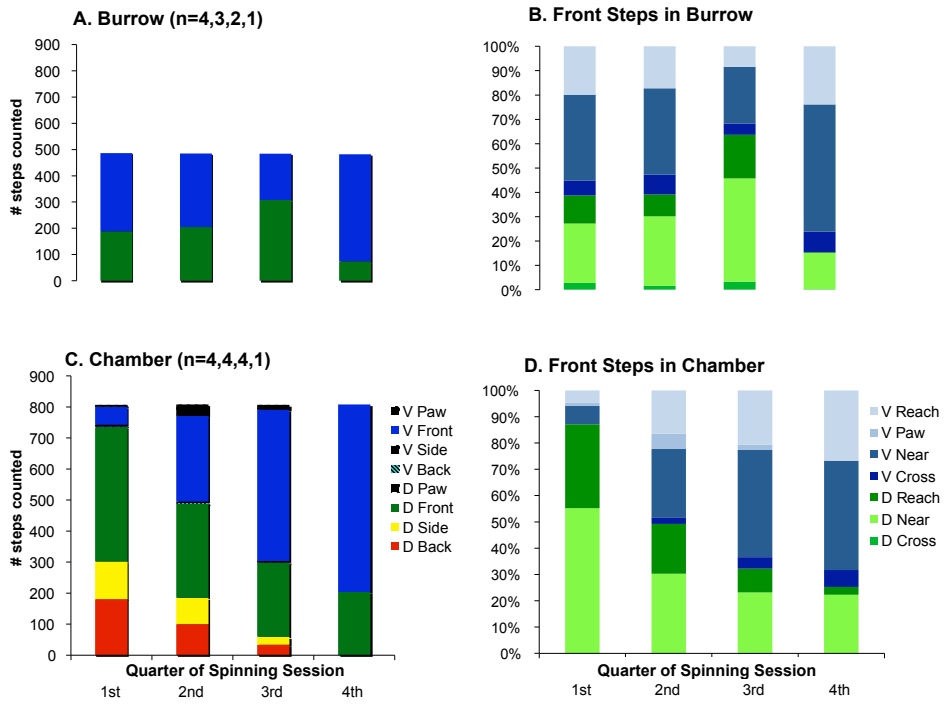

Figure 5.7: Details of spinning over time by *Antipaluria urichi* in a Burrow (A and B) or in a Chamber (C and D) arena. Spinning bouts were split into quarters of spinning and number of steps taken of varying positions displayed as mean values for four (Burrow) or five (Chamber) females. Positions of steps named here are illustrated in Figure 5.6. The split into quarters was determined by dividing the number of steps in a time event report for the female that spun the most in each arena. The records of the other females were related to this most productive spinner. Sample sizes show how many females are represented in each quarter of the session. As example, in the Chamber only one females record is shown for the 4th quarter of spinning because the others had stopped spinning early relative to the most productive spinner. This happened because some of them started to spin late in the hour-long trial and were cut off before they completely switched to full ventral spinning.

As expected if *A. urichi* were responsive to particular microhabitats, they emphasized different spin styles when placed into an open chamber versus a tight burrow. In the open, on bark, they produced more complex steps overall, as illustrated in the significantly higher mean step diversity scores when in the chamber (0.844 0.008 (SE) versus 0.723 0.017 in the burrow; Students t = 6.1716, P ¡ 0.001). In addition, Cham-

ber spinners displayed significantly more spin steps (mean for Chamber = 2785 ± 161 (SE) and for Burrow = 1252 ± 285; Students t = 5.09, P ¡ 0.001) and spent more time spinning (Chamber mean time = 1335 ± 52.5 s and Burrow mean time = 649.3 ± 122.7 s; Students t = 5.55, P = 0.0014). The more complex spinning expressed in the chamber was due to actions early in the trials when they stepped around their bodies and especially over their dorsums, creating the framework necessary for building a sheet of silk. These behaviors are shown in Figure 5.7, which illustrates the changes in spin steps as the silk builds up over time. In contrast, spinners in the burrow showed only spin steps around the anterior of their bodies, actions that would coat the burrows surface but not create a framework of silk. In contrast to these differences, front stepping details were similar for spinners in both arenas. Chamber spinners switched to front steps toward the second half of the trial, while Burrow spinners displayed these steps throughout their time spinning. Chamber spinners gradually shifted from creating a domicile covering, using dorsal steps illustrated in green in the graph, to ventral steps (shown in blue, Figure 5.7C and 5.7D), which appear to reinforce the emerging structure. In sum, spinners that need to build a covering of silk do so first. The rapid, complex spinning steps, such as ventral near, reach, cross and so forth, appear to explain the complex microstructure of their silk walls and these spin steps were expressed in both situations. The transition arrows in the kinematic diagrams show that *A. urichi* switches from foot to foot but also repeats certain steps over and over before stepping to a different position. Silk is ejected throughout these actions and repeat stepping thickens the silk patch. Supplemental Figure 2 shows the overall behavioral acts of individuals in the two arenas demonstrating that throughout the trials they were also traveling, flipping over and turning around as they spin back and forth, rather than in one spot. As they move, a tube builds up that can cover their relatively long bodies (mean body length = 1.6 ± 0.02 cm) [5]. Observations of

females in the field caring for their eggs showed a similar style of spinning by rapid steps taken in one spot and indeed, the eggs are covered with very thick silk [5]. The silk samples used in the subsequent analysis of micro- and nanostructure as well as in the tests for interactions with water were taken from laboratory cultures where the embiopterans would have spun with the full complement of stepping displayed in the kinematics for the open apparatus (Figure 6A; Figure 7C and 7D).

5.5 Conclusions

In summary, we have characterized both the composition and functional use of an alkane or lipid-rich surface coating on webspinner silk of the species *Antipaluria urichi*. Embiopterans create protective shelters and domiciles by spinning silken sheets and tunnels composed of exceptionally thin ($\sim$ 100 nm in diameter) protein-based fibers. In addition to providing physical structure and protection from predators, the silk sheets are hydrophobic surfaces, offering insects protection from tropical rainfall. We have shown that this waterproof nature is a result of a hydrophobic alkane / lipid-rich surface coating on the silk fibers. As revealed by SEM images and FTIR measurements, this surface coating is removed when fibers are washed with 2:1 $CHCl_3$/MeOH, a standard lipid extraction solvent. The lipids extracted using organic solvents were profiled using GC-MS, providing a first look into the types of lipids present in the surface coating of *A. urichi* silk. We revealed the presence of a wide variety of lipid species including straight and branched-chain alkanes, fatty acids and methyl esters of chain-length out to and possibly greater than 36 carbons. The water behavior properties caused by this surface coating and by the silk sheet's fine structure were also investigated using contact angle measurements. Just like how the lotus leaf and the rose petal have evolved fine structure details suited for their habitat, we argue that the combination of a hydrophobic coating on the nanofibers with the micro- and

nanostructural details results in a superhydrophobic surface that is adhesive to water, a property shared with the rose petal, and that the structural detail may be a result of the peculiar and complex spinning behavior of the insect. This concept of spinning behavior adapting to microhabitat is supported by our observations that *A. urichi* adult females spin more silk using more complex stepping patterns in an open (chamber) habitat than in an enclosed (burrow) environment. With its unique properties, embiid silk may provide future inspiration to develop biomimetic materials that are strong, lightweight, and hydrophobic. As the rose-petal effect of the sheets is contingent on the lipid coating, nanoscale fiber polymer sheet materials could be designed to have varying levels of water-permeability based on the fine structure details and the degree to which the fibers are coated in hydrophobic material.

5.6 Supplemental Material

The text and figures below were provided as supplementary material for chapter 5, which was submitted for publication to the Journal of Chemical Ecology. The information describes the methodology for monitoring silk spinning behavior. All of the silk spinning behavior data was collected by Dr. Janice Edgerly and her students at Santa Clara University.

Silk Spinning Behavior Spinning behavior was evaluated only in adult females to minimize variability due to a sex effect and because adult females produce copious silk during their stints as caregivers for their young [46]. To induce spinning in the laboratory at Santa Clara University, five individuals were placed into either a narrow notch into a plywood block, covered with a transparent plastic lid, or into a bark-lined plexiglass arena set-up as shown in Supplemental Figure S1. They cannot reach to spin silk against the top of the box in the chamber arena, unlike in the burrow where they could easily touch the lid. Females typically spin silk when they are removed from their domiciles and placed into silk-free habitats and, for the most part, spinning was elicited with this method. One female was eliminated from the analysis because she wandered back and forth but did not spin in the burrow. Behavioral acts were scored using Observer software (version 5, Noldus Information Technology, Wageningen, The Netherlands). Videos were replayed at 1/2 speed and the same investigator scored the behaviors to minimize investigator error. The proportion of time spent spinning and stepping details were calculated for females in the two different arenas.

Spin steps were represented as positional features of stepping displayed as each individual pressed her silk ejectors against the surfaces of the burrow, the bark, or against the emerging silk structure. Spin step positions (described in a previous study [4]) are labeled in the kinematic diagrams in Figure 5.5, which shows the proportion

of steps taken by the left and right front feet around the body. They usually start by spinning with their feet planted on the wooden floor of the burrow or against the bark of the chamber arena, and their dorsum facing the camera lens, an orientation we named dorsal. They also flip over (to a position dubbed ventral) as they add silk to previously produced silk above their dorsum. We quantified the stepping patterns in the two arenas by calculating the mean relative frequency of each step position and the mean probability of transition between each possible combination of steps. We also calculated and compared the mean total number of spin steps in the burrow vs. the chamber with a Students t-test. Finally, a measure of spin step diversity was computed by adopting a measure used to quantify species diversity in ecology, Simpsons Species Diversity Index [47], which collapses all spin steps into a number that reflects the diversity of stepping, by treating each step as a species. A higher value represents more diverse spin steps during a session. The mean diversity score was compared for spinners in the burrow and chamber with a Students t-test. We predicted that the chamber arena would elicit more complex spinning in *A. urichi* because of the apparent need to create a framework for their silk domiciles. If they display stereotypical spinning and are not responsive to situation, then no difference should emerge between Burrow or Chamber. Either way, the results will provide insight into the dynamics of weaving silk.

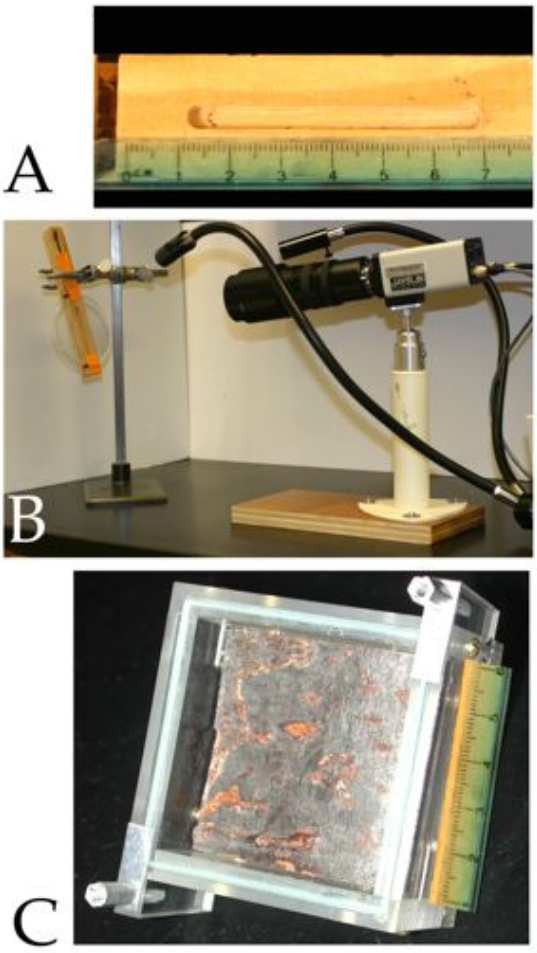

Figure 5.8: Spinning apparatus for filming webspinners as they spin silk in either a (A) Burrow (0.3 cm wide X 0.5 cm dep X 5.8 cm long) drilled into a block of plywood to resemble a crevice in bark or (C)Chamber, a plexiglass box lined on one side with oak bark (inner dimension of 6 cm long by 6 cm wide by 4 cm deep). Each individual was filmed with a (B) solid state video-camera with an 18 mm to 108 mm F 2.5 TV-style zoom lens (Javelin Electronics, Torrance, California, USA) for one hour and recorded onto a DVD to allow playback.

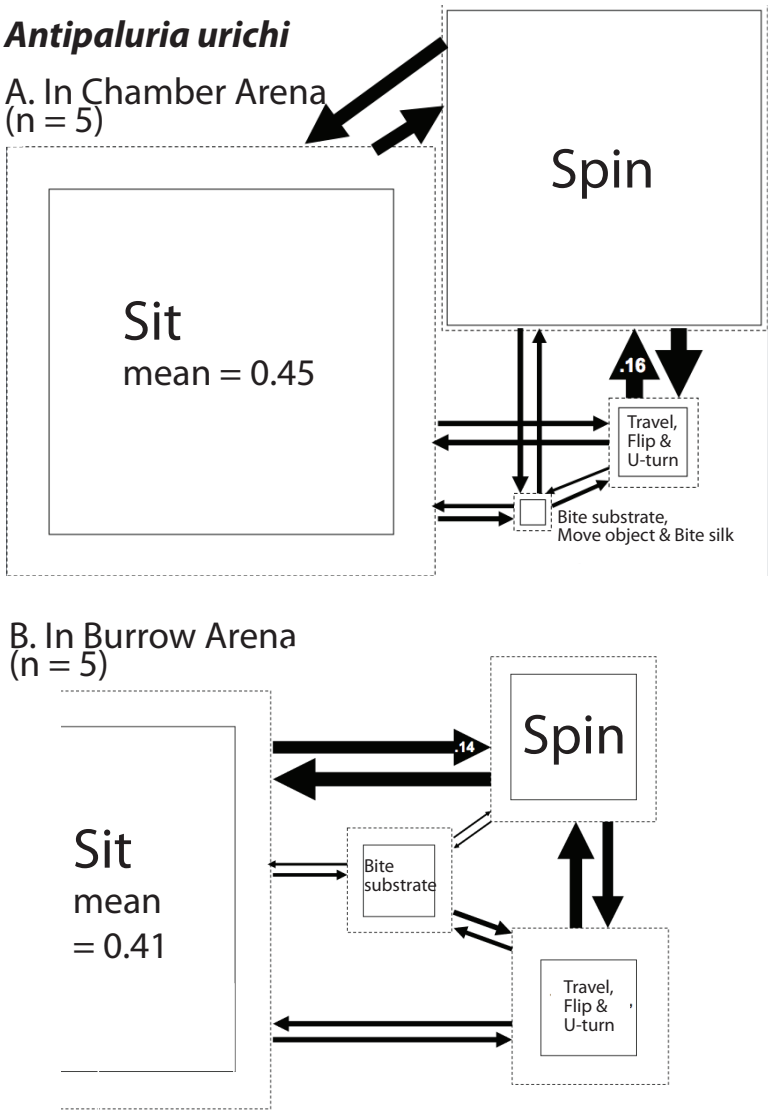

Figure 5.9: Time budgets shown as mean proportion of time (solid black line) (with standard deviation as outer dotted line) spent in various activities during filming in the two arena types (A) Chamber and (B) Burrow. Arrows indicate mean transition probabilities from one behavior to another. Flip is the action of turning over while spinning to face the silk or alternatively to face the substrate. Other behaviors are self-explanatory.

REFERENCES

[1] Janice S Edgerly. Life Beneath Silk Walls: A Review of the Primitively Social Embiidina. In J C Choe and B Crespi, editors, *The Evolution of Social Behavior in Insects and Arachnids*, pages 14–25. Cambridge University Press, 1997.

[2] J S Edgerly, J A Davilla, and N Schoenfeld. Silk Spinning Behavior and Domicile Construction in Webspinners - Springer. *Journal of Insect Behavior*, 15(2):219–242, 2002.

[3] T Nagashima, N Niwa, S Okajima, and T Nonaka. Ultrastructure of silk gland of webspinners, Oligotoma japonica (Insecta, Embioptera). *Cytologia : international journal of cytology*, 1991.

[4] J S Edgerly, S Büsse, and T Hörnschemeyer. Spinning behaviour and morphology of the spinning glands. *Zoologischer Anzeiger*, (251):297–306, 2012.

[5] Janice S Edgerly. Maternal behaviour of a webspinner (Order Embiidina). *Ecological Entomology*, 12(1):1–11, February 1987.

[6] J S Edgerly, S M Shenoy, and V G Werner. Relating the Cost of Spinning Silk to the Tendency to Share It for Three Embiids with Different Lifestyles (Order Embiidina: Clothodidae, Notoligotomidae, and Australembiidae). *Environmental Entomology*, 35(2):448–457, April 2006.

[7] Janice S Edgerly. Is group living an antipredator defense in a facultatively communal webspinner (Embiidina: Clothodidae)? *Journal of Insect Behavior*, 7(2):135–147, March 1994.

[8] J S Edgerly. *Behavioral ecology of a Primitively Social Webspinner (Embiidina: Clothodidae:* Clothoda urichi*)*. . PhD thesis, Cornell University, January 1986.

[9] Stefan Schulz. Composition of the silk lipids of the spider Nephila clavipes. *Lipids*, 36(6):637–647, June 2001.

[10] Sarah Weisman, Holly E Trueman, Stephen T Mudie, Jeffrey S Church, Tara D Sutherland, and Victoria S Haritos. An Unlikely Silk: The Composite Material of Green Lacewing Cocoons. *Biomacromolecules*, 9(11):3065–3069, November 2008.

[11] Alexander Sponner, Wolfram Vater, Shamci Monajembashi, Eberhard Unger, Frank Grosse, and Klaus Weisshart. Composition and Hierarchical Organisation of a Spider Silk. *PLoS ONE*, 2(10):e998, October 2007.

[12] Eliane Victoriano, Daniela O Pinheiro, and Elisa A Gregório. Histochemical and ultrastructural evidence of lipid secretion by the silk gland of the sugarcane borer Diatraea saccharalis (Fabricius) (Lepidoptera: Crambidae). *Neotropical entomology*, 36(5):707–711, September 2007.

[13] Matthew A Collin, Jessica E Garb, Janice S Edgerly, and Cheryl Y Hayashi. Characterization of silk spun by the embiopteran, Antipaluria urichi. *Insect biochemistry and molecular biology*, 39(2):75–82, February 2009.

[14] Matthew A Collin, Edina Camama, Brook O Swanson, Janice S Edgerly, and Cheryl Y Hayashi. Comparison of embiopteran silks reveals tensile and structural similarities across Taxa. *Biomacromolecules*, 10(8):2268–2274, August 2009.

[15] Shoko Okada, Sarah Weisman, Holly E Trueman, Stephen T Mudie, Victoria S Haritos, and Tara D Sutherland. An Australian webspinner species makes the finest known insect silk fibers. *International Journal of Biological Macromolecules*, 43(3):271–275, October 2008.

[16] S Wang and L Jiang. Definition of Superhydrophobic States. *Advanced Materials*, 19(21):3423–3424, November 2007.

[17] Yong Min Park, Myeong Gang, Young Ho Seo, and Byeong Hee Kim. Artificial petal surface based on hierarchical micro- and nanostructures. *Thin Solid Films*, 520(1):362–367, October 2011.

[18] Xin Yong and Lucy T Zhang. Nanoscale Wetting on Groove-Patterned Surfaces. *Langmuir*, 25(9):5045–5053, May 2009.

[19] Ruthven N A H Lewis and Ronald N McElhaney. Fourier transform infrared spectroscopy in the study of lipid phase transitions in model and biological membranes: practical considerations. *Methods in molecular biology (Clifton, N.J.)*, 400:207–226, 2007.

[20] G H Altman, F Diaz, C Jakuba, T Calabro, R L Horan, J Chen, H Lu, J Richmond, and D L Kaplan. Silk-based biomaterials. *Biomaterials*, 24(3):401–416, 2003.

[21] Matthew A Collin, Janice S Edgerly, and Cheryl Y Hayashi. Comparison of fibroin cDNAs from webspinning insects: insight into silk formation and function. *Zoology (Jena, Germany)*, 114(4):239–246, September 2011.

[22] P Manirakiza, A Covaci, and P Schepens. Comparative Study on Total Lipid Determination using Soxhlet, Roese-Gottlieb, Bligh & Dyer, and Modified Bligh & Dyer Extraction Methods. *Journal of Food Composition and Analysis*, 14(1):93–100, February 2001.

[23] Robert C Randall, Henry Lee, II, Robert J Ozretich, James L Lake, and Richard J Pruell. Evaluation of selected lipid methods for normalizing pollutant bioaccumulation. *Environmental Toxicology and Chemistry*, 10(11):1431–1436, November 1991.

[24] Agustín Estrada-Peña, Frantisek Dusbábek, and Joaquím Castellá. Cuticular hydrocarbon variation and progeny phenotypic similarity between laboratory breeds of allopatric populations of Argas (Persicargas) persicus (Oken) (acari: Argasidae). *Acta Tropica*, 59(4):309–322, August 1995.

[25] Jakob A Shimshoni, Oran Erster, Asael Rot, Olga Cuneah, Stefan Soback, and Varda Shkap. Cuticular fatty acid profile analysis of three Rhipicephalus tick species (Acari: Ixodidae). *Experimental & applied acarology*, 61(4):481–489, December 2013.

[26] M A Gough and S J Rowland. Characterization of unresolved complex mixtures of hydrocarbons in petroleum. *Nature*, 344(6267):648–650, April 1990.

[27] Marco Pelillo, Giovanna Iafelice, Emanuele Marconi, and Maria Fiorenza Caboni. Identification of plant sterols in hexaploid and tetraploid wheats using gas chromatography with mass spectrometry. *Rapid communications in mass spectrometry : RCM*, 17(20):2245–2252, 2003.

[28] P Karlson and A Butenandt. Pheromones (ectohormones) in insects. *Annual review of entomology*, 1959.

[29] J H Tumlinson, R M Silverstein, J C Moser, R G Brownlee, and J M Ruth. Identification of the trail pheromone of a leaf-cutting ant, Atta texana. *Nature*, 234(5328):348–349, December 1971.

[30] C B Proaño, S Cruz, D M McMillan, and J S Edgerly. Exploration of substrate vibrations as communication signals in a webspinner from Ecuador (Embioptera: Clothodidae). *Neotropical entomology*, 41(3):196–203, June 2012.

[31] Khaaliq A Dejan, John M Fresquez, Annika M Meyer, and Janice S Edgerly. Maternal territoriality achieved through shaking and lunging: An investigation of patterns in associated behaviors and substrate vibrations in a colonial embiopteran, Antipaluria urichi. *Journal of Insect Science*, 13:1–28, August 2013.

[32] J F Padday. Sessile Drop Profiles: Corrected Methods for Surface Tension and Spreading Coefficients. *Proceedings of the Royal Society A: Mathematical, Physical and Engineering Sciences*, 330(1583):561–572, November 1972.

[33] ABD Cassie. Contact angles. *Discuss Faraday Soc*, 1948.

[34] D Y Kwok and A W Neumann. Contact angle measurement and contact angle interpretation. *Advances in Colloid and Interface Science*, 81(3):167–249, September 1999.

[35] Lichao Gao and Thomas J McCarthy. Contact angle hysteresis explained. *Langmuir*, 22(14):6234–6237, July 2006.

[36] Zhongjun Cheng, Ming Du, Hua Lai, Naiqing Zhang, and Kening Sun. From petal effect to lotus effect: a facile solution immersion process for the fabrication of super-hydrophobic surfaces with controlled adhesion . *Nanoscale*, 5(7):2776–2783, 2013.

[37] Bharat Bhushan and Michael Nosonovsky. The rose petal effect and the modes of superhydrophobicity. *Philosophical transactions. Series A, Mathematical, physical, and engineering sciences*, 368(1929):4713–4728, October 2010.

[38] C Neinhuis and W Barthlott. Characterization and Distribution of Water-repellent, Self-cleaning Plant Surfaces. *Annals of Botany*, 79(6):667–677, June 1997.

[39] Abraham Marmur. The Lotus effect: superhydrophobicity and metastability. *Langmuir*, 20(9):3517–3519, April 2004.

[40] Lin Feng, Yanan Zhang, Jinming Xi, Ying Zhu, Nü Wang, Fan Xia, and Lei Jiang. Petal effect: a superhydrophobic state with high adhesive force. *Langmuir*, 24(8):4114–4119, April 2008.

[41] Juuso T Korhonen, Tommi Huhtamäki, Olli Ikkala, and Robin H A Ras. Reliable measurement of the receding contact angle. *Langmuir*, 29(12):3858–3863, March 2013.

[42] L Feng, S Li, Y Li, H Li, L Zhang, and J Zhai. Super-Hydrophobic Surfaces: From Natural to Artificial - Feng - 2002 - Advanced Materials - Wiley Online Library. *Advanced . . .*, 2002.

[43] Bharat Bhushan and Eun Kyu Her. Fabrication of Superhydrophobic Surfaces with High and Low Adhesion Inspired from Rose Petal. *Langmuir*, 26(11):8207–8217, June 2010.

[44] Bharat Bhushan. Bioinspired structured surfaces. *Langmuir*, 28(3):1698–1714, January 2012.

[45] Elena Celia, Thierry Darmanin, Elisabeth Taffin de Givenchy, Sonia Amigoni, and Frédéric Guittard. Recent advances in designing superhydrophobic surfaces. *Journal of Colloid and Interface Science*, 402:1–18, July 2013.

[46] Janice S Edgerly. Maternal behaviour of a webspinner (Order Embiidina): mother-nymph associations. *Ecological Entomology*, 13(3):263–272, August 1988.

[47] J E Brower, J H Zar, and C N vonEnde. *Field and laboratory methods for general ecology*. WCB McGraw-Hill, Boston, Massachusetts, 4th edition, 1997.

REFERENCES: CHAPTER 1

[1] C Craig. Evolution of arthropod silks. *Annual review of entomology*, 1997.

[2] Fritz Vollrath. Liquid crystalline spinning of spider silk. *Nature*, 2001.

[3] C Wong Po Foo, E Bini, J Hensman, D P Knight, R V Lewis, and D L Kaplan. Role of pH and charge on silk protein assembly in insects and spiders. *Applied Physics A*, 82(2):223–233, 2006.

[4] Danielle N Rockwood, Rucsanda C Preda, Tuna Yücel, Xiaoqin Wang, Michael L Lovett, and David L Kaplan. Materials fabrication from Bombyx mori silk fibroin. *Nature Protocols*, 6(10):1612–1631, September 2011.

[5] Fritz Vollrath. Strength and structure of spiders' silks. *Reviews in Molecular Biotechnology*, 74(2):67–83, August 2000.

[6] John M Gosline, Mark W Denny, and M Edwin DeMont. Spider silk as rubber. *Nature*, 309(5968):551–552, June 1984.

[7] J M Gosline, P A Guerette, C S Ortlepp, and K N Savage. The mechanical design of spider silks: from fibroin sequence to mechanical function. *The Journal of Experimental Biology*, 202(Pt 23):3295–3303, December 1999.

[8] Tara D Sutherland, James H Young, Sarah Weisman, Cheryl Y Hayashi, and David J Merritt. Insect silk: one name, many materials. *Annual review of entomology*, 55:171–188, 2010.

[9] P Duelli. A 'missing link' in the evolution of the egg pedicel in lacewings? *Experientia*, 42(6):624–624, June 1986.

[10] Sarah Weisman, Shoko Okada, Stephen T Mudie, Mickey G Huson, Holly E Trueman, Alagacone Sriskantha, Victoria S Haritos, and Tara D Sutherland. Fifty years later: the sequence, structure and function of lacewing cross-beta silk. *Journal of structural biology*, 168(3):467–475, December 2009.

[11] Andrew A Walker, Sarah Weisman, Jeffrey S Church, David J Merritt, Stephen T Mudie, and Tara D Sutherland. Silk from Crickets: A New Twist on Spinning. *PLoS ONE*, 7(2):e30408, February 2012.

[12] R H Crozier, P S Newey, and E A Schluens. A masterpiece of evolution—Oecophylla weaver ants (Hymenoptera: Formicidae). *Myrmecological News*, 13:57–71, December 2009.

[13] Gary LaFontaine. *Caddisflies*. The Lyons Press, April 1989.

[14] Glenn B Wiggins. *The caddisfly family Phryganeidae (Trichoptera)*. University of Toronto Press Incorporated, 1998.

[15] E S Ross. A synopsis of the embiidina of the United States. *Proceedings of the Entomological Society of Washington*, 86(1):82–93, 1984.

[16] Edward S Ross. Webspinners (Embiidina). In John L Capirena, editor, *Encyclopedia of Entomology*, pages 4169–4172. Springer Netherlands, 2008.

[17] Jacques Bitsch. Ultrastructure of the phallic glands of the firebrat, Thermobia domestica (packard) (Thysanura : Lepismatidae). *International Journal of Insect Morphology and Embryology*, 19(2):65–78, January 1990.

[18] C Craig, M Hsu, and D Kaplan. A comparison of the composition of silk proteins produced by spiders and insects. *International journal of biological ...*, 1999.

[19] E Fischer. About spider silk. *Hoppe-Seyler's Z Physiol Chem*, pages 440–450, 1907.

[20] Yoshihide Tsujimoto and Yoshiaki Suzuki. The dna sequence of bombyx mori fibroin gene including the 5 flanking, mRNA coding, entire intervening and fibroin protein coding regions. *Cell*, 18(2):591–600, October 1979.

[21] F Sehnal and M Zurovec. Construction of silk fiber core in Lepidoptera. *Biomacromolecules*, 5(3):666–674, 2004.

[22] Tetsuo Ohmachi, Hideo Nagayama, and Kensuke Shimura. The isolation of a messenger RNA coding for the small subunit of fibroin from the posterior silkgland of the silkworm, Bombyx mori. *FEBS letters*, 146(2):385–388, September 1982.

[23] M Xu and R V Lewis. Structure of a protein superfiber: spider dragline silk. *Proceedings of the National Academy of Sciences of the United States of America*, 87(18):7120–7124, September 1990.

[24] Michael B Hinman and Randolph V Lewis. Isolation of a clone encoding a second dragline silk fibroin. Nephila clavipes dragline silk is a two-protein fiber. *The Journal of biological chemistry*, 267(27):19320–19324, 1992.

[25] C Y Hayashi, N H Shipley, and R V Lewis. Hypotheses that correlate the sequence, structure, and mechanical properties of spider silk proteins. *International Journal of Biological Macromolecules*, 24(2-3):271–275, March 1999.

[26] Tetsuo Asakura, Yu Suzuki, Yasumoto Nakazawa, Gregory P Holland, and Jeffery L Yarger. Elucidating silk structure using solid-state NMR. *Soft Matter*, 9(48):11440–11450, 2013.

[27] J D van Beek. The molecular structure of spider dragline silk: Folding and orientation of the protein backbone. *Proceedings of the National Academy of Sciences*, 99(16):10266–10271, July 2002.

[28] L Beaulieu, H Schäfer, M Demura, and T Asakura. Solid-state NMR determination of the secondary structure of Samia cynthia ricini silk. *Nature*, 2000.

[29] Gregory P Holland, Melinda S Creager, and Janelle E Jenkins. Determining Secondary Structure in Spider Dragline Silk by Carbon Carbon Correlation Solid-State NMR Spectroscopy. *Journal of the ...*, 2008.

[30] M S Creager, E B Butler, R V Lewis, J L Yarger, and G P Holland. Solid-state NMR evidence for elastin-like β-turn structure in spider dragline silk. *Chemical Communications*, 46(36):6714–6716, 2010.

[31] Xiangyan Shi, Jeffery L Yarger, and Gregory P Holland. Elucidating proline dynamics in spider dragline silk fibre using 2H-13C HETCOR MAS NMR. *Chemical Communications*, 50(37):4856–4859, May 2014.

[32] Sujatha Sampath, Thomas Isdebski, Janelle E Jenkins, Joel V Ayon, Robert W Henning, Joseph P R O Orgel, Olga Antipoa, and Jeffery L Yarger. X-ray diffraction study of nanocrystalline and amorphous structure within major and minor ampullate dragline spider silks. *Soft Matter*, 8(25):6713–6722, 2012.

[33] Tetsuo Asakura, Kosuke Ohgo, Kohei Komatsu, Masakazu Kanenari, and Kenji Okuyama. Refinement of Repeated β-turn Structure for Silk I Conformation of Bombyx moriSilk Fibroin Using 13C Solid-State NMR and X-ray Diffraction Methods. *Macromolecules*, 38(17):7397–7403, August 2005.

[34] A Simmons, E Ray, and LW Jelinski. Solid-state 13C NMR of Nephila clavipes dragline silk establishes structure and identity of crystalline regions. *Macromolecules*, 27(18):5235–5237, 1994.

[35] Janelle E Jenkins, Melinda S Creager, Randolph V Lewis, Gregory P Holland, and Jeffery L Yarger. Quantitative Correlation between the protein primary sequences and secondary structures in spider dragline silks. *Biomacromolecules*, 11(1):192–200, 2009.

[36] Z Yang, DT Grubb, and LW Jelinski. Small-angle X-ray scattering of spider dragline silk. *Macromolecules*, 30(26):8254–8261, 1997.

[37] Gregory P Holland, Randolph V Lewis, and Jeffery L Yarger. WISE NMR characterization of nanoscale heterogeneity and mobility in supercontracted Nephila clavipes spider dragline silk. *J. Am. Chem. Soc*, 126(18):5867–5872, 2004.

[38] Sinan Keten and Markus J Buehler. Atomistic model of the spider silk nanostructure. *Applied physics letters*, 96(15):153701, 2010.

[39] Nathan Becker, Emin Oroudjev, Stephanie Mutz, Jason P Cleveland, Paul K Hansma, Cheryl Y Hayashi, Dmitrii E Makarov, and Helen G Hansma. Molecular nanosprings in spider capture-silk threads. *Nature Materials*, 2(4):278–283, March 2003.

[40] Yi Liu and Zhengzhong Shao. Elasticity of spider silks. *Biomacromolecules*, 9:1782–1786, 2008.

[41] Matthew A Collin, Janice S Edgerly, and Cheryl Y Hayashi. Comparison of fibroin cDNAs from webspinning insects: insight into silk formation and function. *Zoology (Jena, Germany)*, 114(4):239–246, September 2011.

[42] N Yonemura, F Sehnal, and K Mita. Protein composition of silk filaments spun under water by caddisfly larvae. *Biomacromolecules*, 7(12):3370–3378, 2006.

[43] Naoyuki Yonemura, Kazuei Mita, Toshiki Tamura, and František Sehnal. Conservation of Silk Genes in Trichoptera and Lepidoptera. *Journal of molecular evolution*, 68(6):641–653, May 2009.

[44] D M Byler and H Susi. Examination of the secondary structure of proteins by deconvolved FTIR spectra. *Biopolymers*, 25(3):469–487, March 1986.

[45] S Cai and B R Singh. Identification of β-turn and random coil amide III infrared bands for secondary structure estimation of proteins. *Biophysical Chemistry*, 1999.

[46] Md Majibur Rahman Khan, Hideaki Morikawa, Yasuo Gotoh, Mikihiko Miura, Zha Ming, Yuji Sato, and Masayuki Iwasa. Structural characteristics and properties of Bombyx mori silk fiber obtained by different artificial forcibly silking speeds. *International Journal of Biological Macromolecules*, 42(3):264–270, April 2008.

[47] Shengjie Ling, Zeming Qi, David P Knight, Zhengzhong Shao, and Xin Chen. Synchrotron FTIR Microspectroscopy of Single Natural Silk Fibers. *Biomacromolecules*, 12(9):3344–3349, September 2011.

[48] Nicholas N Ashton, Daniel R Roe, Robert B Weiss, Thomas E Cheatham, III, and Russell J Stewart. Self-Tensioning Aquatic Caddisfly Silk: Ca 2+-Dependent Structure, Strength, and Load Cycle Hysteresis. *Biomacromolecules*, 14(10):3668–3681, October 2013.

[49] Matthew A Collin, Edina Camama, Brook O Swanson, Janice S Edgerly, and Cheryl Y Hayashi. Comparison of embiopteran silks reveals tensile and structural similarities across Taxa. *Biomacromolecules*, 10(8):2268–2274, August 2009.

[50] Andrew A Walker, Jeffrey S Church, Andrea L Woodhead, and Tara D Sutherland. Silverfish silk is formed by entanglement of randomly coiled protein chains. *Insect biochemistry and molecular biology*, 43(7):572–579, July 2013.

[51] Sarah Weisman, Holly E Trueman, Stephen T Mudie, Jeffrey S Church, Tara D Sutherland, and Victoria S Haritos. An Unlikely Silk: The Composite Material of Green Lacewing Cocoons. *Biomacromolecules*, 9(11):3065–3069, November 2008.

[52] P Papadopoulos, J Sölter, and F Kremer. Structure-property relationships in major ampullate spider silk as deduced from polarized FTIR spectroscopy. *The European physical journal. E, Soft matter*, 24(2):193–199, October 2007.

[53] Shengjie Ling, Zeming Qi, David P Knight, Yufang Huang, Lei Huang, Huan Zhou, Zhengzhong Shao, and Xin Chen. Insight into the Structure of Single Antheraea pernyi Silkworm Fibers Using Synchrotron FTIR Microspectroscopy. *Biomacromolecules*, 14(6):1885–1892, June 2013.

[54] J O Warwicker. Comparative studies of fibroins. II. The crystal structures of various fibroins. *Journal of Molecular Biology*, 2(6):350–362, December 1960.

[55] DT Grubb and LW Jelinski. Fiber morphology of spider silk: the effects of tensile deformation. *Macromolecules*, 30(10):2860–2867, 1997.

[56] C Riekel, C Bränden, C Craig, C Ferrero, F Heidelbach, and M Müller. Aspects of X-ray diffraction on single spider fibers. *International Journal of Biological Macromolecules*, 24(2-3):179–186, March 1999.

[57] Lawrence F Drummy, B L Farmer, and Rajesh R Naik. Correlation of the ?-sheet crystal size in silk fibers with the protein amino acid sequence. *Soft Matter*, 3(7):877–882, 2007.

[58] Janelle E Jenkins, Sujatha Sampath, Emily Butler, Jihyun Kim, Robert W Henning, Gregory P Holland, and Jeffery L Yarger. Characterizing the secondary protein structure of black widow dragline silk using solid-state NMR and X-ray diffraction. *Biomacromolecules*, 14(10):3472–3483, October 2013.

[59] Ku Liang, Yu Gong, Jianlong Fu, Shi Yan, Yuanyuan Tan, Rong Du, Xueqing Xing, Guang Mo, Zhongjun Chen, Quan Cai, Dongbai Sun, and Zhonghua Wu. Microstructural change of degummed Bombyx mori silk: an in situ stretching wide-angle X-ray-scattering study. *International Journal of Biological Macromolecules*, 57:99–104, June 2013.

[60] Tetsuo Asakura, Juming Yao, Tsutomu Yamane, Kosuke Umemura, and Anne S Ulrich. Heterogeneous Structure of Silk Fibers from BombyxmoriResolved by 13C Solid-State NMR Spectroscopy. *J. Am. Chem. Soc*, 124(30):8794–8795, July 2002.

[61] K Schmidt-Rohr and H W Spiess. *Multidimensional Solid-State NMR and Polymers*. Academic Press, 1 edition, November 1994.

[62] H Saito, I Ando, and A Naito. *Solid State NMR Spectroscopy for Biopolymers*. Springer, July 2006.

[63] S Hartmann. Nuclear double resonance in the rotating frame. *Physical Review*, 1962.

[64] Tetsuo Asakura, Yu Suzuki, Yasumoto Nakazawa, Koji Yazawa, Gregory P Holland, and Jeffery L Yarger. Silk structure studied with nuclear magnetic resonance. *Progress in Nuclear Magnetic Resonance Spectroscopy*, 69(Complete):23–68, 2013.

[65] DS Wishart, CG Bigam, A Holm, RS Hodges, and BD Sykes. 1 H, 13 C and 15 N random coil NMR chemical shifts of the common amino acids. I. Investigations of nearest-neighbor effects. *Journal of biomolecular NMR*, 5(1):67–81, 1995.

[66] Akira Shoji, Takuo Ozaki, Hazime Saito, Ryoko Tabeta, and Isao Ando. Conformational characterization of solid polypeptides by carbon-13 NMR recorded by the cross polarization-magic angle spinning method: conformation-dependent carbon-13 chemical shifts of oligo- and poly(γ-benzyl L-glutamates) and sequential copolymers of γ-benzyl and γ-methyl L-glutamates and qualitative evaluation of side-chain orientation. *Macromolecules*, 17(8):1472–1479, August 1984.

[67] Hans R Kricheldorf and Detlef Mueller. Secondary structure of peptides. 3. Carbon-13 NMR cross polarization/magic angle spinning spectroscopic characterization of solid polypeptides. *Macromolecules*, 16(4):615–623, July 1983.

[68] Hazime Saito, Yoshihiro Iwanaga, Ryoko Tabeta, Mitsuaki Narita, and Tetsuo Asakura. A high resolution 13C NMR study of silk fibroin in solid state by the cross polarization-magic angle spinning method: Conformational characterization utilizing conformation-dependent 13C chemical shifts. *Chemistry Letters*, (4):427–430, 1983.

[69] Zhengyu Dong, Randolph V Lewis, and C Russell Middaugh. Molecular mechanism of spider silk elasticity. *Archives of biochemistry and biophysics*, 284(1):53–57, January 1991.

[70] Gregory P Holland, Melinda S Creager, Janelle E Jenkins, Randolph V Lewis, and Jeffery L Yarger. Determining Secondary Structure in Spider Dragline Silk by Carbon Carbon Correlation Solid-State NMR Spectroscopy. *J. Am. Chem. Soc*, 130(30):9871–9877, 2008.

[71] G P Holland, J E Jenkins, M S Creager, R V Lewis, and J L Yarger. Quantifying the fraction of glycine and alanine in β-sheet and helical conformations in spider dragline silk using solid-state NMR. *Chemical Communications*, (43):5568–5570, 2008.

[72] Shoko Okada, Sarah Weisman, Holly E Trueman, Stephen T Mudie, Victoria S Haritos, and Tara D Sutherland. An Australian webspinner species makes the finest known insect silk fibers. *International Journal of Biological Macromolecules*, 43(3):271–275, October 2008.

[73] K M Kjer, R J Blahnik, and R W Holzenthal. Phylogeny of caddisflies (Insecta, Trichoptera). *Zoologica Scripta*, 31(1):83–91, 2002.

[74] J C Morse. Phylogeny of trichoptera. *Annual review of entomology*, 42(1):427–450, 1997.

[75] Kensuke Shimura, Aiko Kikuchi, Kohei Ohtomo, Yōtarō Katagata, and Akio Hyodo. Studies on Silk Fibroin of Bombyx mori. I. Fractionation of Fibroin Prepared from the Posterior Silk Gland. *The Journal of Biochemistry*, 80(4):693–702, 1976.

[76] Russell J Stewart, Ching Shuen Wang, and Hui Shao. Complex coacervates as a foundation for synthetic underwater adhesives. *Advances in Colloid and Interface Science*, 167:85–93, 2011.

[77] R J Stewart and C S Wang. Adaptation of Caddisfly Larval Silks to Aquatic Habitats by Phosphorylation of H-Fibroin Serines. *Biomacromolecules*, 11(4):969–974, 2010.

[78] J S Edgerly, J A Davilla, and N Schoenfeld. Silk Spinning Behavior and Domicile Construction in Webspinners - Springer. *Journal of Insect Behavior*, 15(2):219–242, 2002.

[79] Janice S Edgerly. Life Beneath Silk Walls: A Review of the Primitively Social Embiidina. In J C Choe and B Crespi, editors, *The Evolution of Social Behavior in Insects and Arachnids*, pages 14–25. Cambridge University Press, 1997.

[80] Matthew A Collin, Jessica E Garb, Janice S Edgerly, and Cheryl Y Hayashi. Characterization of silk spun by the embiopteran, Antipaluria urichi. *Insect biochemistry and ...*, 39:79–82, 2009.

[81] Laurel R Fox. Cannibalism in natural populations. *Annual review of ecology and systematics*, pages 87–106, 1975.

[82] Hadley Leggett. 1 Million Spiders Make Golden Silk for Rare Cloth, September 2009.

[83] Amy E Albertson, Florence Teulé, Warner Weber, Jeffery L Yarger, and Randolph V Lewis. Effects of different post-spin stretching conditions on the mechanical properties of synthetic spider silk fibers. *Journal of the Mechanical Behavior of Biomedical Materials*, 29:225–234, January 2014.

[84] Florence Teulé, Bennett Addison, Alyssa R Cooper, Joel Ayon, Robert W Henning, Chris J Benmore, Gregory P Holland, Jeffery L Yarger, and Randolph V Lewis. Combining flagelliform and dragline spider silk motifs to produce tunable synthetic biopolymer fibers. *Biopolymers*, 97(6):418–431, October 2011.

[85] Lingling Xu, Jan K Rainey, Qing Meng, and Xiang-Qin Liu. Recombinant Minimalist Spider Wrapping Silk Proteins Capable of Native-Like Fiber Formation. *PLoS ONE*, 7(11):e50227, November 2012.

[86] Paul Geurts, Liang Zhao, Yang Hsia, Eric Gnesa, Simon Tang, Felicia Jeffery, Coby La Mattina, Andreas Franz, Leah Larkin, and Craig Vierra. Synthetic Spider Silk Fibers Spun from Pyriform Spidroin 2, A Glue Silk Protein Discovered in Orb-Weaving Spider Attachment Discs. *Biomacromolecules*, 11(12):3495–3503, 2010.

[87] Gustavo R Plaza, Paola Corsini, Enrico Marsano, José Pérez-Rigueiro, Lautaro Biancotto, Manuel Elices, Christian Riekel, Fernando Agulló-Rueda, Eva Gallardo, José M Calleja, and Gustavo V Guinea. Old Silks Endowed with New Properties. *Macromolecules*, 42(22):8977–8982, November 2009.

[88] John G Hardy, Lin M Römer, and Thomas R Scheibel. Polymeric materials based on silk proteins. *Polymer*, 49(20):4309–4327, September 2008.

[89] Kristin Schacht and Thomas Scheibel. Processing of recombinant spider silk proteins into tailor-made materials for biomaterials applications. *Current opinion in biotechnology*, 29:62–69, 2014.

[90] Jonathan A Kluge, Olena Rabotyagova, Gary G Leisk, and David L Kaplan. Spider silks and their applications. *Trends in biotechnology*, 26(5):244–251, May 2008.

[91] L Meinel, S Hofmann, V Karageorgiou, and C Kirker-Head. The inflammatory responses to silk films in vitro and in vivo. *Biomaterials*, 2005.

[92] Rebecca L Horan, Kathryn Antle, Adam L Collette, Yongzhong Wang, Jia Huang, Jodie E Moreau, Vladimir Volloch, David L Kaplan, and Gregory H Altman. In vitro degradation of silk fibroin. *Biomaterials*, 26(17):3385–3393, June 2005.

[93] Rei Nemoto, Satoshi Nakamura, Tetsuhiko Isobe, and Mamoru Senna. Direct Synthesis of Hydroxyapatite-Silk Fibroin Nano-Composite Sol via a Mechanochemical Route. *Journal of Sol-Gel Science and Technology*, 21(1/2):7–12, 2001.

[94] A Murphy and P John. Modification of silk fibroin using diazonium coupling chemistry and the effects on hMSC proliferation and differentiation. *Biomaterials*, 2008.

[95] T Arai, H Ishikawa, and G Freddi. Chemical modification of Bombyx mori silk using isocyanates. *Journal of applied ...*, 2001.

[96] Z Cai and G Jiang. Chemical modification of Bombyx mori silk with epoxide EPSIB. *Journal of applied polymer science*, 2004.

[97] Z Cai. Using an aqueous epoxide in Bombyx mori silk fabric finishing. *Textile Research Journal*, 2003.

[98] M Tsukada, Y Goto, G Freddi, and H Shiozaki. Chemical modification of silk with aromatic acid anhydrides. *Journal of applied polymer science*, 45(7):1189–1194, 1992.

[99] Susan Sofia, Mary Beth McCarthy, Gloria Gronowicz, and David L Kaplan. Functionalized silk-based biomaterials for bone formation. *Journal of Biomedical Materials Research Part A*, 54(1):139–148, 2000.

[100] T Kardestuncer, M B McCarthy, V Karageorgiou, D Kaplan, and G Gronowicz. RGD-tethered Silk Substrate Stimulates the Differentiation of Human Tendon Cells. *Clinical Orthopaedics and Related Research*, 448:234–239, July 2006.

[101] Tzahi Cohen-Karni, Kyung Jae Jeong, Jonathan H Tsui, Gally Reznor, Mirela Mustata, Meni Wanunu, Adam Graham, Carolyn Marks, David C Bell, Robert Langer, and Daniel S Kohane. Nanocomposite gold-silk nanofibers. *Nano letters*, 12(10):5403–5406, October 2012.

[102] Felix Bauer and Thomas Scheibel. Artificial Egg Stalks Made of a Recombinantly Produced Lacewing Silk Protein. *Angewandte Chemie International Edition*, 51(26):6521–6524, May 2012.

[103] Russell J Stewart. Protein-based underwater adhesives and the prospects for their biotechnological production. *Applied microbiology and biotechnology*, 89(1):27–33, 2011.

[104] H Shao. Biomimetic underwater adhesives with environmentally triggered setting mechanisms. *Advanced Materials*, 2010.

[105] Bruce P Lee, P B Messersmith, J N Israelachvili, and J H Waite. Mussel-Inspired Adhesives and Coatings. *Annual Review of Materials Research*, 41(1):99–132, August 2011.

REFERENCES: CHAPTER 2

[1] K M Kjer, R J Blahnik, and R W Holzenthal. Phylogeny of caddisflies (Insecta, Trichoptera). *Zoologica Scripta*, 31(1):83–91, 2002.

[2] J C Morse. Phylogeny of trichoptera. *Annual review of entomology*, 42(1):427–450, 1997.

[3] Gary LaFontaine. *Caddisflies*. The Lyons Press, April 1989.

[4] Glenn B Wiggins. *The caddisfly family Phryganeidae (Trichoptera)*. University of Toronto Press Incorporated, 1998.

[5] Russell J Stewart, Ching Shuen Wang, and Hui Shao. Complex coacervates as a foundation for synthetic underwater adhesives. *Advances in Colloid and Interface Science*, 167:85–93, 2011.

[6] Carrie E Brubaker and Phillip B Messersmith. The Present and Future of Biologically Inspired Adhesive Interfaces and Materials. *Langmuir*, 28(4):2200–2205, January 2012.

[7] Kensuke Shimura, Aiko Kikuchi, Kohei Ohtomo, Yōtarō Katagata, and Akio Hyodo. Studies on Silk Fibroin of Bombyx mori. I. Fractionation of Fibroin Prepared from the Posterior Silk Gland. *The Journal of Biochemistry*, 80(4):693–702, 1976.

[8] N Yonemura, F Sehnal, and K Mita. Protein composition of silk filaments spun under water by caddisfly larvae. *Biomacromolecules*, 7(12):3370–3378, 2006.

[9] Naoyuki Yonemura, Kazuei Mita, Toshiki Tamura, and František Sehnal. Conservation of Silk Genes in Trichoptera and Lepidoptera. *Journal of molecular evolution*, 68(6):641–653, May 2009.

[10] M S Engster. Studies on silk secretion in the trichoptera (F. Limnephilidae). *Cell and Tissue Research*, 169(1):77–92, June 1976.

[11] F Sehnal and M Zurovec. Construction of silk fiber core in Lepidoptera. *Biomacromolecules*, 5(3):666–674, 2004.

[12] R J Stewart and C S Wang. Adaptation of Caddisfly Larval Silks to Aquatic Habitats by Phosphorylation of H-Fibroin Serines. *Biomacromolecules*, 11(4):969–974, 2010.

[13] Richard E Marsh, Robert B Corey, and Linus Pauling. An investigation of the structure of silk fibroin. *Biochimica et Biophysica Acta*, 16:1–34, January 1955.

[14] Osman Rathore and Dotsevi Y Sogah. Self-assembly of β-sheets into nanostructures by poly (alanine) segments incorporated in multiblock copolymers inspired by spider silk. *J. Am. Chem. Soc*, 123(22):5231–5239, 2001.

[15] A Simmons, E Ray, and LW Jelinski. Solid-state 13C NMR of Nephila clavipes dragline silk establishes structure and identity of crystalline regions. *Macromolecules*, 27(18):5235–5237, 1994.

[16] Wei-Qiang Chen, Helga Priewalder, Julius Paul Pradeep John, and Gert Lubec. Silk cocoon of Bombyx mori: Proteins and posttranslational modifications - heavy phosphorylation and evidence for lysine-mediated cross links. *PROTEOMICS*, 10(3):369–379, February 2010.

[17] Nicholas N Ashton, Daniel S Taggart, and Russell J Stewart. Silk tape nanostructure and silk gland anatomy of trichoptera. *Biopolymers*, 97(6):432–445, 2012.

[18] G H Altman, F Diaz, C Jakuba, T Calabro, R L Horan, J Chen, H Lu, J Richmond, and D L Kaplan. Silk-based biomaterials. *Biomaterials*, 24(3):401–416, 2003.

[19] B Lotz and F C Cesari. Chemical-Structure and the Crystalline-Structures of Bombyx-Mori Silk Fibroin. *Biochimie*, 61(2):205–214, 1979.

[20] M Tsukada, MMR Khan, E Inoue, and G Kimura. Physical properties and structure of aquatic silk fiber from Stenopsyche marmorata 10.1016/j.ijbiomac.2009.10.003 : International Journal of Biological Macromolecules — ScienceDirect.com. *International Journal of Biological Macromolecules*, 46:54–58, 2010.

[21] Y Wang, K Sanai, H Wen, and T Zhao. Characterization of unique heavy chain fibroin filaments spun underwater by the caddisfly Stenopsyche marmorata (Trichoptera; Stenopsychidae). *Molecular biology reports*, 37:2885–2892.

[22] M S Creager, E B Butler, R V Lewis, J L Yarger, and G P Holland. Solid-state NMR evidence for elastin-like β-turn structure in spider dragline silk. *Chemical Communications*, 46(36):6714–6716, 2010.

[23] R W Williams, A Chang, D Juretić, and S Loughran. Secondary structure predictions and medium range interactions. *Biochimica et Biophysica Acta*, 916(2):200–204, 1987.

[24] Jan Johansson, Charlotte Nerelius, Hanna Willander, and Jenny Presto. Conformational preferences of non-polar amino acid residues: An additional factor in amyloid formation. *Biochemical and biophysical research communications*, 402(3):515–518, November 2010.

[25] Janusz W. Strzelecki, Joanna Strzelecka, Karolina Mikulska, Mariusz Tszydel, Aleksander Balter, and Wieslaw Nowak. Nanomechanics of new materials - AFM and computer modelling studies of trichoptera silk. *Central European Journal of Physics*, 9(2):482–491, 2011.

[26] Emma Lang, Gyorgyi I Szendrei, Ilona Elekes, Virginia M-Y Lee, and Laszlo Otvos Jr. Reversible β-pleated sheet formation of a phosphorylated synthetic τ peptide. *Biochemical and biophysical research communications*, 182(1):63–69, January 1992.

[27] M Hollosi, L Urge, A Perczel, J Kajtar, I Teplan, J Otvos, and G D Fasman. Metal Ion-Induced Conformational-Changes of Phosphorylated Fragments of Human Neurofilament (Nf-M) Protein. *Journal of Molecular Biology*, 223(3):673–682, 1992.

[28] S Holly, I Laczko, G D Fasman, and M Hollosi. FT-IR Spectroscopy Indicates That Ca2+-Binding to Phosphorylated C-Terminal Fragments of the Midsized Neurofilament Protein Subunit Results in [beta]-Sheet Formation and [beta]-Aggregation. *Biochemical and biophysical research communications*, 197(2):755–762, 1993.

[29] Andrew E Bennett, Chad M Rienstra, Michèle Auger, K V Lakshmi, and Robert G Griffin. Heteronuclear decoupling in rotating solids. *The Journal of Chemical Physics*, 103(16):6951, 1995.

[30] K Takegoshi, S Nakamura, and T Terao. 13C–1H dipolar-assisted rotational resonance in magic-angle spinning NMR. *Chemical Physics Letters*, 344(5):631–637, 2001.

[31] K Takegoshi, S Nakamura, and T Terao. C–H dipolar-driven C–C recoupling without C rf irradiation in nuclear magnetic resonance of rotating solids. *The Journal of Chemical Physics*, 118(5):2325–2341, 2003.

[32] J Schaefer, R A McKay, and E O Stejskal. Double-Cross-Polarization Nmr of Solids. *Journal of Magnetic Resonance*, 34(2):443–447, 1979.

[33] E O Stejskal, Jacob Schaefer, and R A McKay. Analysis of double cross-polarization rates in solid proteins. *Journal of Magnetic Resonance (1969)*, 57(3):471–485, May 1984.

[34] Wlodzimierz Ciesielski, Hassan Kassassir, and Marek J Potrzebowski. A practical guide for the setup of a 1H–31P–13C double cross-polarization (DCP) experiment. *Solid State Nuclear Magnetic Resonance*, 39(3-4):151–157, May 2011.

[35] J Herzfeld and A E Berger. Sideband Intensities in Nmr-Spectra of Samples Spinning at the Magic Angle. *Journal of Chemical Physics*, 73(12):6021–6030, 1980.

[36] D Massiot, F Fayon, M Capron, I King, S Le Calvé, B Alonso, J O Durand, B Bujoli, Z Gan, and G Hoatson. Modelling oneand twodimensional solidstate NMR spectra. *Magnetic Resonance in Chemistry*, 40(1):70–76, 2002.

[37] J G Hardy and T R Scheibel. Production and processing of spider silk proteins. *Journal of Polymer Science Part A: Polymer Chemistry*, 47(16):3957–3963, 2009.

[38] Z Yang, O Liivak, A Seidel, G LaVerde, DB Zax, and LW Jelinski. Supercontraction and backbone dynamics in spider silk: 13C and 2H NMR studies. *J. Am. Chem. Soc*, 122(37):9019–9025, 2000.

[39] Gregory P Holland, Janelle E Jenkins, Melinda S Creager, Randolph V Lewis, and Jeffery L Yarger. Solid-state NMR investigation of major and minor ampullate spider silk in the native and hydrated states. *Biomacromolecules*, 9(2):651–657, 2008.

[40] Akira Shoji, Takuo Ozaki, Hazime Saito, Ryoko Tabeta, and Isao Ando. Conformational characterization of solid polypeptides by carbon-13 NMR recorded by the cross polarization-magic angle spinning method: conformation-dependent carbon-13 chemical shifts of oligo- and poly(γ-benzyl L-glutamates) and sequential copolymers of γ-benzyl and γ-methyl L-glutamates and qualitative evaluation of side-chain orientation. *Macromolecules*, 17(8):1472–1479, August 1984.

[41] T Asakura. 13C CP/MAS NMR study on structural heterogeneity in Bombyx mori silk fiber and their generation by stretching. *Protein Science*, 11:2706–2713, 2002.

[42] Hans R Kricheldorf and Detlef Mueller. Secondary structure of peptides. 3. Carbon-13 NMR cross polarization/magic angle spinning spectroscopic characterization of solid polypeptides. *Macromolecules*, 16(4):615–623, July 1983.

[43] DS Wishart, CG Bigam, A Holm, RS Hodges, and BD Sykes. 1 H, 13 C and 15 N random coil NMR chemical shifts of the common amino acids. I. Investigations of nearest-neighbor effects. *Journal of biomolecular NMR*, 5(1):67–81, 1995.

[44] Ewa A Bienkiewicz and Kevin J Lumb. Journal of Biomolecular NMR, Volume 15, Number 3 - SpringerLink. *Journal of biomolecular NMR*, 15(3):203–206, 1999.

[45] Tetsuo Asakura, Mingying Yang, Taiji Kawase, and Yasumoto Nakazawa. 13C Solid-State NMR Study of Structural Heterogeneity in Peptides Containing Both Polyalanine and Repeated GGA Sequences as a Local Structural Model of NephilaclavipesDragline Silk (Spidroin 1). *Macromolecules*, 38(8):3356–3363, April 2005.

[46] J D van Beek. The molecular structure of spider dragline silk: Folding and orientation of the protein backbone. *Proceedings of the National Academy of Sciences*, 99(16):10266–10271, July 2002.

[47] Gregory P Holland, Melinda S Creager, Janelle E Jenkins, Randolph V Lewis, and Jeffery L Yarger. Determining Secondary Structure in Spider Dragline Silk by Carbon Carbon Correlation Solid-State NMR Spectroscopy. *J. Am. Chem. Soc*, 130(30):9871–9877, 2008.

[48] M S Creager, T Izdebski, A E Brooks, and R V Lewis. Elucidating Metabolic Pathways for Amino Acid Incorporation Into Dragline Spider Silk using 13C Enrichment and Solid State NMR. *Comparative Biochemistry and Physiology-Part A: Molecular & Integrative Physiology*, 2011.

[49] Carole Gardiennet-Doucet, Xavier Assfeld, Bernard Henry, and Piotr Tekely. Revealing Successive Steps of Deprotonation of l- Phosphoserine through 13C and 31P Chemical Shielding Tensor Fingerprints. *The Journal of Physical Chemistry A*, 110(29):9137–9144, July 2006.

[50] T M Duncan and D C Douglas. On the 31P chemical shift anisotropy in condensed phosphates. *Chemical Physics*, 87(3):339–349, July 1984.

[51] J O Warwicker. Comparative studies of fibroins. II. The crystal structures of various fibroins. *Journal of Molecular Biology*, 2(6):350–362, December 1960.

[52] Sujatha Sampath, Thomas Isdebski, Janelle E Jenkins, Joel V Ayon, Robert W Henning, Joseph P R O Orgel, Olga Antipoa, and Jeffery L Yarger. X-ray diffraction study of nanocrystalline and amorphous structure within major and minor ampullate dragline spider silks. *Soft Matter*, 8(25):6713–6722, 2012.

[53] Yi Liu and Zhengzhong Shao. Elasticity of spider silks. *Biomacromolecules*, 9:1782–1786, 2008.

[54] Xiao Hu, David Kaplan, and Peggy Cebe. Determining Beta-Sheet Crystallinity in Fibrous Proteins by Thermal Analysis and Infrared Spectroscopy. *Macromolecules*, 39(18):6161–6170, September 2006.

[55] C Riekel, C Bränden, C Craig, C Ferrero, F Heidelbach, and M Müller. Aspects of X-ray diffraction on single spider fibers. *International Journal of Biological Macromolecules*, 24(2-3):179–186, March 1999.

REFERENCES: CHAPTER 3

[1] Gary LaFontaine. *Caddisflies*. The Lyons Press, April 1989.

[2] Glenn B Wiggins. *The caddisfly family Phryganeidae (Trichoptera)*. University of Toronto Press Incorporated, 1998.

[3] J C Morse. Phylogeny of trichoptera. *Annual review of entomology*, 42(1):427–450, 1997.

[4] K M Kjer, R J Blahnik, and R W Holzenthal. Phylogeny of caddisflies (Insecta, Trichoptera). *Zoologica Scripta*, 31(1):83–91, 2002.

[5] Richard E Marsh, Robert B Corey, and Linus Pauling. An investigation of the structure of silk fibroin. *Biochimica et Biophysica Acta*, 16:1–34, January 1955.

[6] Osman Rathore and Dotsevi Y Sogah. Self-assembly of β-sheets into nanostructures by poly (alanine) segments incorporated in multiblock copolymers inspired by spider silk. *J. Am. Chem. Soc*, 123(22):5231–5239, 2001.

[7] O Rabotyagova and P Cebe. Role of Polyalanine Domains in βSheet Formation in Spider Silk Block Copolymers. *Macromolecular Bioscience*, 10:49–59, 2010.

[8] G P Holland, J E Jenkins, M S Creager, R V Lewis, and J L Yarger. Quantifying the fraction of glycine and alanine in β-sheet and helical conformations in spider dragline silk using solid-state NMR. *Chemical Communications*, (43):5568–5570, 2008.

[9] N Yonemura, F Sehnal, and K Mita. Protein composition of silk filaments spun under water by caddisfly larvae. *Biomacromolecules*, 7(12):3370–3378, 2006.

[10] Naoyuki Yonemura, Kazuei Mita, Toshiki Tamura, and František Sehnal. Conservation of Silk Genes in Trichoptera and Lepidoptera. *Journal of molecular evolution*, 68(6):641–653, May 2009.

[11] M S Engster. Studies on silk secretion in the trichoptera (F. Limnephilidae). *Cell and Tissue Research*, 169(1):77–92, June 1976.

[12] M Tsukada, MMR Khan, E Inoue, and G Kimura. Physical properties and structure of aquatic silk fiber from Stenopsyche marmorata 10.1016/j.ijbiomac.2009.10.003 : International Journal of Biological Macromolecules — ScienceDirect.com. *International Journal of Biological Macromolecules*, 46:54–58, 2010.

[13] Y Wang, K Sanai, H Wen, T Zhao, and M Nakagaki. Characterization of unique heavy chain fibroin filaments spun underwater by the caddisfly Stenopsyche marmorata (Trichoptera; Stenopsychidae). *Molecular biology reports*, 37(6):2885–2892, 2010.

[14] J Bennett Addison, Nicholas N Ashton, Warner S Weber, Russell J Stewart, Gregory P Holland, and Jeffery L Yarger. β-Sheet Nanocrystalline Domains Formed from Phosphorylated Serine-Rich Motifs in Caddisfly Larval Silk: A Solid State NMR and XRD Study. *Biomacromolecules*, 14(4):1140–1148, April 2013.

[15] R J Stewart and C S Wang. Adaptation of Caddisfly Larval Silks to Aquatic Habitats by Phosphorylation of H-Fibroin Serines. *Biomacromolecules*, 11(4):969–974, 2010.

[16] Nicholas N Ashton, Daniel R Roe, Robert B Weiss, Thomas E Cheatham, III, and Russell J Stewart. Self-Tensioning Aquatic Caddisfly Silk: Ca 2+-Dependent Structure, Strength, and Load Cycle Hysteresis. *Biomacromolecules*, 14(10):3668–3681, October 2013.

[17] Nicholas N Ashton, Daniel S Taggart, and Russell J Stewart. Silk tape nanostructure and silk gland anatomy of trichoptera. *Biopolymers*, 97(6):432–445, 2012.

[18] M S Creager, E B Butler, R V Lewis, J L Yarger, and G P Holland. Solid-state NMR evidence for elastin-like β-turn structure in spider dragline silk. *Chemical Communications*, 46(36):6714–6716, 2010.

[19] R W Williams, A Chang, D Juretić, and S Loughran. Secondary structure predictions and medium range interactions. *Biochimica et Biophysica Acta*, 916(2):200–204, 1987.

[20] Jan Johansson, Charlotte Nerelius, Hanna Willander, and Jenny Presto. Conformational preferences of non-polar amino acid residues: An additional factor in amyloid formation. *Biochemical and biophysical research communications*, 402(3):515–518, November 2010.

[21] Russell J Stewart, Ching Shuen Wang, and Hui Shao. Complex coacervates as a foundation for synthetic underwater adhesives. *Advances in Colloid and Interface Science*, 167:85–93, 2011.

[22] Janusz W. Strzelecki, Joanna Strzelecka, Karolina Mikulska, Mariusz Tszydel, Aleksander Balter, and Wieslaw Nowak. Nanomechanics of new materials - AFM and computer modelling studies of trichoptera silk. *Central European Journal of Physics*, 9(2):482–491, 2011.

[23] Emma Lang, Gyorgyi I Szendrei, Ilona Elekes, Virginia M-Y Lee, and Laszlo Otvos Jr. Reversible β-pleated sheet formation of a phosphorylated synthetic τ peptide. *Biochemical and biophysical research communications*, 182(1):63–69, January 1992.

[24] M Hollosi, L Urge, A Perczel, J Kajtar, I Teplan, J Otvos, and G D Fasman. Metal Ion-Induced Conformational-Changes of Phosphorylated Fragments of Human Neurofilament (Nf-M) Protein. *Journal of Molecular Biology*, 223(3):673–682, 1992.

[25] S Holly, I Laczko, G D Fasman, and M Hollosi. FT-IR Spectroscopy Indicates That Ca2+-Binding to Phosphorylated C-Terminal Fragments of the Midsized Neurofilament Protein Subunit Results in [beta]-Sheet Formation and [beta]-Aggregation. *Biochemical and biophysical research communications*, 197(2):755–762, 1993.

[26] Andrew E Bennett, Chad M Rienstra, Michèle Auger, K V Lakshmi, and Robert G Griffin. Heteronuclear decoupling in rotating solids. *The Journal of Chemical Physics*, 103(16):6951, 1995.

[27] E Fukushima and SBW Roeder. *Experimental Pulse Nmr: A Nuts and Bolts Approach*. Westview Press, 1983.

[28] DT Grubb and LW Jelinski. Fiber morphology of spider silk: the effects of tensile deformation. *Macromolecules*, 30(10):2860–2867, 1997.

[29] Carole Gardiennet-Doucet, Xavier Assfeld, Bernard Henry, and Piotr Tekely. Revealing Successive Steps of Deprotonation of l- Phosphoserine through 13C and 31P Chemical Shielding Tensor Fingerprints. *The Journal of Physical Chemistry A*, 110(29):9137–9144, July 2006.

[30] Carole Gardiennet, Bernard Henry, Paul Kuad, Bernard Spiess, and Piotr Tekely. Straightforward detection of the secondary ionisation of the phosphate group and pK determinations by high-resolution solid-state 31P NMR. *Chemical communications (Cambridge, England)*, (2):180–182, January 2005.

[31] Christian Jäger, Thea Welzel, Wolfgang Meyer-Zaika, and Matthias Epple. A solid-state NMR investigation of the structure of nanocrystalline hydroxyapatite. *Magnetic Resonance in Chemistry*, 44(6):573–580, 2006.

[32] Xavier Marchandise, Patrick Belgrand, and André-Pierre Legrand. Solid-State 31P NMR Spectroscopy of Bone and Bone Substitutes. *Magnetic Resonance in Medicine*, 28(1):1–8, November 1992.

REFERENCES: CHAPTER 4

[1] J S Edgerly, J A Davilla, and N Schoenfeld. Silk Spinning Behavior and Domicile Construction in Webspinners - Springer. *Journal of Insect Behavior*, 15(2):219–242, 2002.

[2] Janice S Edgerly. Life Beneath Silk Walls: A Review of the Primitively Social Embiidina. In J C Choe and B Crespi, editors, *The Evolution of Social Behavior in Insects and Arachnids*, pages 14–25. Cambridge University Press, 1997.

[3] J S Edgerly, S Büsse, and T Hörnschemeyer. Spinning behaviour and morphology of the spinning glands. *Zoologischer Anzeiger*, (251):297–306, 2012.

[4] Shoko Okada, Sarah Weisman, Holly E Trueman, Stephen T Mudie, Victoria S Haritos, and Tara D Sutherland. An Australian webspinner species makes the finest known insect silk fibers. *International Journal of Biological Macromolecules*, 43(3):271–275, October 2008.

[5] Matthew A Collin, Edina Camama, Brook O Swanson, Janice S Edgerly, and Cheryl Y Hayashi. Comparison of embiopteran silks reveals tensile and structural similarities across Taxa. *Biomacromolecules*, 10(8):2268–2274, August 2009.

[6] Matthew A Collin, Jessica E Garb, Janice S Edgerly, and Cheryl Y Hayashi. Characterization of silk spun by the embiopteran, Antipaluria urichi. *Insect biochemistry and ...*, 39:79–82, 2009.

[7] J S Edgerly, A TADIMALLA, and E P DAHLHOFF. Adaptation to thermal stress in lichen-eating webspinners (Embioptera): habitat choice, domicile construction and the potential role of heat shock proteins. *Functional Ecology*, 19(2):255–262, April 2005.

[8] Edward S Ross. Webspinners (Embiidina). In John L Capirena, editor, *Encyclopedia of Entomology*, pages 4169–4172. Springer Netherlands, 2008.

[9] Kelly B Miller, Cheryl Y Hayashi, Michael F Whiting, Gavin J Svenson, and Janice S Edgerly. The phylogeny and classification of Embioptera (Insecta). *Systematic Entomology*, 37(3):550–570, 2012.

[10] Matthew A Collin, Janice S Edgerly, and Cheryl Y Hayashi. Comparison of fibroin cDNAs from webspinning insects: insight into silk formation and function. *Zoology (Jena, Germany)*, 114(4):239–246, September 2011.

[11] Randolph V Lewis. Spider silk: ancient ideas for new biomaterials. *Chemical reviews*, 106(9):3762–3774, September 2006.

[12] G H Altman, F Diaz, C Jakuba, T Calabro, R L Horan, J Chen, H Lu, J Richmond, and D L Kaplan. Silk-based biomaterials. *Biomaterials*, 24(3):401–416, 2003.

[13] Tara D Sutherland, James H Young, Sarah Weisman, Cheryl Y Hayashi, and David J Merritt. Insect silk: one name, many materials. *Annual review of entomology*, 55:171–188, 2010.

[14] C Z Zhou, F Confalonieri, N Medina, Y Zivanovic, C Esnault, T Yang, M Jacquet, J Janin, M Duguet, R Perasso, and Z G Li. Fine organization of Bombyx mori fibroin heavy chain gene. *Nucleic Acids Research*, 28(12):2413–2419, June 2000.

[15] M Xu and R V Lewis. Structure of a protein superfiber: spider dragline silk. *Proceedings of the National Academy of Sciences of the United States of America*, 87(18):7120–7124, September 1990.

[16] Sinan Keten, Zhiping Xu, Britni Ihle, and Markus J Buehler. Nanoconfinement controls stiffness, strength and mechanical toughness of β-sheet crystals in silk. *Nature Materials*, 9(4):359–367, March 2010.

[17] Sinan Keten and Markus J Buehler. Atomistic model of the spider silk nanostructure. *Applied physics letters*, 96(15):153701, 2010.

[18] C Y Hayashi, N H Shipley, and R V Lewis. Hypotheses that correlate the sequence, structure, and mechanical properties of spider silk proteins. *International Journal of Biological Macromolecules*, 24(2-3):271–275, March 1999.

[19] Jan Johansson, Charlotte Nerelius, Hanna Willander, and Jenny Presto. Conformational preferences of non-polar amino acid residues: An additional factor in amyloid formation. *Biochemical and biophysical research communications*, 402(3):515–518, November 2010.

[20] R W Williams, A Chang, D Juretić, and S Loughran. Secondary structure predictions and medium range interactions. *Biochimica et Biophysica Acta*, 916(2):200–204, 1987.

[21] David L Minor, Jr and Peter S Kim. Measurement of the b-sheet-forming propensities of amino acids. *Nature*, 367(6464):660–663, 1994.

[22] Sujatha Sampath, Thomas Isdebski, Janelle E Jenkins, Joel V Ayon, Robert W Henning, Joseph P R O Orgel, Olga Antipoa, and Jeffery L Yarger. X-ray diffraction study of nanocrystalline and amorphous structure within major and minor ampullate dragline spider silks. *Soft Matter*, 8(25):6713–6722, 2012.

[23] Janelle E Jenkins, Sujatha Sampath, Emily Butler, Jihyun Kim, Robert W Henning, Gregory P Holland, and Jeffery L Yarger. Characterizing the secondary protein structure of black widow dragline silk using solid-state NMR and X-ray diffraction. *Biomacromolecules*, 14(10):3472–3483, October 2013.

[24] Ku Liang, Yu Gong, Jianlong Fu, Shi Yan, Yuanyuan Tan, Rong Du, Xueqing Xing, Guang Mo, Zhongjun Chen, Quan Cai, Dongbai Sun, and Zhonghua Wu. Microstructural change of degummed Bombyx mori silk: an in situ stretching wide-angle X-ray-scattering study. *International Journal of Biological Macromolecules*, 57:99–104, June 2013.

[25] Tetsuo Asakura, Juming Yao, Tsutomu Yamane, Kosuke Umemura, and Anne S Ulrich. Heterogeneous Structure of Silk Fibers from BombyxmoriResolved by 13C Solid-State NMR Spectroscopy. *J. Am. Chem. Soc*, 124(30):8794–8795, July 2002.

[26] Janelle E Jenkins, Melinda S Creager, Randolph V Lewis, Gregory P Holland, and Jeffery L Yarger. Quantitative Correlation between the protein primary sequences and secondary structures in spider dragline silks. *Biomacromolecules*, 11(1):192–200, 2009.

[27] Alexander Sponner, Wolfram Vater, Shamci Monajembashi, Eberhard Unger, Frank Grosse, and Klaus Weisshart. Composition and Hierarchical Organisation of a Spider Silk. *PLoS ONE*, 2(10):e998, October 2007.

[28] Gregory P Holland, Randolph V Lewis, and Jeffery L Yarger. WISE NMR characterization of nanoscale heterogeneity and mobility in supercontracted Nephila clavipes spider dragline silk. *J. Am. Chem. Soc*, 126(18):5867–5872, 2004.

[29] Z Yang, DT Grubb, and LW Jelinski. Small-angle X-ray scattering of spider dragline silk. *Macromolecules*, 30(26):8254–8261, 1997.

[30] DT Grubb and LW Jelinski. Fiber morphology of spider silk: the effects of tensile deformation. *Macromolecules*, 30(10):2860–2867, 1997.

[31] C Riekel, C Bränden, C Craig, C Ferrero, F Heidelbach, and M Müller. Aspects of X-ray diffraction on single spider fibers. *International Journal of Biological Macromolecules*, 24(2-3):179–186, March 1999.

[32] Fritz Vollrath, Thor Holtet, Hans C Thogersen, and Sebastian Frische. Structural organization of spider silk. *Proceedings of the Royal Society of London. Series B: Biological Sciences*, 263(1367):147–151, 1996.

[33] S Frische, Maunsbach, AB, and F Vollrath. Elongate cavities and skin-core structure in Nephila spider silk observed by electron microscopy. *Journal of Microscopy*, 189(1):64–70, 1998.

[34] Stefan Schulz. Composition of the silk lipids of the spider Nephila clavipes. *Lipids*, 36(6):637–647, June 2001.

[35] Eliane Victoriano, Daniela O Pinheiro, and Elisa A Gregório. Histochemical and ultrastructural evidence of lipid secretion by the silk gland of the sugarcane borer Diatraea saccharalis (Fabricius) (Lepidoptera: Crambidae). *Neotropical entomology*, 36(5):707–711, September 2007.

[36] Sarah Weisman, Holly E Trueman, Stephen T Mudie, Jeffrey S Church, Tara D Sutherland, and Victoria S Haritos. An Unlikely Silk: The Composite Material of Green Lacewing Cocoons. *Biomacromolecules*, 9(11):3065–3069, November 2008.

[37] David Nečas and Petr Klapetek. Gwyddion: an open-source software for SPM data analysis. *Central European Journal of Physics*, 10(1):181–188, November 2011.

[38] Andrew E Bennett, Chad M Rienstra, Michèle Auger, K V Lakshmi, and Robert G Griffin. Heteronuclear decoupling in rotating solids. *The Journal of Chemical Physics*, 103(16):6951, 1995.

[39] Ruthven N A H Lewis and Ronald N McElhaney. Fourier transform infrared spectroscopy in the study of lipid phase transitions in model and biological membranes: practical considerations. *Methods in molecular biology (Clifton, N.J.)*, 400:207–226, 2007.

[40] Maxime Boulet-Audet, Thierry Lefèvre, Thierry Buffeteau, and Michel Pézolet. Attenuated Total Reflection Infrared Spectroscopy: An Efficient Technique to Quantitatively Determine the Orientation and Conformation of Proteins in Single Silk Fibers. *Applied Spectroscopy*, 62(9):956–962, September 2008.

[41] Jianzhong Shao, Jinhuan Zheng, Jinqiang Liu, and C M Carr. Fourier transform Raman and Fourier transform infrared spectroscopy studies of silk fibroin. *Journal of applied polymer science*, 96(6):1999–2004, 2005.

[42] Shengjie Ling, Zeming Qi, David P Knight, Zhengzhong Shao, and Xin Chen. Synchrotron FTIR Microspectroscopy of Single Natural Silk Fibers. *Biomacromolecules*, 12(9):3344–3349, September 2011.

[43] Shengjie Ling, Zeming Qi, David P Knight, Yufang Huang, Lei Huang, Huan Zhou, Zhengzhong Shao, and Xin Chen. Insight into the Structure of Single Antheraea pernyi Silkworm Fibers Using Synchrotron FTIR Microspectroscopy. *Biomacromolecules*, 14(6):1885–1892, June 2013.

[44] Periklis Papadopoulos, Roxana Ene, Immanuel Weidner, and Friedrich Kremer. Similarities in the Structural Organization of Major and Minor Ampullate Spider Silk. *Macromolecular Rapid Communications*, 30(9-10):851–857, May 2009.

[45] Nicholas N Ashton, Daniel R Roe, Robert B Weiss, Thomas E Cheatham, III, and Russell J Stewart. Self-Tensioning Aquatic Caddisfly Silk: Ca 2+-Dependent Structure, Strength, and Load Cycle Hysteresis. *Biomacromolecules*, 14(10):3668–3681, October 2013.

[46] Andrew A Walker, Jeffrey S Church, Andrea L Woodhead, and Tara D Sutherland. Silverfish silk is formed by entanglement of randomly coiled protein chains. *Insect biochemistry and molecular biology*, 43(7):572–579, July 2013.

[47] P Papadopoulos, J Sölter, and F Kremer. Structure-property relationships in major ampullate spider silk as deduced from polarized FTIR spectroscopy. *The European physical journal. E, Soft matter*, 24(2):193–199, October 2007.

[48] Venyaminov SYu and N N Kalnin. Quantitative IR spectrophotometry of peptide compounds in water (H2O) solutions. II. Amide absorption bands of polypeptides and fibrous proteins in alpha-, beta-, and random coil conformations. *Biopolymers*, 30(13-14):1259–1271, 1990.

[49] J O Warwicker. Comparative studies of fibroins. II. The crystal structures of various fibroins. *Journal of Molecular Biology*, 2(6):350–362, December 1960.

[50] Hazime Saito. Conformationdependent 13C chemical shifts: A new means of conformational characterization as obtained by highresolution solidstate 13C NMR. *Magnetic Resonance in Chemistry*, 24(10):835–852, 1986.

[51] Akira Shoji, Takuo Ozaki, Hazime Saito, Ryoko Tabeta, and Isao Ando. Conformational characterization of solid polypeptides by carbon-13 NMR recorded by the cross polarization-magic angle spinning method: conformation-dependent carbon-13 chemical shifts of oligo- and poly(γ-benzyl L-glutamates) and sequential copolymers of γ-benzyl and γ-methyl L-glutamates and qualitative evaluation of side-chain orientation. *Macromolecules*, 17(8):1472–1479, August 1984.

[52] Tetsuo Asakura, Kohei Suita, Tsunenori Kameda, Sergii Afonin, and Anne S Ulrich. Structural role of tyrosine inBombyx mori silk fibroin, studied by solidstate NMR and molecular mechanics on a model peptide prepared as silk I and II. *Magnetic Resonance in Chemistry*, 42(2):258–266, January 2004.

[53] Tetsuo Asakura, Rena Sugino, Tatsushi Okumura, and Yasumoto Nakazawa. The role of irregular unit, GAAS, on the secondary structure of Bombyx mori silk fibroin studied with 13C CP/MAS NMR and wide-angle X-ray scattering. *Protein science : a publication of the Protein Society*, 11(8):1873–1877, August 2002.

[54] D Massiot, F Fayon, M Capron, I King, S Le Calvé, B Alonso, J O Durand, B Bujoli, Z Gan, and G Hoatson. Modelling oneand twodimensional solidstate NMR spectra. *Magnetic Resonance in Chemistry*, 40(1):70–76, 2002.

[55] Melinda S Creager, Janelle E Jenkins, Leigh A Thagard-Yeaman, Amanda E Brooks, Justin A Jones, Randolph V Lewis, Gregory P Holland, and Jeffery L Yarger. Solid-state NMR comparison of various spiders' dragline silk fiber. *Biomacromolecules*, 11(8):2039–2043, August 2010.

[56] Gregory P Holland, Janelle E Jenkins, Melinda S Creager, Randolph V Lewis, and Jeffery L Yarger. Solid-state NMR investigation of major and minor ampullate spider silk in the native and hydrated states. *Biomacromolecules*, 9(2):651–657, 2008.

[57] Z Yang, O Liivak, A Seidel, G LaVerde, DB Zax, and LW Jelinski. Supercontraction and backbone dynamics in spider silk: 13C and 2H NMR studies. *J. Am. Chem. Soc*, 122(37):9019–9025, 2000.

[58] J Bennett Addison, Nicholas N Ashton, Warner S Weber, Russell J Stewart, Gregory P Holland, and Jeffery L Yarger. β-Sheet Nanocrystalline Domains Formed from Phosphorylated Serine-Rich Motifs in Caddisfly Larval Silk: A Solid State NMR and XRD Study. *Biomacromolecules*, 14(4):1140–1148, April 2013.

REFERENCES: CHAPTER 5

[1] Janice S Edgerly. Life Beneath Silk Walls: A Review of the Primitively Social Embiidina. In J C Choe and B Crespi, editors, *The Evolution of Social Behavior in Insects and Arachnids*, pages 14–25. Cambridge University Press, 1997.

[2] J S Edgerly, J A Davilla, and N Schoenfeld. Silk Spinning Behavior and Domicile Construction in Webspinners - Springer. *Journal of Insect Behavior*, 15(2):219–242, 2002.

[3] T Nagashima, N Niwa, S Okajima, and T Nonaka. Ultrastructure of silk gland of webspinners, Oligotoma japonica (Insecta, Embioptera). *Cytologia : international journal of cytology*, 1991.

[4] J S Edgerly, S Büsse, and T Hörnschemeyer. Spinning behaviour and morphology of the spinning glands. *Zoologischer Anzeiger*, (251):297–306, 2012.

[5] Janice S Edgerly. Maternal behaviour of a webspinner (Order Embiidina). *Ecological Entomology*, 12(1):1–11, February 1987.

[6] J S Edgerly, S M Shenoy, and V G Werner. Relating the Cost of Spinning Silk to the Tendency to Share It for Three Embiids with Different Lifestyles (Order Embiidina: Clothodidae, Notoligotomidae, and Australembiidae). *Environmental Entomology*, 35(2):448–457, April 2006.

[7] Janice S Edgerly. Is group living an antipredator defense in a facultatively communal webspinner (Embiidina: Clothodidae)? *Journal of Insect Behavior*, 7(2):135–147, March 1994.

[8] J S Edgerly. *Behavioral ecology of a Primitively Social Webspinner (Embiidina: Clothodidae:* Clothoda urichi*)*. . PhD thesis, Cornell University, January 1986.

[9] Stefan Schulz. Composition of the silk lipids of the spider Nephila clavipes. *Lipids*, 36(6):637–647, June 2001.

[10] Sarah Weisman, Holly E Trueman, Stephen T Mudie, Jeffrey S Church, Tara D Sutherland, and Victoria S Haritos. An Unlikely Silk: The Composite Material of Green Lacewing Cocoons. *Biomacromolecules*, 9(11):3065–3069, November 2008.

[11] Alexander Sponner, Wolfram Vater, Shamci Monajembashi, Eberhard Unger, Frank Grosse, and Klaus Weisshart. Composition and Hierarchical Organisation of a Spider Silk. *PLoS ONE*, 2(10):e998, October 2007.

[12] Eliane Victoriano, Daniela O Pinheiro, and Elisa A Gregório. Histochemical and ultrastructural evidence of lipid secretion by the silk gland of the sugarcane borer Diatraea saccharalis (Fabricius) (Lepidoptera: Crambidae). *Neotropical entomology*, 36(5):707–711, September 2007.

[13] Matthew A Collin, Jessica E Garb, Janice S Edgerly, and Cheryl Y Hayashi. Characterization of silk spun by the embiopteran, Antipaluria urichi. *Insect biochemistry and molecular biology*, 39(2):75–82, February 2009.

[14] Matthew A Collin, Edina Camama, Brook O Swanson, Janice S Edgerly, and Cheryl Y Hayashi. Comparison of embiopteran silks reveals tensile and structural similarities across Taxa. *Biomacromolecules*, 10(8):2268–2274, August 2009.

[15] Shoko Okada, Sarah Weisman, Holly E Trueman, Stephen T Mudie, Victoria S Haritos, and Tara D Sutherland. An Australian webspinner species makes the finest known insect silk fibers. *International Journal of Biological Macromolecules*, 43(3):271–275, October 2008.

[16] S Wang and L Jiang. Definition of Superhydrophobic States. *Advanced Materials*, 19(21):3423–3424, November 2007.

[17] Yong Min Park, Myeong Gang, Young Ho Seo, and Byeong Hee Kim. Artificial petal surface based on hierarchical micro- and nanostructures. *Thin Solid Films*, 520(1):362–367, October 2011.

[18] Xin Yong and Lucy T Zhang. Nanoscale Wetting on Groove-Patterned Surfaces. *Langmuir*, 25(9):5045–5053, May 2009.

[19] Ruthven N A H Lewis and Ronald N McElhaney. Fourier transform infrared spectroscopy in the study of lipid phase transitions in model and biological membranes: practical considerations. *Methods in molecular biology (Clifton, N.J.)*, 400:207–226, 2007.

[20] G H Altman, F Diaz, C Jakuba, T Calabro, R L Horan, J Chen, H Lu, J Richmond, and D L Kaplan. Silk-based biomaterials. *Biomaterials*, 24(3):401–416, 2003.

[21] Matthew A Collin, Janice S Edgerly, and Cheryl Y Hayashi. Comparison of fibroin cDNAs from webspinning insects: insight into silk formation and function. *Zoology (Jena, Germany)*, 114(4):239–246, September 2011.

[22] P Manirakiza, A Covaci, and P Schepens. Comparative Study on Total Lipid Determination using Soxhlet, Roese-Gottlieb, Bligh & Dyer, and Modified Bligh & Dyer Extraction Methods. *Journal of Food Composition and Analysis*, 14(1):93–100, February 2001.

[23] Robert C Randall, Henry Lee, II, Robert J Ozretich, James L Lake, and Richard J Pruell. Evaluation of selected lipid methods for normalizing pollutant bioaccumulation. *Environmental Toxicology and Chemistry*, 10(11):1431–1436, November 1991.

[24] Agustín Estrada-Peña, Frantisek Dusbábek, and Joaquím Castellá. Cuticular hydrocarbon variation and progeny phenotypic similarity between laboratory breeds of allopatric populations of Argas (Persicargas) persicus (Oken) (acari: Argasidae). *Acta Tropica*, 59(4):309–322, August 1995.

[25] Jakob A Shimshoni, Oran Erster, Asael Rot, Olga Cuneah, Stefan Soback, and Varda Shkap. Cuticular fatty acid profile analysis of three Rhipicephalus tick species (Acari: Ixodidae). *Experimental & applied acarology*, 61(4):481–489, December 2013.

[26] M A Gough and S J Rowland. Characterization of unresolved complex mixtures of hydrocarbons in petroleum. *Nature*, 344(6267):648–650, April 1990.

[27] Marco Pelillo, Giovanna Iafelice, Emanuele Marconi, and Maria Fiorenza Caboni. Identification of plant sterols in hexaploid and tetraploid wheats using gas chromatography with mass spectrometry. *Rapid communications in mass spectrometry : RCM*, 17(20):2245–2252, 2003.

[28] P Karlson and A Butenandt. Pheromones (ectohormones) in insects. *Annual review of entomology*, 1959.

[29] J H Tumlinson, R M Silverstein, J C Moser, R G Brownlee, and J M Ruth. Identification of the trail pheromone of a leaf-cutting ant, Atta texana. *Nature*, 234(5328):348–349, December 1971.

[30] C B Proaño, S Cruz, D M McMillan, and J S Edgerly. Exploration of substrate vibrations as communication signals in a webspinner from Ecuador (Embioptera: Clothodidae). *Neotropical entomology*, 41(3):196–203, June 2012.

[31] Khaaliq A Dejan, John M Fresquez, Annika M Meyer, and Janice S Edgerly. Maternal territoriality achieved through shaking and lunging: An investigation of patterns in associated behaviors and substrate vibrations in a colonial embiopteran, Antipaluria urichi. *Journal of Insect Science*, 13:1–28, August 2013.

[32] J F Padday. Sessile Drop Profiles: Corrected Methods for Surface Tension and Spreading Coefficients. *Proceedings of the Royal Society A: Mathematical, Physical and Engineering Sciences*, 330(1583):561–572, November 1972.

[33] ABD Cassie. Contact angles. *Discuss Faraday Soc*, 1948.

[34] D Y Kwok and A W Neumann. Contact angle measurement and contact angle interpretation. *Advances in Colloid and Interface Science*, 81(3):167–249, September 1999.

[35] Lichao Gao and Thomas J McCarthy. Contact angle hysteresis explained. *Langmuir*, 22(14):6234–6237, July 2006.

[36] Zhongjun Cheng, Ming Du, Hua Lai, Naiqing Zhang, and Kening Sun. From petal effect to lotus effect: a facile solution immersion process for the fabrication of super-hydrophobic surfaces with controlled adhesion . *Nanoscale*, 5(7):2776–2783, 2013.

[37] Bharat Bhushan and Michael Nosonovsky. The rose petal effect and the modes of superhydrophobicity. *Philosophical transactions. Series A, Mathematical, physical, and engineering sciences*, 368(1929):4713–4728, October 2010.

[38] C Neinhuis and W Barthlott. Characterization and Distribution of Water-repellent, Self-cleaning Plant Surfaces. *Annals of Botany*, 79(6):667–677, June 1997.

[39] Abraham Marmur. The Lotus effect: superhydrophobicity and metastability. *Langmuir*, 20(9):3517–3519, April 2004.

[40] Lin Feng, Yanan Zhang, Jinming Xi, Ying Zhu, Nü Wang, Fan Xia, and Lei Jiang. Petal effect: a superhydrophobic state with high adhesive force. *Langmuir*, 24(8):4114–4119, April 2008.

[41] Juuso T Korhonen, Tommi Huhtamäki, Olli Ikkala, and Robin H A Ras. Reliable measurement of the receding contact angle. *Langmuir*, 29(12):3858–3863, March 2013.

[42] L Feng, S Li, Y Li, H Li, L Zhang, and J Zhai. Super-Hydrophobic Surfaces: From Natural to Artificial - Feng - 2002 - Advanced Materials - Wiley Online Library. *Advanced ...*, 2002.

[43] Bharat Bhushan and Eun Kyu Her. Fabrication of Superhydrophobic Surfaces with High and Low Adhesion Inspired from Rose Petal. *Langmuir*, 26(11):8207–8217, June 2010.

[44] Bharat Bhushan. Bioinspired structured surfaces. *Langmuir*, 28(3):1698–1714, January 2012.

[45] Elena Celia, Thierry Darmanin, Elisabeth Taffin de Givenchy, Sonia Amigoni, and Frédéric Guittard. Recent advances in designing superhydrophobic surfaces. *Journal of Colloid and Interface Science*, 402:1–18, July 2013.

[46] Janice S Edgerly. Maternal behaviour of a webspinner (Order Embiidina): mother-nymph associations. *Ecological Entomology*, 13(3):263–272, August 1988.

[47] J E Brower, J H Zar, and C N vonEnde. *Field and laboratory methods for general ecology*. WCB McGraw-Hill, Boston, Massachusetts, 4th edition, 1997.